NASA Contractor Report CR-154631

FEDERAL ELECTRIC CORPORATION

An Accuracy Analysis of the LDAR System

Dr. Horst A. Poehler

PREPARED FOR
JOHN F. KENNEDY SPACE CENTER
CONTRACT NAS10-4967

National Aeronautics and
Space Administration

John F. Kennedy Space Center

NASA

KSC FORM 16-12 (REV. 8/76)

AN ACCURACY ANALYSIS OF THE LDAR SYSTEM

FEC-7146

FEDERAL ELECTRIC CORPORATION
RF SYSTEMS BRANCH
KENNEDY SPACE CENTER

8 March 1977

APPROVAL

AN ACCURACY ANALYSIS OF THE LDAR SYSTEM

ORIGINATOR:

Horst A. Poehler

Dr. Horst A. Poehler
Senior Scientist

APPROVAL:

Jesse W. Taylor

Jesse W. Taylor
Branch Manager
RF Systems Branch, FEC-720

Carl L. Lennon

Carl L. Lennon, Project Manager
EMA Section Chief, IN-TEL-32

SUMMARY

An accuracy report of the LDAR system is presented. The effect of quantizing errors are modelled by use of a computer. The errors in the four configurations of the LDAR system are compared to the limiting errors in an ideal hyperbolic system. Performance data from the track of a jet airplane and for the indicated position of a fixed lightning simulator are analyzed for dispersions in the data. Error models show the quality and the areas of highly accurate data, and show how the data deteriorates outside the primary measuring range.

TABLE OF CONTENTS

LIST OF ILLUSTRATIONS

LIST OF TABLES

I. INTRODUCTION

The LDAR System, References (1,2), determines the location of an electrical discharge in the clouds from the time of arrival of the pulsed RF radiation emitted by the discharge. The accuracy of the LDAR System is determined by how precisely the time of arrival of the discharge waveform can be determined. Potential sources of inaccuracy in the basic measurement are variations in the transmission delay from the outlying site to the central site, waveform distortion, noise, and the quantizing error inherent in the conversion of analogue to digital data.

The accuracy of the measurement is also degraded by the Geometric Dilution of Precision GDOP (sometimes called the Factor of Geometric Precision), that is inherent in the geometry of the system. The error of the measurement at any given point in the measurement field is the product of the basic error in the measurement by the Geometric Dilution of Precision, GDOP for that point in space.

We will first present the GDOPs to give a picture of how the basic measurement accuracy is diluted in different parts of the measurement field. Then we will discuss in some detail the accuracy of the basic measurement.

As a standard for the performance of a time-of-arrival system, such as LDAR, we will present GDOPs for an optimized hyperbolic system. In practice, physical limitations do not permit the implementation of the geometry dictated by the optimum configuration. As a result, the accuracy in certain regions of space will be degraded.

We will clarify the GDOPs of the actual LDAR configuration by a series of computer-generated error curves. This will tell us in what area of space

the four configurations of the LDAR system have their best and their poorest accuracy.

Finally, we will use the scatter in the LDAR's forty-mile track of a jet plane, and in the location of fixed lightning simulators to compare calculated and measured random errors, and to illustrate the precision which LDAR is capable of.

II. THE IDEAL HYPERBOLIC SYSTEM

The position of a point in space can be uniquely determined from measurements of the delay in the time-of-arrival between each of three stations and a central receiver station. The sought-for position is the intersection of three hyperbolic surfaces, hence the system is referred to as a hyperbolic system.

In configuring a time-of-arrival system, the goal is to find a configuration that will optimize the RMS errors in position over the largest possible volume in space. The question of the optimum configuration of the receiving stations has already been answered by Holmes and Reedy[3]. They found that the optimum configuration is that of a Y, with the master station at the center and with a separation of 120 degrees between the three stations. Their analysis showed further that reasonable departures ($\pm$ 10 to 15 degrees) could be tolerated.

In practice, it is generally not possible to locate three stations equidistant and at a 120 degree separation - especially at Kennedy Space Center where such a configuration would put at least one of these stations in the river.

We start by presenting the GDOP curves for the ideal hyperbolic configuration to set a standard against which we can measure the performance of the LDAR system.

The station configuration of the ideal hyperbolic system and the coordinate system used in the GDOP plots are shown in Figure 1 and Figure 2. The GDOP curves developed by Holmes and Reedy will be given in Figures 3 to 10.

The curves, as originally presented, were given in parametric form, that is in units of baseline length, and in units of measurement uncertainty, du.

To make the GDOP plots more specific, and to offer a more ready comparison with LDAR, the parametric values have been supplemented with numbers appropriate to the LDAR system, using a baseline of 8000 meters and a basic measurement uncertainty, du, of 6 meters.

In Figure 3 we show the geometric dilution of precision (GDOP) in X at an azimuth angle of 30 degrees for altitudes of 800, 4000, and 8000 meters. The GDOP curves are essentially the same for azimuths of 0 to 360 degrees, except that some differences will show up at those azimuths on which the stations lie, that is a 120, 240, and 360 degrees. (See Figures 1 and 6).

Note that at all distances up to 6000 meters (3.75 mi.) the error in the X measurement is very small, that is, less than 7 meters. At 8000 meters (5 mi.) range, the error is 11 meters. For greater distances, the error increases rapidly, being some 54 meters at 16 km. (10 mi.). From the parametric nature of the plots, it is clear that the system performance is good up to distances equal to the baseline, that is up to k=ratio of distance/baseline length=1.

Figure 4 shows how the error in the measurement of height (elevation) Z varies with the horizontal distance for a measurement error of 6 meters (0.02 microseconds) in the range difference measurement.

For the higher altitudes (that is for heights greater than 1000 meters) the error in the height is reasonably low, that is less than 72 meters for

ranges up to 6000 meters (3.75 mi.). At 8000 meters (10 mi.), the height error is 110 meters. Comparison with Figure 3 shows that the error in height is much greater than the error in distance.

At heights less than 800 meters (2,600 ft.) the error in the measurement of height Z increases rapidly as the height decreases. For example at a height of 80 meters (262 ft.), at a range of 8000 meters (5 mi.), the error in the height measurement is 1080 meters (3543 ft.).

Figures 5 and 6 show GDOPs for an azimuth that runs through a station. While the GDOP for X is only slightly different, the GDOP for height Z shows a marked difference. Note that the error in the measurement decreases remarkably for points over the measuring station. For example, at a height of 80 meters the measurement error decreases from 480 to 24 meters.

Figures 7 and 8 show contours of constant dilution factor for X for heights of 800, and 8000 meters. Note that at ranges up to 8000 meters (5 mi.) the error in the X measurement is less than 6 meters.

Figures 9 and 10 show contours of constant dilution for height Z at heights of 800 and 8000 meters. Note the marked improvement with height. Not only does the magnitude of the measurement error decrease with height, but the distribution in the error is much more uniform. Finally, note that the decrease in error above the station already shown in Figure 6 is very apparent in Figure 9.

III. THE LDAR SYSTEM

The configuration of the LDAR system is shown in Figure 11. One extra station was added to the four stations required in order to (1) achieve redundancy, permitting continued operation in case one station should fail during an operation, (2) to obtain a second configuration which could be used to check on the first, the primary configuration.

With five station, four time-of-arrival configurations are possible. These will be referred to as Configurations #1, #2, #3, and #4, and are shown in Figure 12. The time of arrival at the stations will be designated as TØ, T1, T2, T3, and T4, where TØ refers to the central station.

Computer-generated error plots were produced by assigning to TØ, T1, T2, T3, and T4 the values required to plot out a circle, and then letting TØ T1, T2, T3, and T4, assume values 0.05 microseconds below, equal to, and above their nominal values. For each of the possible combinations of the slightly different values of TØ, T1, T2, T3, and T4 the computer calculated the corresponding X, Y, and Z, using the hyperbolic solution previously programmed, and produced an LDAR plot showing the central or nominal point, as well as the scatter in X, Y, and Z caused by fluctuations in the input-time values of 0.05 microseconds. Plots were produced for ground-range circles of 5, 10, 20, 40 and 160 miles for a height of 10,000 meters.

The 5, 10, 20, 40 and 160 mile error plots for the primary configuration, Configuration #1, are shown in Figures 13 to 17.

To characterize the scatter in the data we have added the value of the standard deviation σ_R, and have further expressed σ_R as a percentage of the nominal value.

At the five mile range, the range error is small, with a σ_R of 37 meters or 0.46% at 0 degree azimuth.

The 10 mile curve shows an increase in the errors, here σ_R is 192 meters or 1.2%. Note that the size of the error depends on the azimuth, being less around 270 degrees.

The 20, 40, and 160 mile error plots show an increasing error with range. At 160 miles σ_R is 141 km. or 55%. Bear in mind that the extreme values shown in the plots are maxima and minima, and do not represent plus and minus the standard deviation.

The standard deviation is a quantity smaller than the maximum or the minimum. Also note, that because of overlap problems in computer plotting, we have built in a maximum value of 1.1 times the extreme range indicated in the plot. Any data point having a range larger than this will not be plotted at the proper azimuth, but will be plotted at an azimuth of 45 degrees, at a range of 1.3 times the maximum range, that is in the upper right-hand corner of the plot.

Figures 13 to 17 also show the error in the height. The height plots are shown at the left. The upper plot refers to data for azimuth from 270 to 90 degrees, while the lower plot shows height data for azimuth from 90 to 270 degrees. Again the degree of dispersion is expressed by the standard deviation, here σ_Z, which also is expressed as a percentage of the nominal value. As before, note that the extreme values indicated are the

maximum and the minimum values, not plus or minus the standard deviation (a smaller quantity). The scatter in height increases with range and becomes intolerable at a range of 160 miles.

Particularly in Figures 15 to 17 it is clear that the scatter in range is much greater than the scatter in azimuth. Because of this, the data is spread out along the radius vector. This is quite characteristic of the hyperbolic system and can be seen in all the data. Where there are random errors, the data points tend to spread out along the radius.

A more detailed plot of the error in elevation is given in Figures 18 to 22 for ranges of 5, 10, 20, 40, and 160 miles. There is some variation of the elevation error with azimuth. The 40 mile plot, Figure 21, clearly shows the elevation error to be lowest around 60, around 200, and around 330 degrees. The elevation error is unacceptably high at 160 miles. Points below the X-axis indicate that the input time delays are inconsistent with the geometrical assumptions, and hence are not acceptable.

In addition to the primary configuration, which provides a uniform and an acceptable good coverage up to a 20 mile range, other configurations (four at a time) of the five stations are possible, as already shown in Figure 12.

Error plots for Configuration #2, Configuration #3, and Configuration #4 will be shown in turn. We shall see that these configurations do not give uniform error curves, but that these error curves have unacceptably high peaks. Because of the geometry, the errors rise to high levels near critical azimuths. The critical azimuths turn out to be those azimuths for which three stations come close to lying on a line.

The 5, 10, 20, 40, and 160 mile range-azimuth error plots for Configuration #2 are shown in Figures 23 to 27. The smallest range errors are found at azimuths between 240 and 300 degrees. Usable data, however, can be obtained from 40 to 120 degrees and from 220 to 300 degrees.

For 20 miles and beyond, the range errors become unacceptably high over the azimuths between 300 and 40 degrees and between 120 to 220 degrees. As noted earlier, no range data larger than 1.1 times the maximum indicated range are shown because of overlap problems in computer plotting. This gives the range-azimuth plots an artificially smooth outer edge. We have an excellent example of the geometric dilution of precision. Unfavorable geometry (the lining up of the north, the central and the south stations) leads to a severe degration of the accuracy for these azimuths. Note that the most severe scatter occurs along azimuths near base lines that are approximately 180 degrees apart. For Configuration #2 these base lines are 200 and 339 degrees.

The elevation-azimuth error plots for Configuration #2 are shown in Figures 28 to 32. At ranges less than 5 miles the elevation errors are low and the configuration is suitable for use at all azimuths. At the 10 mile range, the 180 degree azimuth must be excluded because of large errors. At the 20 mile range azimuths from150 to 210 and from 320 to 20 must be excluded. At the 160 mile range, the errors in elevation are excessive at all azimuths.

Range-azimuth error plots for Configuration #3 are shown in Figures 33 to 37, and the associated elevation-azimuth error plots are shown in Figures 38 to 42. Similar to Configuration #2, Configuration #3 has regions

of good and bad data.

Range-azimuth error plots for Configuration #4 are shown in Figures 43 to 47, and the corresponding elevation-azimuth error plots are shown in Figures 48 to 52. Again we find regions of low, and regions of unacceptably high errors.

It should be noted that Configuration #2 and Configuration #4 supplement each other, and that they can be combined as shown in Figures 53 and 54 to give acceptable data for all azimuths.

In the operation of the LDAR system, Configuration #1 is used as the primary configuration. Configuration #2 and Configuration #4 are used as backup over the regions indicated in Figures 53 and 54, and are used to check the data obtained from the primary configurations. Where the data does not agree within a prescribed level, the data is rejected.

All the LDAR elevation error plots presented so far have been for an elevation of 10,000 meters. From the GDOP plots for an ideal hyperbolic system (Figures 4 and 6, and 9 and 10) we expect the elevation error plots to show higher errors at elevations below 10,000 meters. This is indeed what we find when we compare the LDAR elevation error plot at 3000 meters elevation, Figure 55, with that at 10,000 meters, Figure 56.

IV. ESTIMATE OF RANDOM AND SYSTEMATIC ERRORS

1. Types of Errors

The discussion of system accuracy conventionally divides errors into two types because their different characteristics and behavior. The first are the bias, or static, errors, also known as the systematic errors. To evaluate these one must have available a more accurate system to use as a reference, or to have available, a number of fixed, known, data points. Generally the bias errors are sufficiently stable that they can be removed by calibration. The second are the random errors.

Random errors are unpredictable perturbations that can only be defined in statistical terms, such as the mean and the standard deviation. For example, if the data has a standard deviation of sigma σ, for a normal distribution we can expect that 68% of all the data points will lie within plus or minus one σ of the mean, and 95% of the data points will lie within plus or minus two σ of the mean. The standard deviation is a measure of the dispersion of the data.

The random error of the LDAR system can be determined from the scatter of the data points in LDAR's forty-mile track of a jet plane, and from the scatter of the data in LDAR's measurement of two, fixed lightning simulators.

The bias, or static error of the system can be estimated from LDAR's measurement of the position of known, fixed, lightning simulators.

We shall treat the two types of errors separately, but first we will say a few words about the sources of the errors.

2. Source of Errors

Errors arise in the quantizing of the input signal inherent in converting the analogue signal to a digital signal, in the changes in the

time of transmission time from the outlying sites, from noise at low signal levels, and finally from the use of too restricted a bandwidth.

a. Quantizing Errors

The quantizing errors have a maximum value of ± 0.025 microseconds. They will be shown to be the primary errors, and will be discussed further in the report.

b. Speed of Propagation

While the speed of propagation is constant in vacuum, in air it varies with the index of refraction. Further the path of an electromagnetic wave in air is not a straight line, but somewhat longer, since the path is curved, depending on the change in the index of refraction along the path. The magnitude of the refactive errors has been discussed in detail by Crane[5]. Crane's assessment of the maximum difference in the transmission to two separate stations is of particular interest to us. For a baseline of 30 km, Crane gives this maximum difference as 0.3 meters. Our baseline is considerably smaller, (8 km), so that we should expect errors smaller than 0.3 meters or 0.001 microseconds.

c. Transmission Line Delays

Fixed delays in transmission along wide band lines used to carry the LDAR signal from the outlying stations can be calibrated out. Changes in delays due to temperature changes or to malfunctions in distribution amplifiers can cause problems. No statistical data is available here. Changes in delays due to malfunctioning amplifiers would show up in our daily calibration against the fixed lightning simulators. It is recommended that in the future, periodic measurements of the delays of the wide-

band lines be made so that we will be able to assess the size of these random errors for inclusion in our error budget.

d. Noise

At low signal levels, noise will alter the waveshape of the signal. This will lead to errors in the determination of the exact time of arrival. Safeguards against these errors are built into the LDAR system, in that the computer checks the signal strength level to assure that its level is above 75 signal strength units before accepting any data. A level of 75 signal strength units corresponds to a signal to noise ratio of at least 10 db, thereby setting a threshold 10 db for the lowest acceptable S/N ratio.

In routine operation of the LDAR system, the signal level is not recorded. This is a limitation in the determination of the accuracy of a particular measurement. It is recommended that the signal strength be routinely recorded, so that S/N ratio can be coupled with the test data, permitting a meaningful assessment of the accuracy of the test.

Poor signal to noise ratios can degrade the accuracy of the data. Fortunately the computer signal checks prevented the use of low S/N ratio data. Further, it is fortunate that lightning supplies a very strong signal, expecially for storms less than 40 miles away.

e. Bandwidth Limitations

Bandwidth limits the fidelity of the pulse that can be transmitted. The limiting bandwidth is the 5 MHz video cable that links two of the remote sites to the central station.

With a 5 MHz bandwidth, the video cable is capable of transmitting

a 0.2 microsecond pulse. Bandwidth, of course limits the rise time of an output pulse. With a bandwidth of 5 MHz, the output pulse cannot rise faster than $0.5/(5X10^6)$ seconds, or 0.1 microseconds, regardless of how fast the input pulse rises.

Pulses having a rise time longer than several times 0.1 microsecond would be reproduced faithfully. Here limiting bandwidth should not be a problem.

Pulses rising faster than 0.1 microsecond would all appear to have a limiting risetime of 0.1 microsecond, or two 0.05 microsecond sampling intervals.

As Lewis[6] points out, while it might appear that a bandwidth of 1 MHz would be required to made a time-difference measurement to one microsecond, this is not the case. In principle two narrow band impulses can be matched to any desired degree of accuracy, provided that they are identical and that there is sufficient structural detail in the pulses to permit recognition of the corresponding cycles. Correlation of the two waveforms would be the ultimate technique for determining the time shift. In our case, since we are using a reasonably wide bandwidth, the search for the highest peak in the waveform seems adequate. Certainly the analysis of the errors contained in this report do not indicate any errors that begin to compare with the quantizing errors, which are the principal errors.

3. Random Errors

a. Airplane Track

On August 18, 1976, LDAR tracked a jet plane flying at a nominal

altitude of 29,000 feet, on a heading of 350 degrees, for some 40 miles. The LDAR plot of the plane track is shown in Figure 57. The LDAR plot shows the plane flying on a heading of 350 degrees, at an altitude of 30,000 feet. Calculations from the time and position given by the LDAR data, showed the average speed to be 447 knots. As pointed out before, the lower "elevation plot" shows the height of all data points having an azimuth from 90 to 270 degrees, i.e. from the southern hemisphere. The upper "elevation plot" shows the height of all data points having an azimuth between 270 and 90 degrees (the northern hemisphere). Both elevation plots show the elevation to be approximately 30,000 feet.

The plane was picked up at a point some 30 miles in the southwest. Track was lost in the northwest, at a range of some 30 miles. Some scatter in range and in elevation is apparent, with greater scatter being evident in the elevation.

Conversations with the Patrick Air Force Base office of the Federal Aircraft Administration identified the plane as a C-140 jet, SAM-12493, flying at a nominal speed of 450 knots, at a nominal altitude of 29,000 feet, on a course from Fort Lauderdale to Andrews Air Force Base. The LDAR data indicates the average speed to be 447 knots, and gives 29,740 feet as the mean altitude.

It is not quite clear why this plane should have been tracked by the LDAR system. In twelve months of LDAR operation, only one other plane was tracked. To be tracked by the LDAR system the plane either must have emitted a strong radiation in the 30 to 50 MHz band having a sharp, peaked envelope, similar to the radiation from a lightning pulse, or must have reflected lightning signals from lightning that the LDAR plot shown to be

present in the west at the time.

An enlarged portion of the track is reproduced in Figure 58, together with a least-squares line fitting the data points. Of primary interest is the scatter in the LDAR data, since this is a measure of the random error of the system.

A standard deviation σ_R in range of 255 meters is shown in the upper portion of the track. This is a measure of the random tracking error of the LDAR system, in range, at this azimuth and elevation.

In Table I we show the X, Y, Z position of the plane, as measured by LDAR, for various points along the plane's track, including a point near the beginning, and a point near the end of the track. Also shown is the standard deviation of the LDAR data as calculated by the variate difference method, Reference (4), for twenty one data points.

As should be expected from the GDOP plots already presented, the data dispersion increases with range, being the largest at the greatest range. Here we note the standard deviation σ_R to have a value of 242 meters (or 0.7%) at a ground range of 30.6 km, and to increase to 736 meters (or 1.8%) at a range of 40.4 km.

The standard deviation σ_Z of the elevation measurement Z is 202 meters or 2.2%. The percentage error in elevation is obviously greater than that in range, a characteristic of hyperbolic systems that we have already pointed to and illustrated our discussion of the GDOPs.

Also shown in Table I are the standard deviations σ_R of the dispersions in ground range and the standard deviations σ_Z of the dispersions in elevation calculated on an assumed $\pm$ 0.05 microsecond quantizing error in the times of arrival TØ, T1, T2, T3, and T4.

TABLE I. PLANE TRACK, COMPARISON OF MEASURED AND CALCULATED DISPERSIONS

	Position, Meters			Dispersions, Meters		Ground Range, km
	X	Y	Z	σ_R	σ_Z	
Measured (LDAR)	-25,847	-24,744	8932	473	230	35.78
Calculated * (for ± 0.05 μs)	...	...	...	1271	449	
Measured (LDAR)	-30,406	-3,151	9045	242	202	30.57
Calculated	...	...	...	495	451	
Measured (LDAR)	-33,114	13,322	9152	256	170	35.69
Calculated	...	...	...	708	441	
Measured (LDAR)	-33,400	22,789	9132	736	248	10.4
Calculated	...	...	...	1038	403	

* Calculated from error model assuming an uncertainty of ± 0.05 microseconds in TØ, T1, T2, T3, and T4.

It is significant to note that the standard deviations calculated on an assumed $\pm$ 0.05 microsecond uncertainty in the times of arrival are at least two times as large as the standard deviations in the LDAR measurement. For example, at the start of the track at a range of 35.8 km, the standard deviation in the measured data is 473 meters in range and 230 meters in elevation. The standard deviation calculated on an assumed $\pm$ 0.05 microsecond uncertainty are 1271 and 449 meters, respectively, that is over two times as large. For the next data point shown in the table (that of closest approach, 30.6 km), the LDAR dispersions in the measured data show a standard deviation σ_R of 242 meters in range and 202 meters in altitude. The calculated values are 495 and 451 meters, respectively. Again, over two times as large.

Similar observations were made in the measurements of the fixed lightning calibrators. Let us proceed to discuss the lightning simulator data. With this additional data in mind, we shall return to a discussion of the significance of the observation that the dispersions calculated for an assumed $\pm$ 0.05 microsecond uncertainty in the measured times of arrival, are approximately two times those measured by the LDAR system.

b. Fixed Lightning Simulators

Periodic measurements of the position of two lightning simulators, not only provides an overall calibration for the system, but also provides us with information as to the dispersion and as to the bias in the LDAR data.

In Table II we present a summary of data that was taken of the position measurement of the VAB and of the CIF lightning simulators. The VAB simulator is located on top of the Vertical Assembly Building at an azimuth of 354.7 degrees, 5.011 km to the north. The CIF lightning

TABLE II. SUMMARY OF THE POSITION AND DISPERSION MEASURED BY LDAR, AND THE DISPERSION IN POSITION CALCULATED FROM ERROR MODELS FOR THE POSITION OF THE VAB AND THE CIF LIGHTNING SIMULATORS

		Position, Meters		Dispersions, Meters	
		X	Y	σ_X	σ_Y
VAB Lightning Simulator	Measured (LDAR)	-475.5	+5090.9	6.7	4.5
	Calculated *	...	...	11.5	9.1
	Actual	-474.08	+5088.88	...	...
	Bias	-1.4	+2	...	...
CIF Lightning Simulator	Measured (LDAR	340.9	-113.7	6.6	7.9
	Calculated *	...	...	11.9	9.4
	Actual	351.9	-113.7	...	...
	Bias	-11	+4	...	...

* Calculated from an error model, assuming an uncertainty of ± 0.05 microseconds in the measurement of the times of arrival of TØ, T1, T2, T3, and T4.

simulator is located at an azimuth of 107.9 degrees 369.8 meters to the east.

Also shown in Table II is the actual position of the lightning simulators, as determined by survey.

Of particular interest is the comparison of the standard deviation of the dispersions in the LDAR measurement with the standard deviation of the dispersions calculated from an error model which assumes an uncertainty of $\pm$ 0.05 microseconds in the times of arrival TØ, T1, T2, T3, and T4. The VAB position data was based on over 160 measurements. It shows a standard deviation σ_X of the data dispersions in X of 6.7 meters, and σ_Y in Y of 4.5 meters. The calculated standard deviations of the dispersions, based on an error model that assumes an uncertainty of $\pm$ 0.05 microseconds in the times of arrival, are 11.5 for σ_X and 9.1 for σ_Y. As before the ratio of the calculated dispersions (based on $\pm$ 0.05 microseconds) to the dispersions in the measurement data is approximately 2 to 1.

Data for the CIF lightning simulator gives ratios of 1.8 to 1 and 1.2 to 1. The smaller ratios observed here are ascribed to the limited sample size (less than 12) of the data.

A typical series of measurements in units of 0.05 microseconds is shown in Table III. The readings can be seen to fluctuate in unit steps (that is in units of 0.05 microseconds).

4. Systematic Errors

In order to obtain a reliable estimate of the systematic errors, one must have available data from a more accurate system to use as a reference, or to have available, over the range of measurement, a number of fixed, known data points.

TABLE III. TYPICAL SERIES OF DIGITIZED TIME-OF-ARRIVAL READINGS FOR THE VAB LIGHTNING SIMULATOR, ILLUSTRATING QUANTIZING FLUCTUATIONS (IN UNITS OF 0.05 MICROSECONDS)

T0	T1	T2	T3	T4
1058	29	466	313	202
1059	30	466	312	203
1058	29	467	314	202
1059	29	466	312	202
1059	29	467	314	203
1058	30	466	314	203
1059	30	466	312	203
1058	30	467	312	203
1059	30	466	313	202
1059	29	466	313	202
1058	29	466	312	202
1059	29	466	314	202
1058	29	467	314	202
1057	29	468	313	202
1058	30	467	313	203
1057	31	467	313	203

Since LDAR is unique there is no other system, much less a more accurate system to locate the position of electrical discharges in the sky.

An ideal way to evaluate the systematic errors would be to fly a lightning simulator through the LDAR tracking area, providing an accurate measure of position with a tracking radar. This is not impossible and is under consideration. The airplane track referred to earlier would have supplied the necessary estimate, if a tracking radar's track of the plane's position along its course had been available. The airplane track did, however, provide us with data for an estimate of the bias in the elevation measurement. The elevation measured in the airplane, and reported to us was 29,000 feet or 8839 meters. The elevation measured by LDAR was 9065 meters. This gives us an estimate for the bias error in elevation of + 226 meters.

Limited data on the systematic error of the LDAR system is available in LDAR's measurement of the position of two lightning simulators, whose position is accurately known. Using this limited data for an approximate estimate of the systematic error we find that the estimate of the systematic error in X to be the average of -1.4 and -11 or -6.2 meters, and we find the estimate of the systematic error in Y to be the average of +2 and +4 or +3 meters. Of course, many more known data points would be required to make the estimate of the systematic error meaningful.

Errors in the measurement of the elevation at the VAB site are too large to make any estimate of the systematic error in elevation, because of the large errors in elevation that occur at a range of 5,000 meters for elevations less than 200 meters (see Figure 4).

5. Discussion of Errors

Comparison of the dispersions in the experimental data with the dispersions calculated assuming a ± 0.05 microsecond error in the times of arrival TØ, T1, T2, T3, and T4 have shown that the dispersions calculated for an assumed error of ± 0.05 microseconds to be about two times the experimentally observed dispersions.

A closer examination* of the quantizing error that occurs in converting the analogue to a digital signal explains the discrepancy and leads to the conclusion that the quantizing error in the determination of the times of arrival TØ, T1, T2, T3, and T4 is not ± 0.05 microseconds but ± 0.025 microseconds.

Since the error plots of Figures 13 to 56 were based on an assumed quantizing error of ± 0.05 microseconds, the errors shown in these plots should be interpreted as being 1/2 of the values shown.

The GDOP plots of Figures 3 to 10 do not need re-interpretation. They are parametric in nature, and therefore apply equally well to any given basic measurement uncertainty, du. The basic measurement uncertainty used in the overlays to the parametric plots of Figure 3 to 10, is 0.02 microseconds** (equivalent to 6 meters).

---

* The Biomation units that convert the incoming analogue signals to a digital signals utilized a clock which counts in increments of 0.05 microseconds. An event that occurs after nx(0.05) microseconds is assigned a value of n time units. The same value is assigned to all events lying between nx(0.05) and (n+1)x(0.05) microseconds. Hence sampling results in an offset or bias error of 0.025 microseconds with a uniform probability distribution lying between -0.025 and +0.025 microseconds, that is a peak sampling error of +0.025 microseconds.

** To arrive at the measurement uncertainty to be used with the GDOP curves we must take the difference between two station measurements. In taking the difference, the bias error of 0.025 microseconds will cancel out, and we are left with a triangular probability distribution with a peak probability at zero microseconds and a zero probability at ± 0.05 microseconds. The calculated standard deviation for such a probability distribution is 0.02 microseconds (equivalent to 6 meters), which is the value for the basic measurement uncertainty that is used in the overlays for the GDOP plots.

V. CONCLUSIONS

1. The best accuracy of the LDAR system is obtained at points within the baseline of the system, i.e. within 5 miles. Acceptably good data can be obtained out to four baseline lengths, that is out to 20 miles.

2. The most accurate data available from the LDAR system is azimuth, the least accurate is elevation, especially at low elevations.

3. For a hyperbolic system, the accuracy of low elevation data improves the shorter the baseline. The accuracy of long range data improves the longer the baseline. The baseline length actually used must be a compromise between these conflicting requirements. The length of the baseline used in LDAR reflects the need for good range data out to ten miles, and thereby sacrifices accuracy in elevation at low elevations.

4. The primary LDAR configuration comes close to the accuracy available for an ideal hyperbolic system, because the stations approximate the equidistant, and the 120 degree separation requirements. The other three configurations of the LDAR system fall considerably short of the accuracies available from an ideal hyperbolic system.

5. The need for an improvement in the accuracy of the elevation data is obvious. It is recommended that this be achieved through the use of an additional, vertical leg, that would provide time-of-arrival data.

VI. REFERENCES

1. Lennon, C. L., "LDAR - A Lightning Detection and Ranging System", Minutes of the Frequency Management Group, Range Commanders Council, 7-9 October, 1975, Washington, D.C., Published by the Secretariat, Range Commanders Council, White Sands Missile Range, New Mexico, 99002, Pages R1-R25.

2. Lennon, C. L, "The Performance of a Real-Time, Time-of-Arrival Lightning Location System (LDAR)", Presented at the 1976 Fall Annual Meeting, American Geophysical Union, December 6-10. Abstract appears in EOS, Transactions, American Geophysical Union, Vol. 57, No. 12, December 1976. Full paper available from NASA, IN-TEL-32, Kennedy Space Center, Florida, 32899.

3. Holmes, T. G. and Reedy, P.H., "Geometrical Dilution of Precision", Air Force Technical Report Number 21, 12 April 1951. Air Force Missile Test Center, Patrick Air Force Base, Florida.

4. Morse, A. P., "The Estimate of Dispersion from Differences" BRL Report No. 557, 13 July 1945, Ballistics Research Laboratories, Aberdeen Proving Ground, Maryland.

5. Crane, R. K., "Estimates of Errors in Mistram Due to Tropospheric Refraction", Technical Documentary Report No. ESD-TDR-63-158, TM-3422, May 1963, Contract AF33(600)-39852 Project 701, The Mitre Corp., Bedford, Massachussetts.

6. Lewis, E. A., Harvey, R. B., and Rasmussen, J. E., "Hyperbolic Direction Finding with Sferics of Transatlantic Origin", Journal of Geophysical Research, Vol. 65, No. 7, pp. 1879-1905, July 1960.

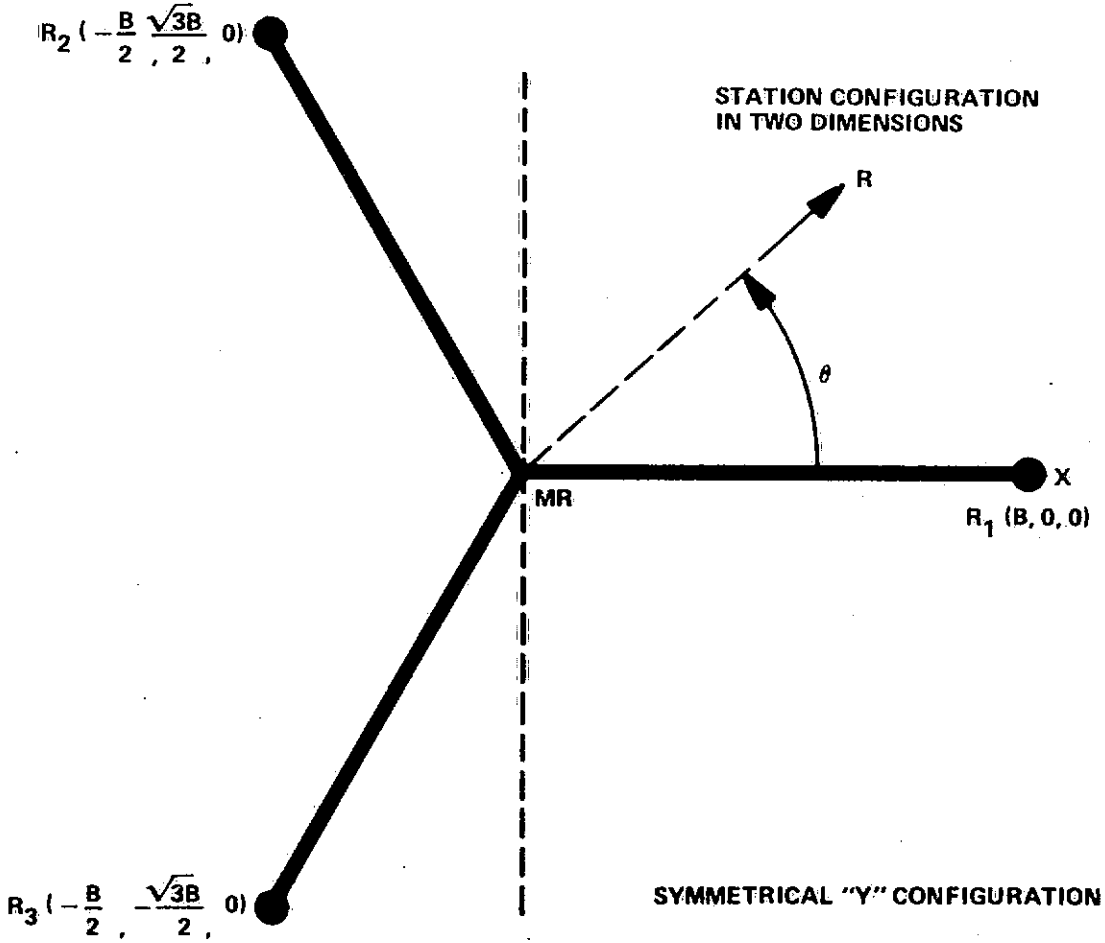

Figure 1. Ideal Hyperbolic System, Y-Configuration (Adapted from Holmes & Reedy, Ref. 3)

FIG. 2 COORDINATE SYSTEM (ADAPTED FROM HOLMES & REEDY, REF. 3)

Three Dimensional Hyperbolic System

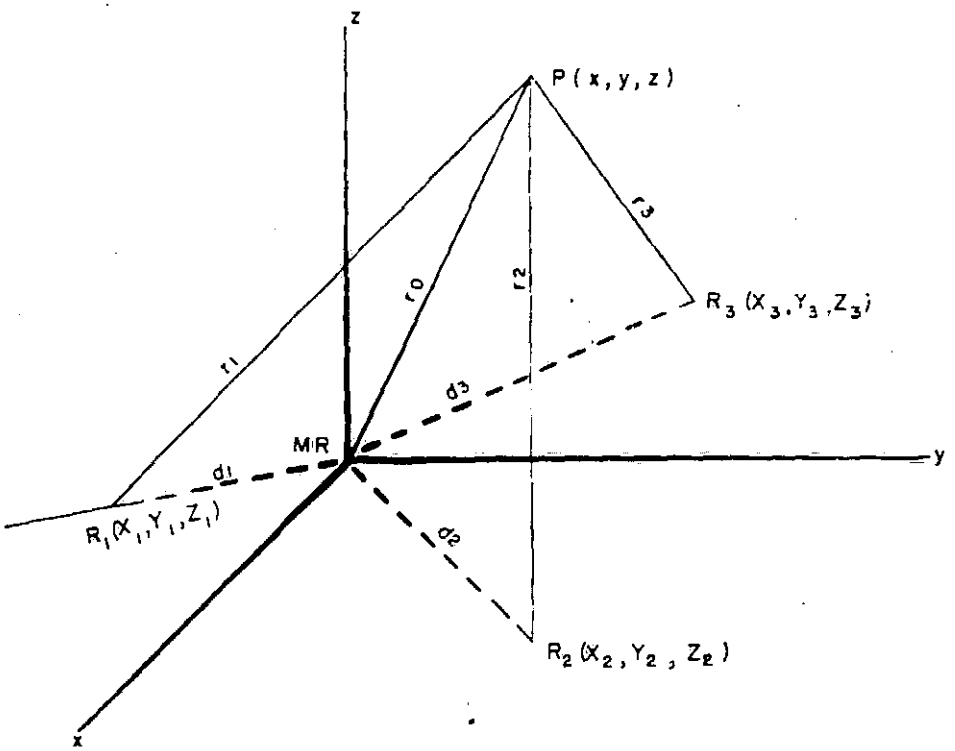

Measured Parameters

$u_1 = r_0 - r_1$

$u_2 = r_0 - r_2$

$u_3 = r_0 - r_3$

MR = Master Receiver

FIG. 3 GDOP PLOT - DILUTION IN X COORDINATE 30 DEGREES
(ADAPTED FROM HOLMES AND REEDY, REF. 3)

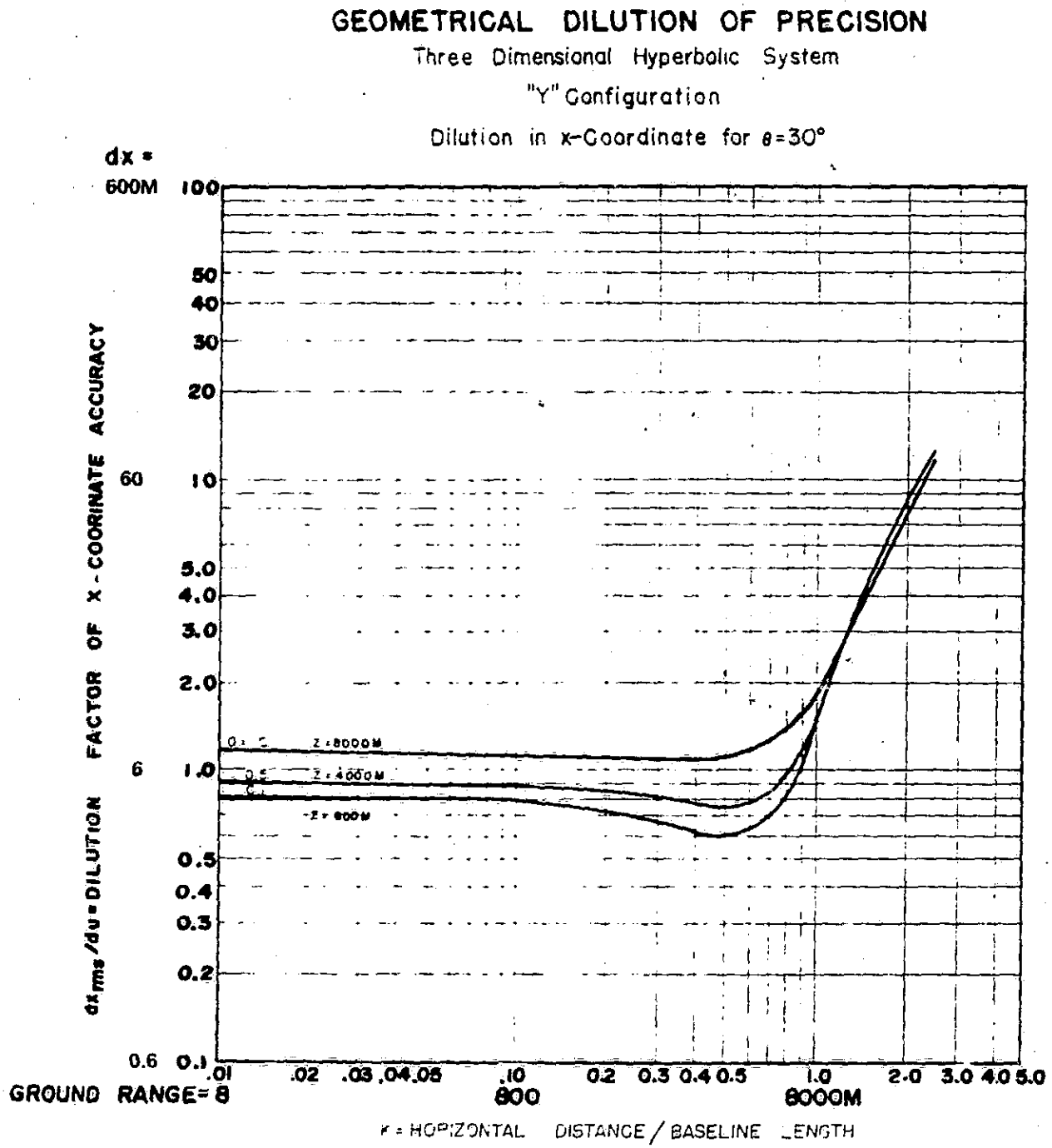

FIG. 4 GDOP Plot - Dilution In Z Coordinate 30 Degrees (ADAPTED FROM HOLMES & REEDY, REF. 3

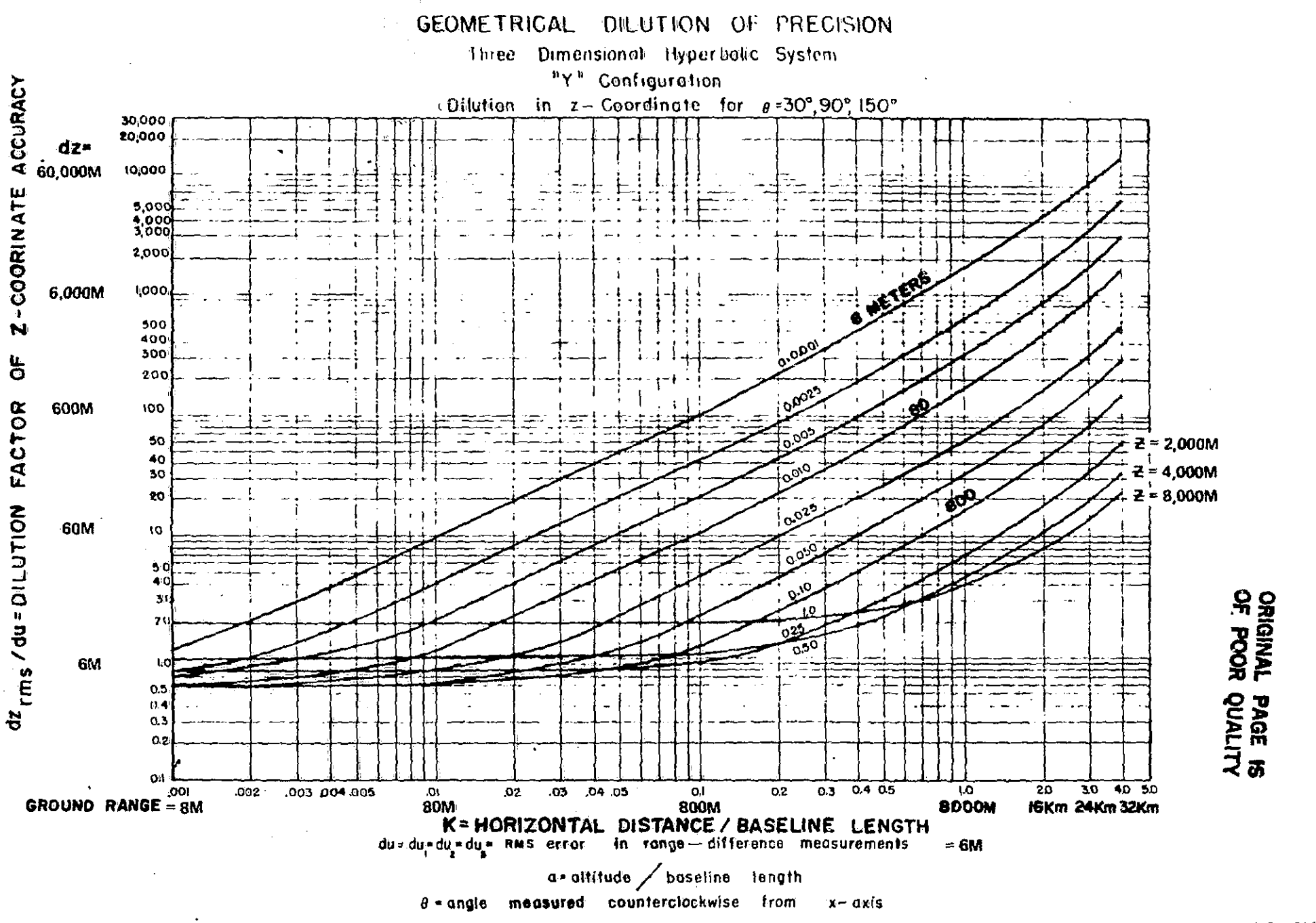

ORIGINAL PAGE IS
OF POOR QUALITY

FIG. 5 GDOP PLOT - DILUTION IN X COORDINATE, 120 DEGREES
(ADAPTED FROM HOLMES AND REEDY, REF. 3)

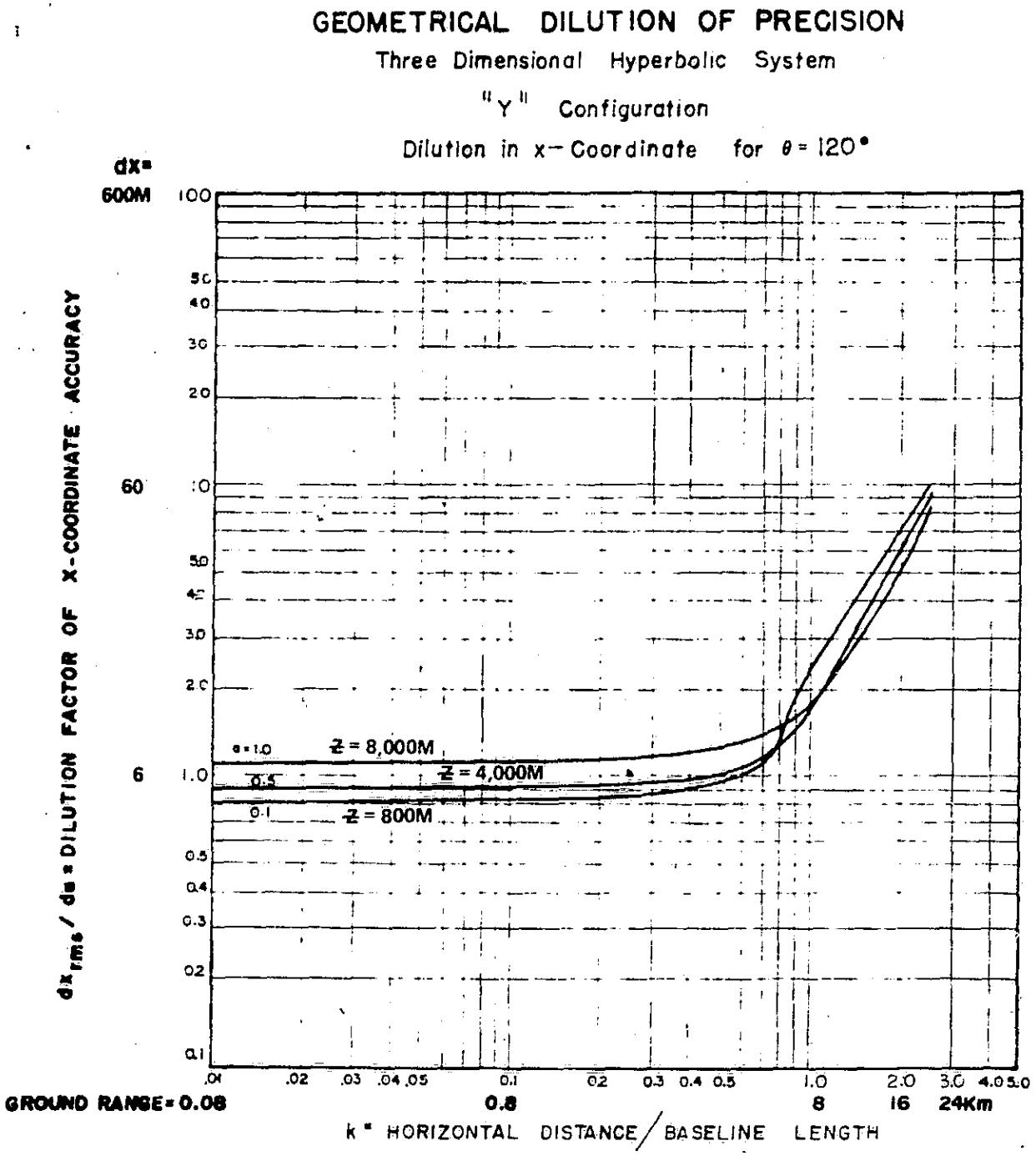

du = du_1 = du_2 = du_3 = RMS error in range-difference measurements
a = altitude / baseline length
θ = angle measured counterclockwise from x-axis

du = 6M

FIG. 6 GDOP PLOT - DILUTION IN Z COORDINATE; 120 DEGREES
(ADAPTED FROM HOLMES AND REEDY, REF. 3)

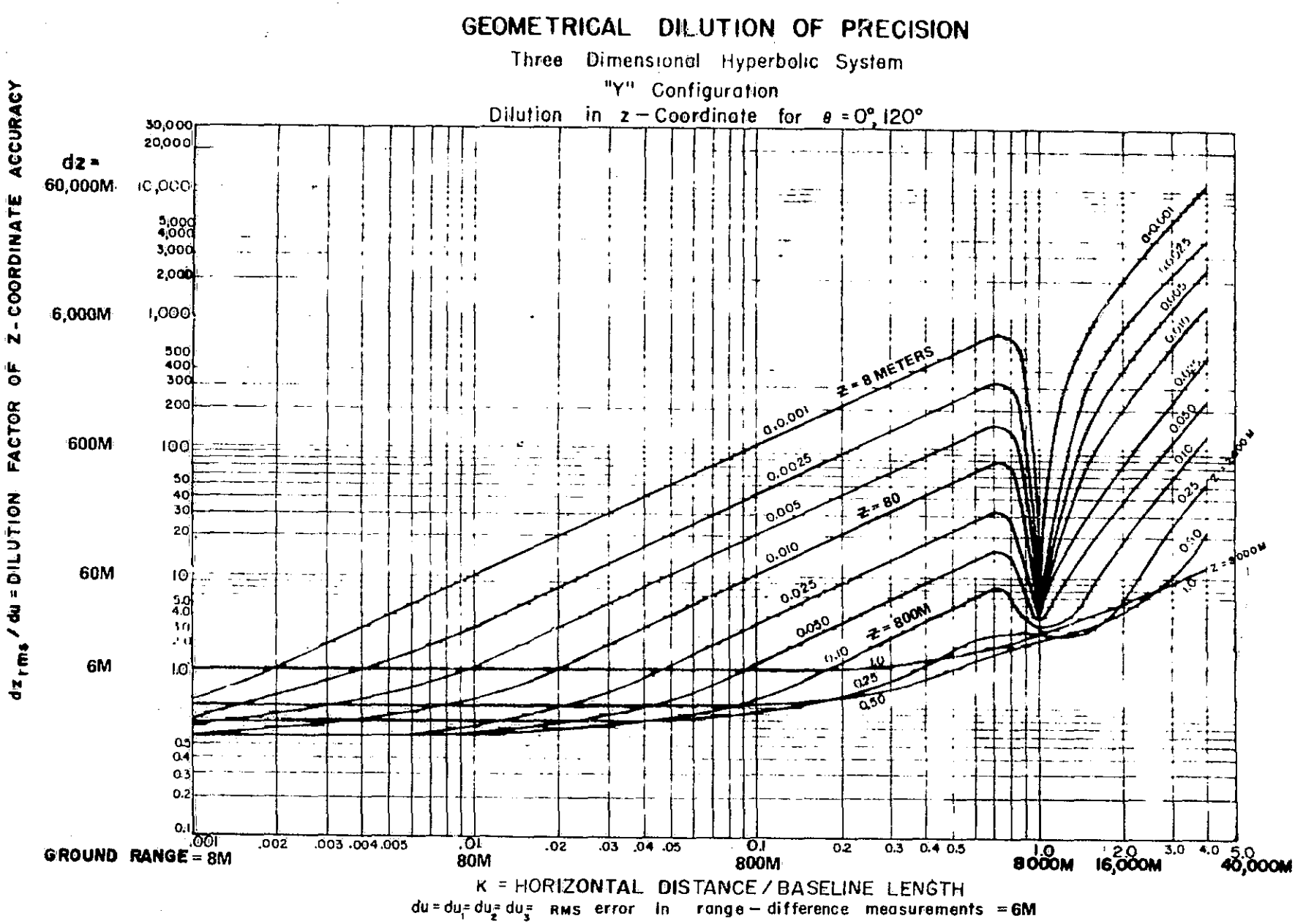

FIG. 7 CONTOUR OF CONSTANT DILUTION, (dx/du), 800 M (ADAPTED FROM HOLMES AND REEDY, REF. 3)

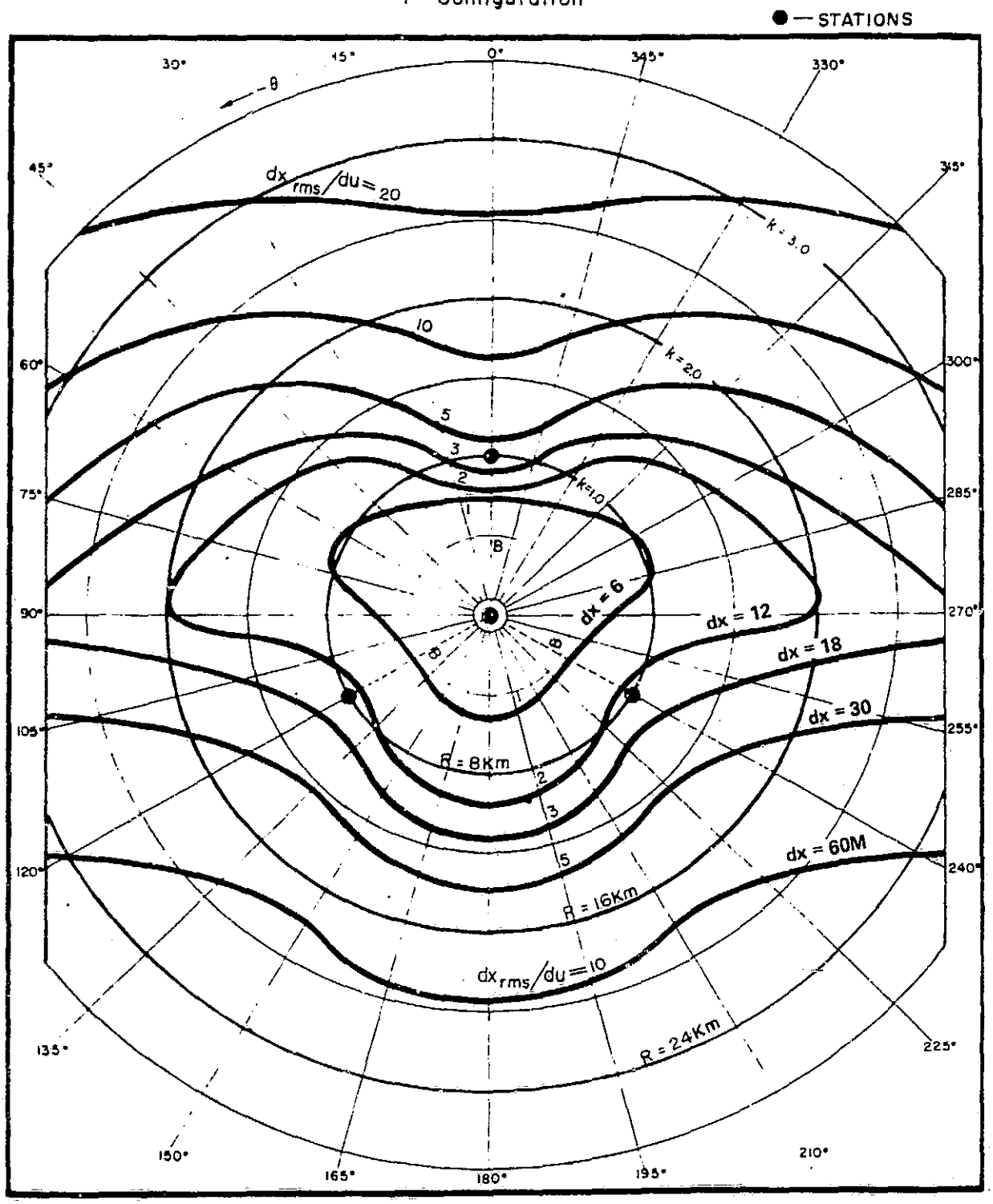

CONTOURS OF CONSTANT-DILUTION FACTOR

dx_{rms}/du for a = 0.1, R = GROUND RANGE

Z = 800 M

du = 6M

FIG. 8 CONTOUR OF CONSTANT DILTION, (dx/du), 80000 M (ADAPTED FROM HOLMES AND REEDY, REF. 1)

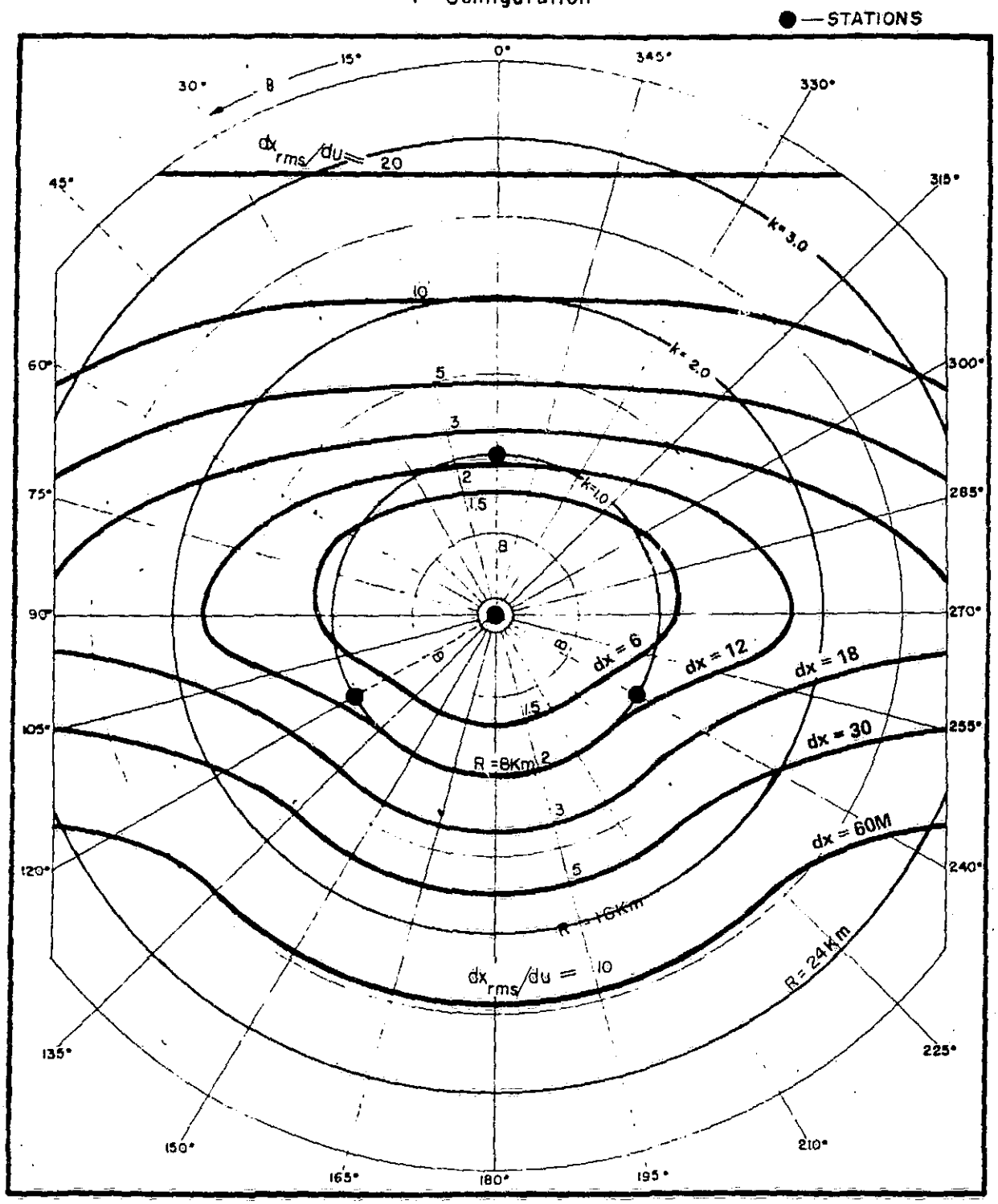

CONTOURS OF CONSTANT-DILUTION FACTOR

dx_{rms}/du for $a = 1.0$, R = GROUND RANGE

Z = 8000 M

du = 6M

FIG. 9 CONTOUR OF CONSTANT DILUTION(dz/du),800 M (ADAPTED FROM HOLMES AND REEDY, REF. 3)

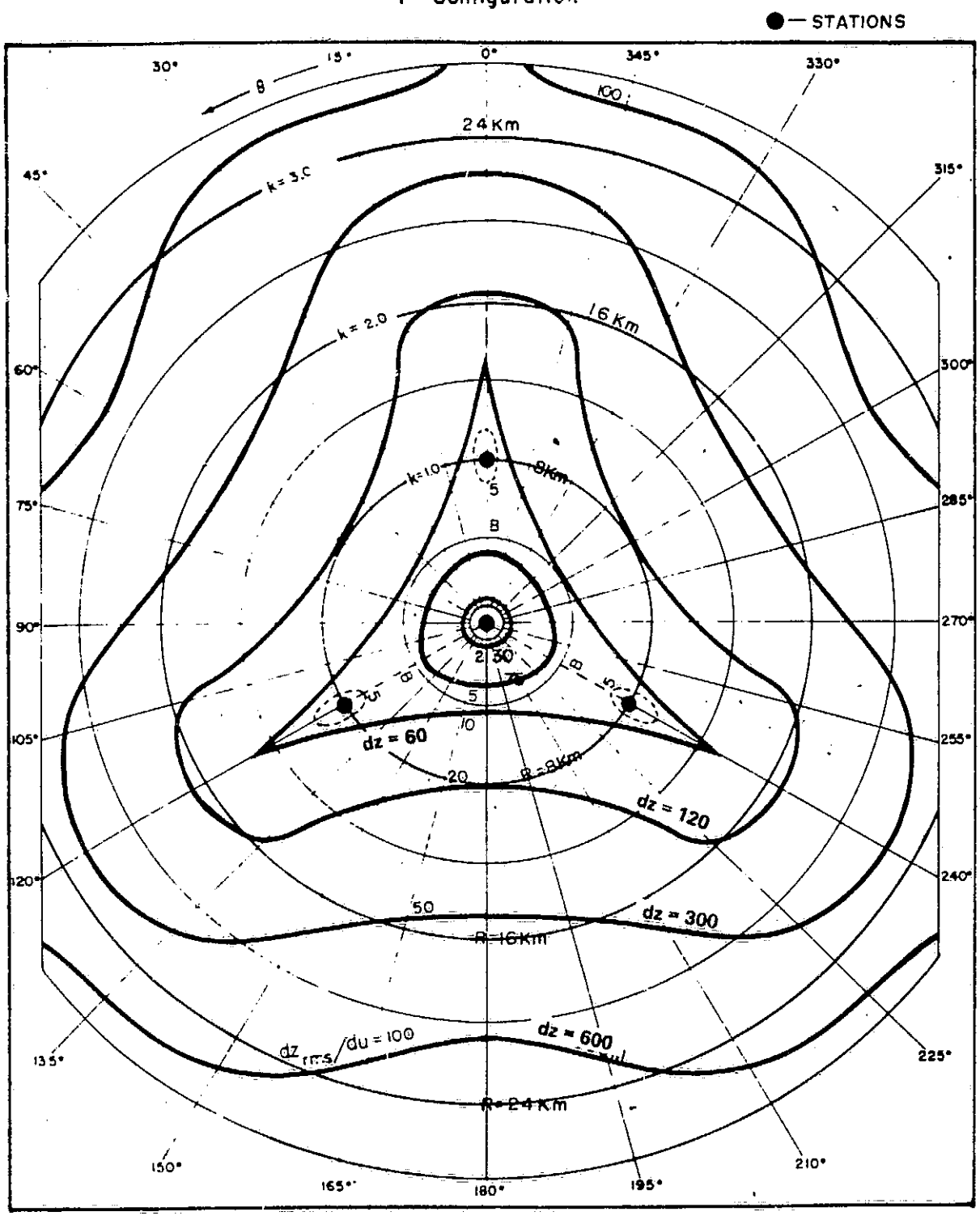

CONTOURS OF CONSTANT-DILUTION FACTOR

dz_{rms}/du for $\sigma = 0.1$, R=GROUND RANGE

Z = 800M

du = 6M

FIG. 10 CONTOUR OF CONSTANT DILUTION, (dz/du), 8000 M (ADAPTED FROM HOLMES AND REEDY, REF. 3)

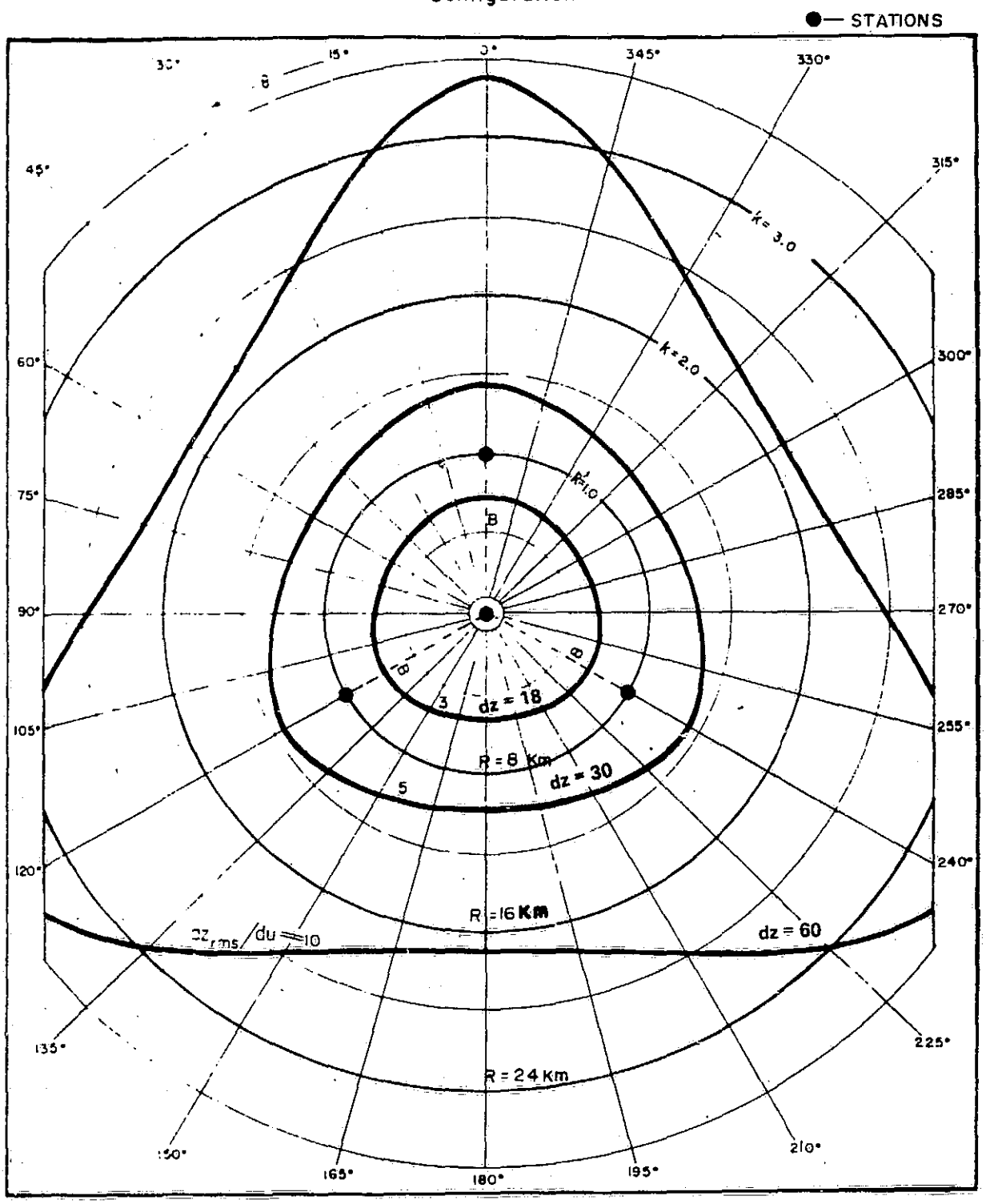

CONTOURS OF CONSTANT-DILUTION FACTOR

dz_{rms}/du for $a = 1.0$, R = GROUND RANGE

Z = 8000 M

du = 6M

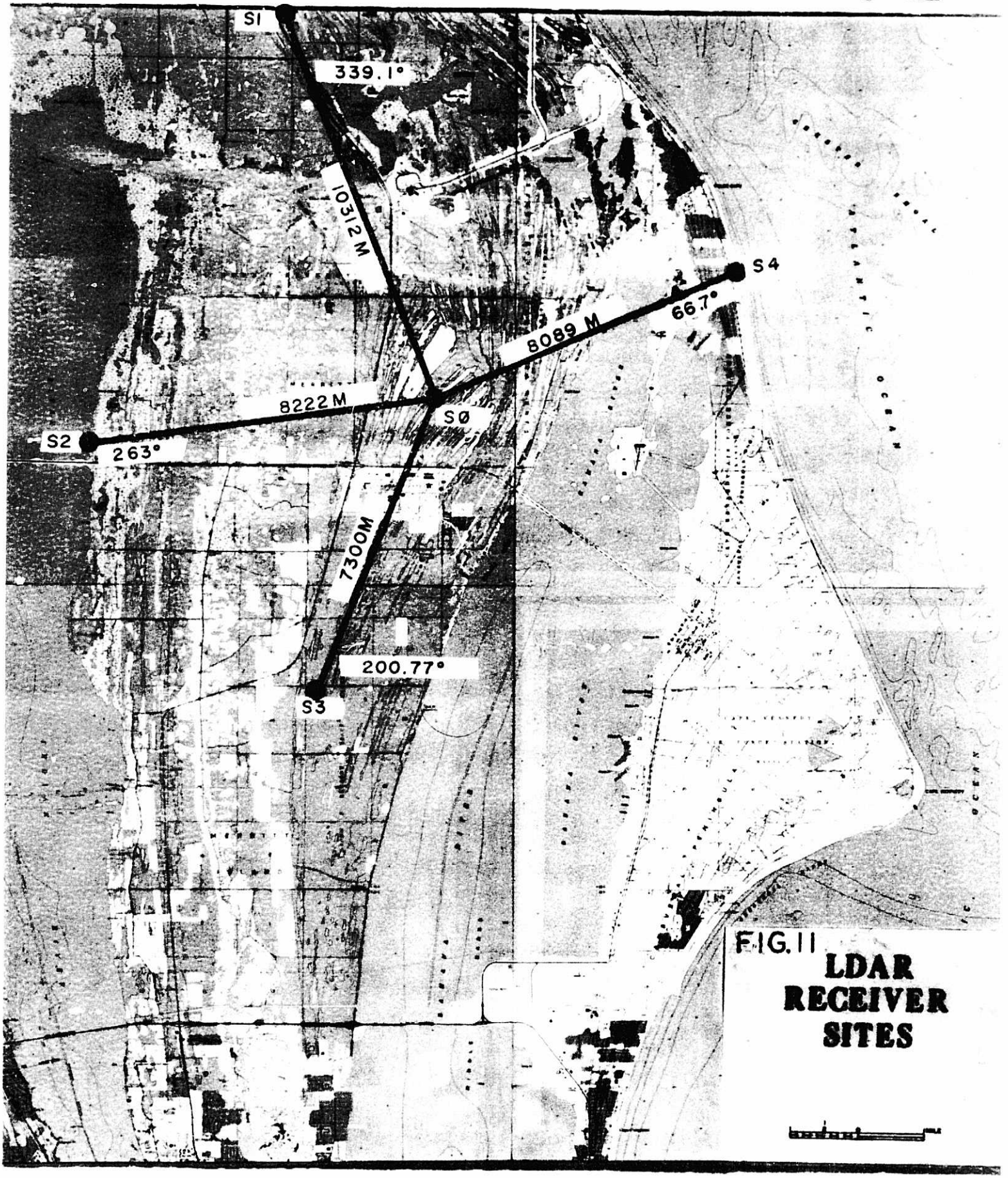

FIG. 11

LDAR RECEIVER SITES

FIG. 12 THE FOUR LDAR CONFIGURATIONS

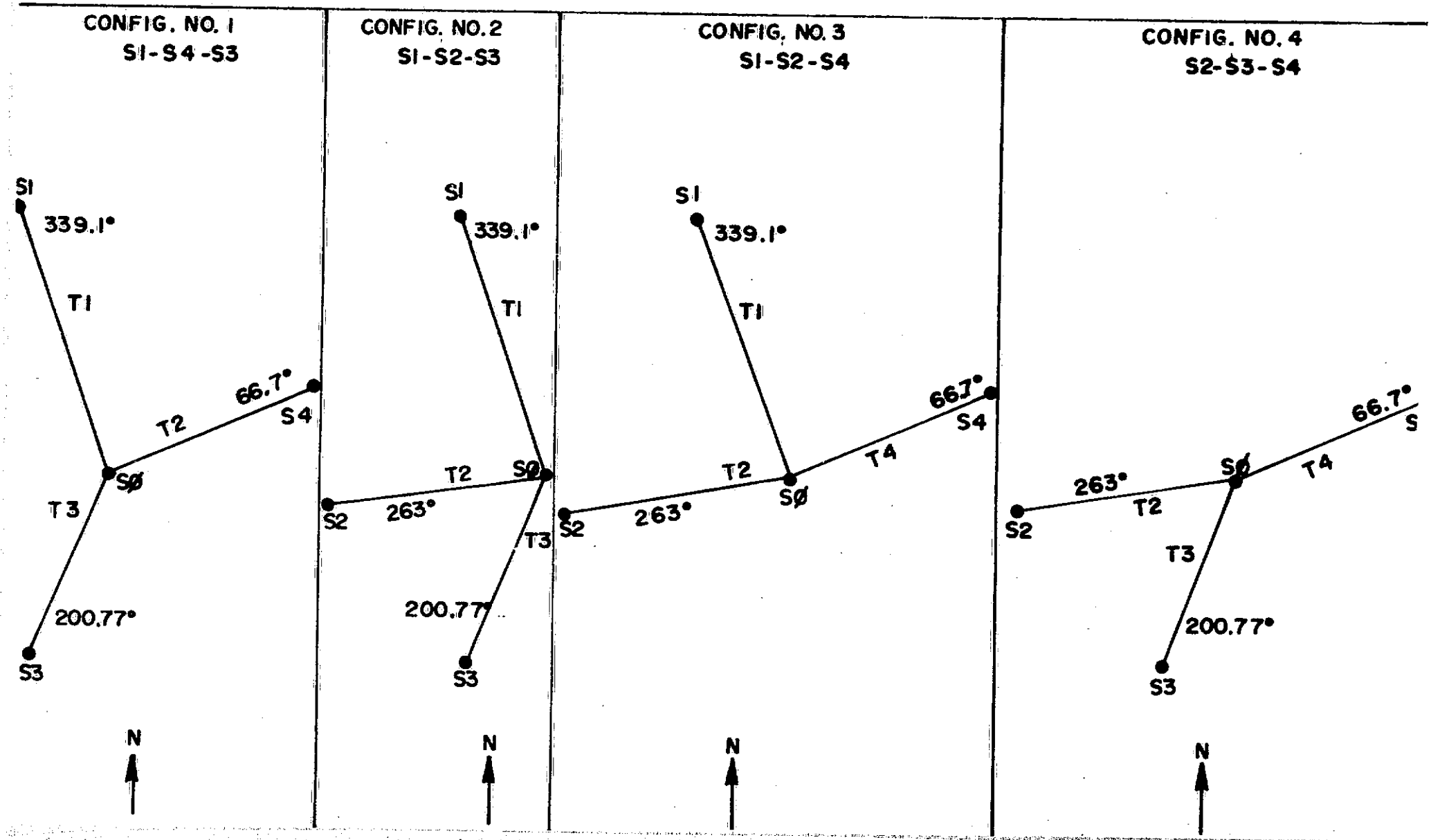

FIG. 13 RANGE-AZIMUTH ERROR PLOT, CONFIGURATION NO. 1, 5 MILES

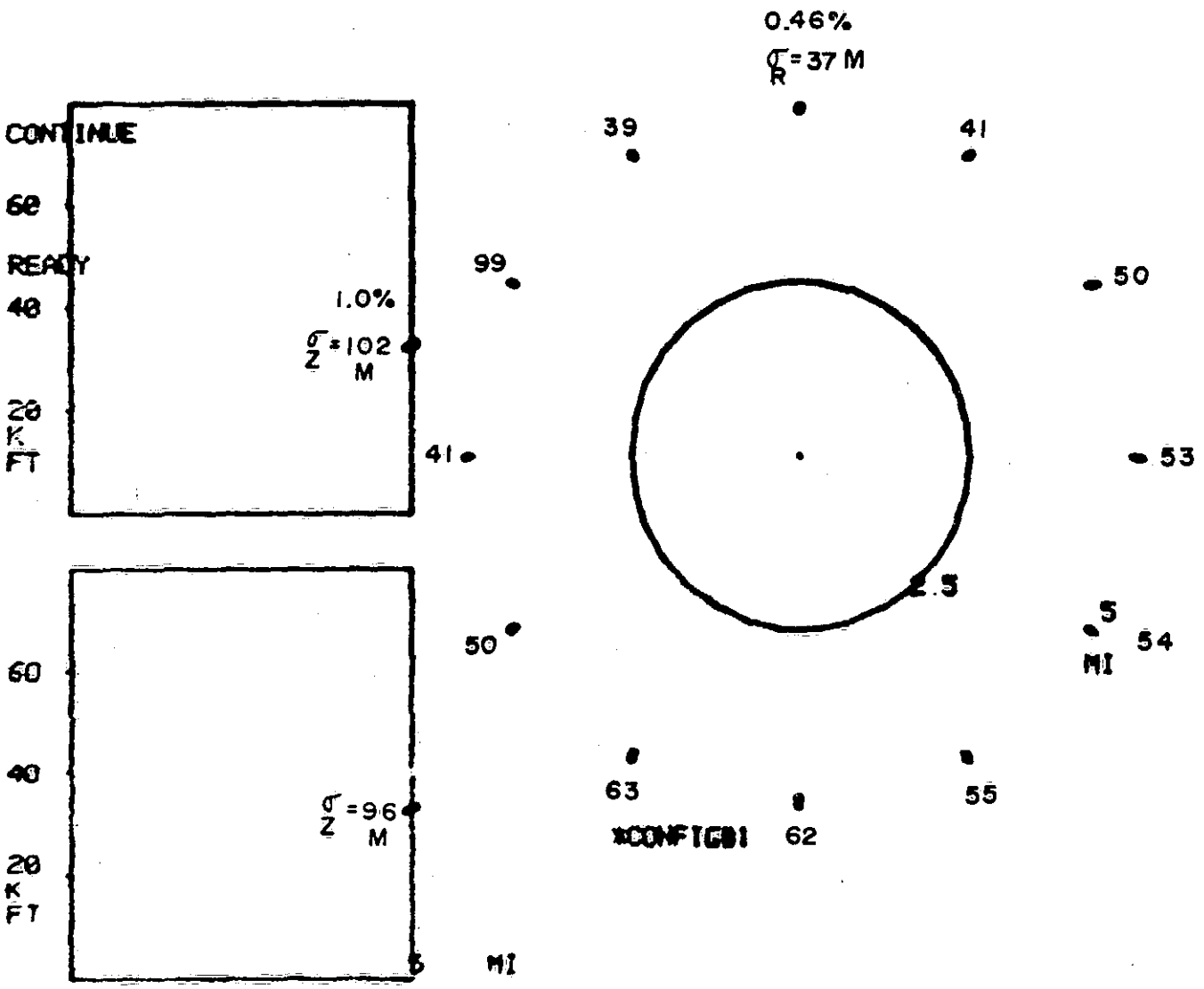

FIG. 14 RANGE-AZIMUTH ERROR PLOT, CONFIGURATION NO. 1, 10 MILES

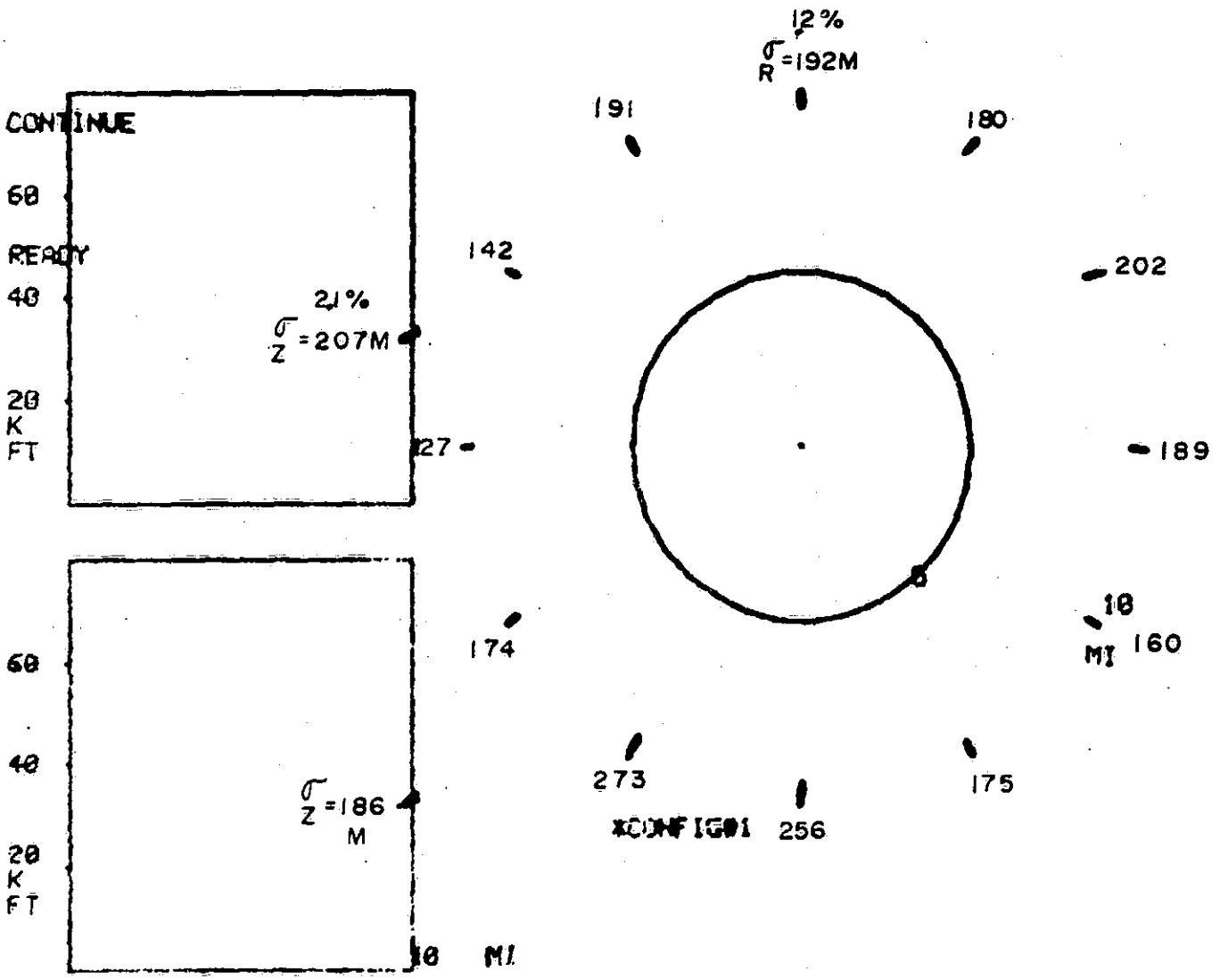

FIG. 15 RANGE-AZIMUTH ERROR PLOT, CONFIGURATION NO. 1, 20 MILES

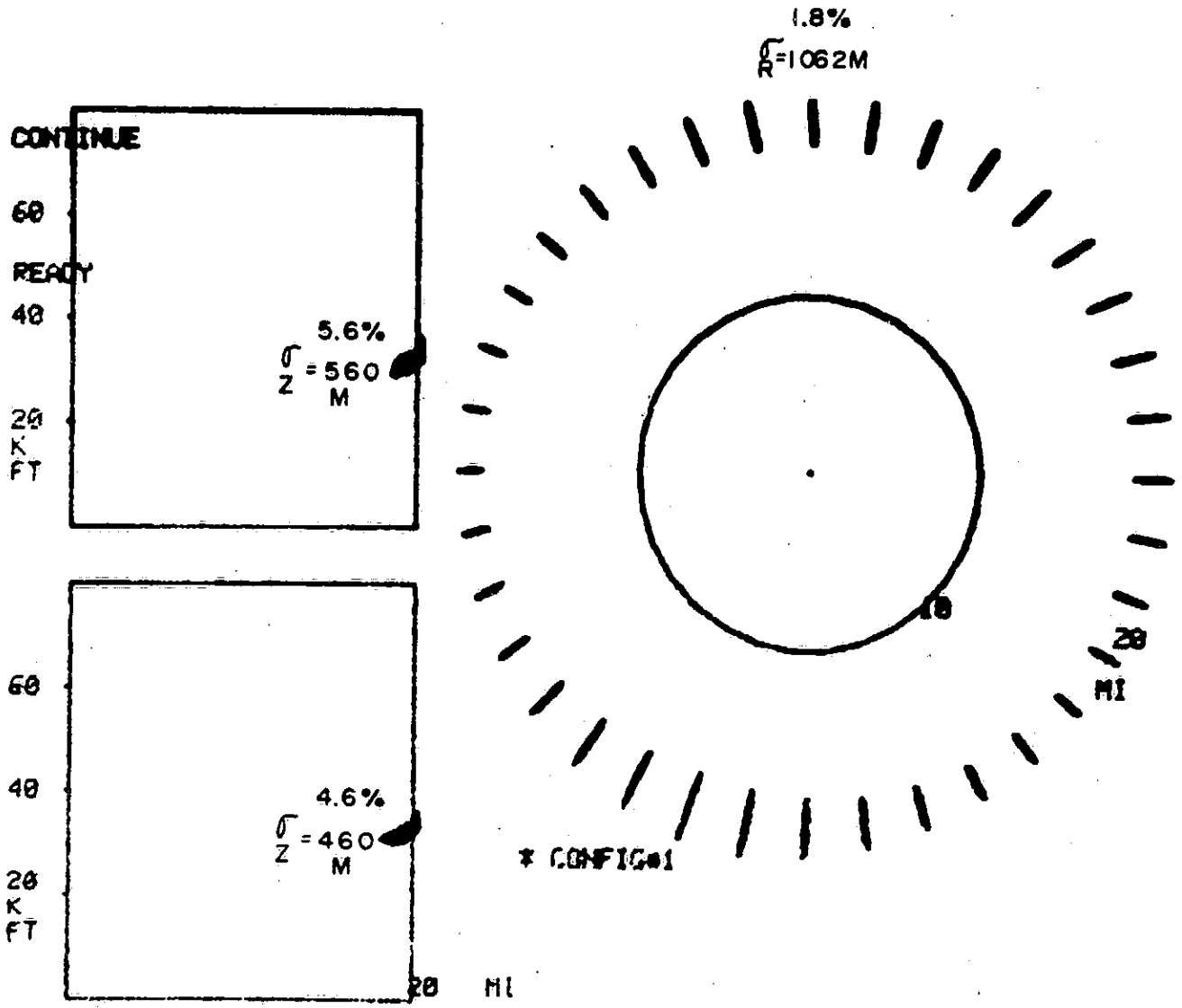

FIG. 16 RANGE-AZIMUTH ERROR PLOT, CONFIGURATION NO. 1, 40 MILES

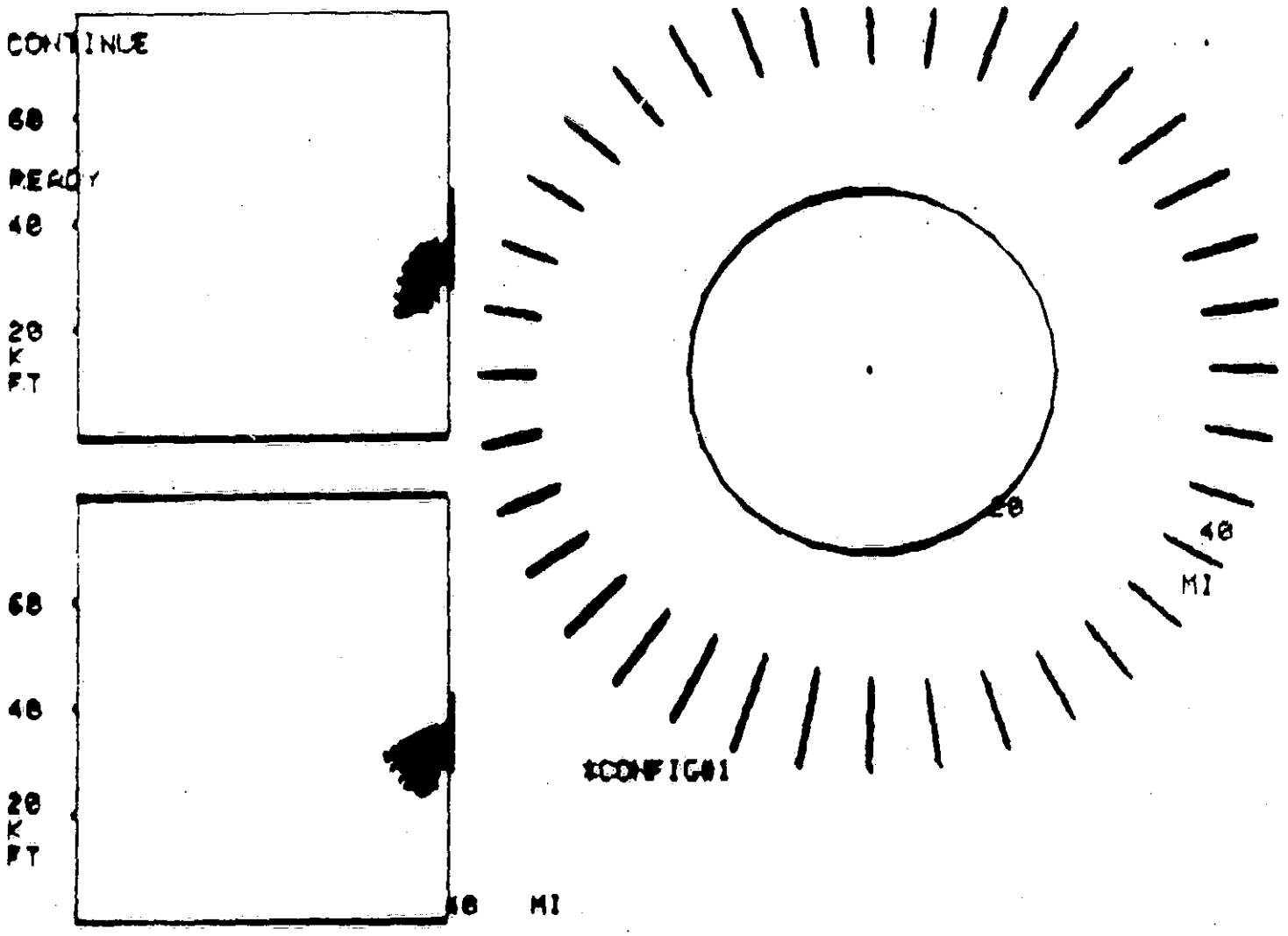

FIG. 17 RANGE-AZIMUTH ERROR PLOT, CONFIGURATION NO. 1, 160 MILES

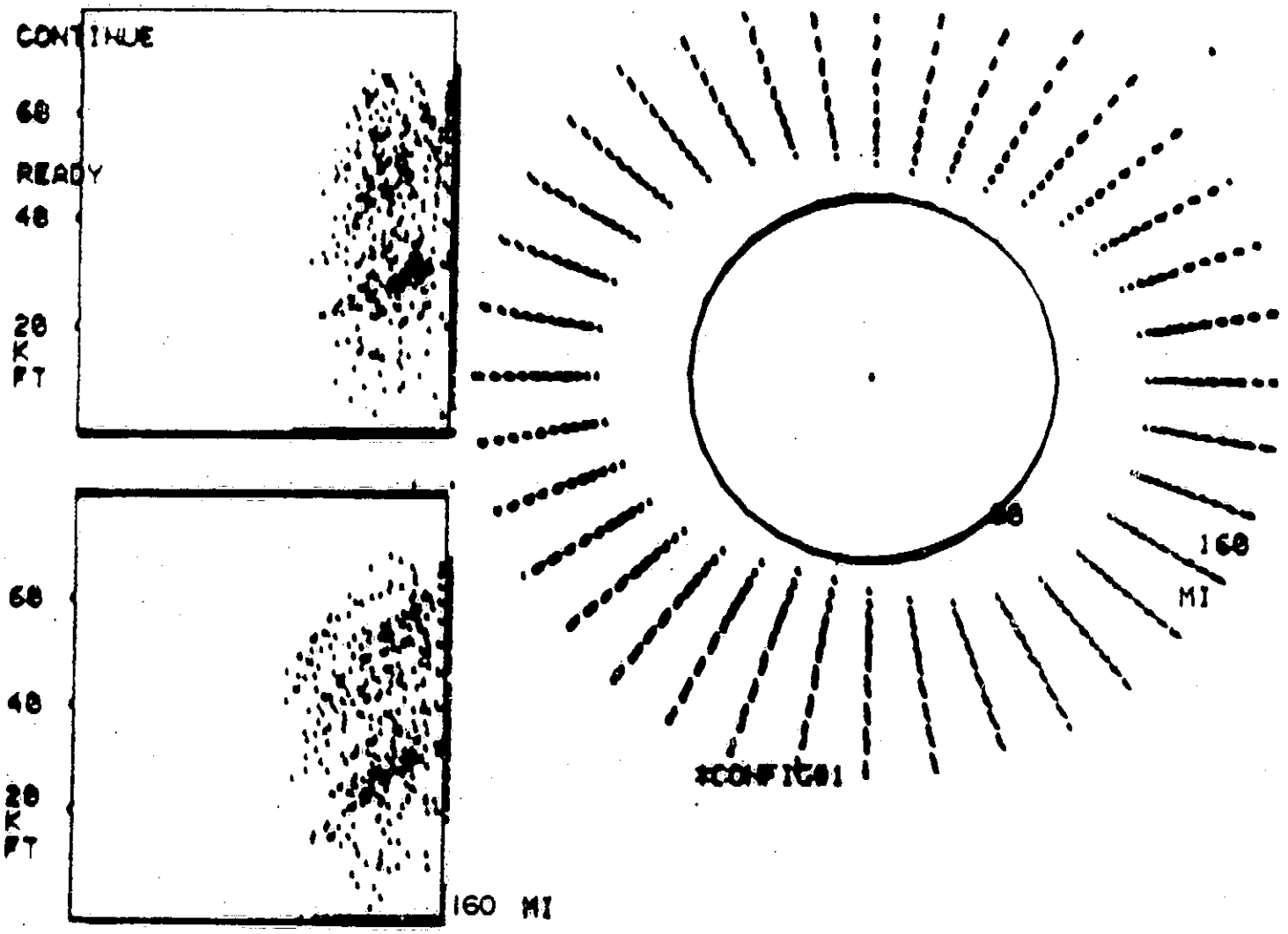

FIG. 18 ELEVATION-AZIMUTH ERROR PLOT, CONFIGURATION NO. 1, 5 MILES

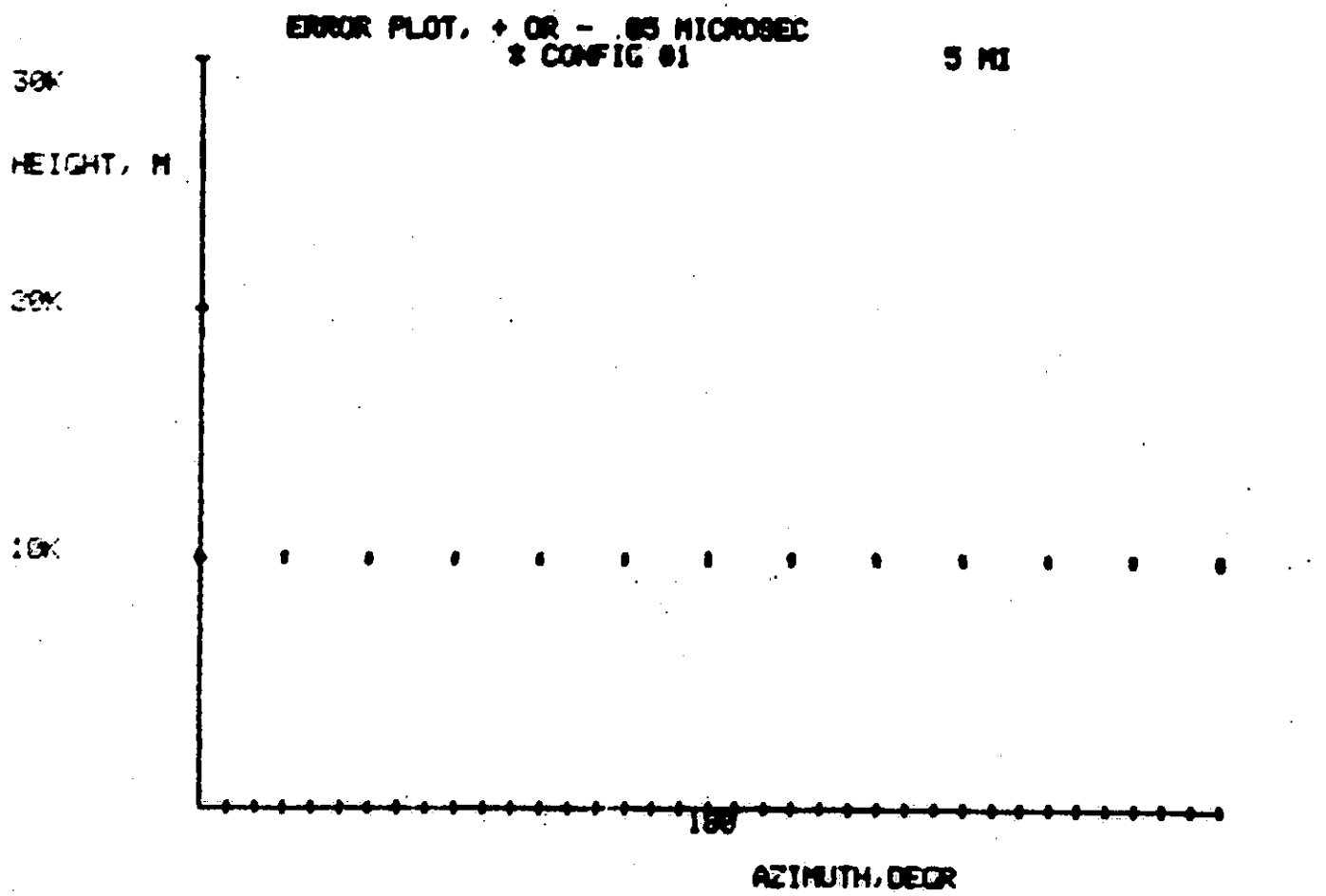

FIG. 19 ELEVATION-AZIMUTH ERROR PLOT, CONFIGURATION NO. 1, 10 MILES

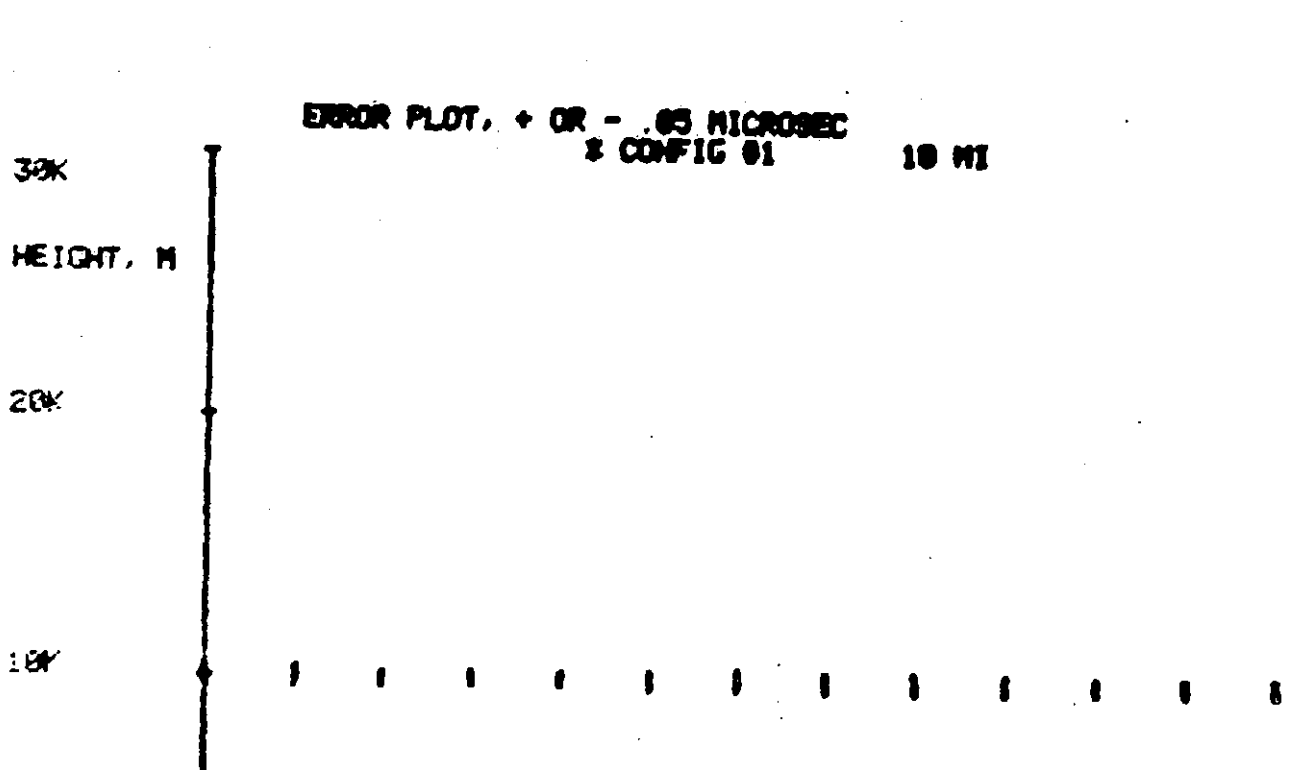

FIG. 20 ELEVATION-AZIMUTH ERROR PLOT, CONFIGURATION NO. 1, 20 MILES

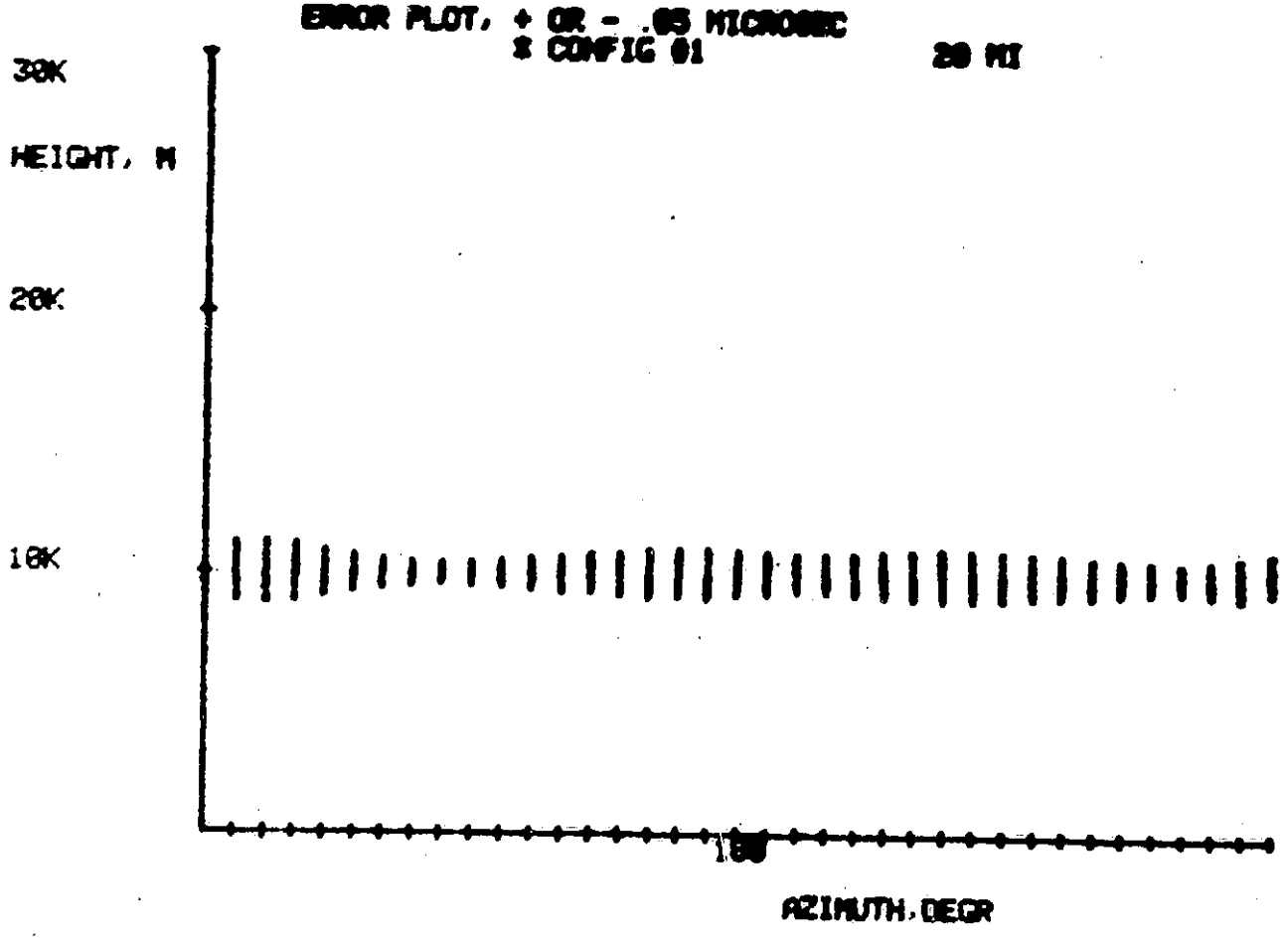

FIG. 21 ELEVATION-AZIMUTH ERROR PLOT, CONFIGURATION NO 1, 40 MILES

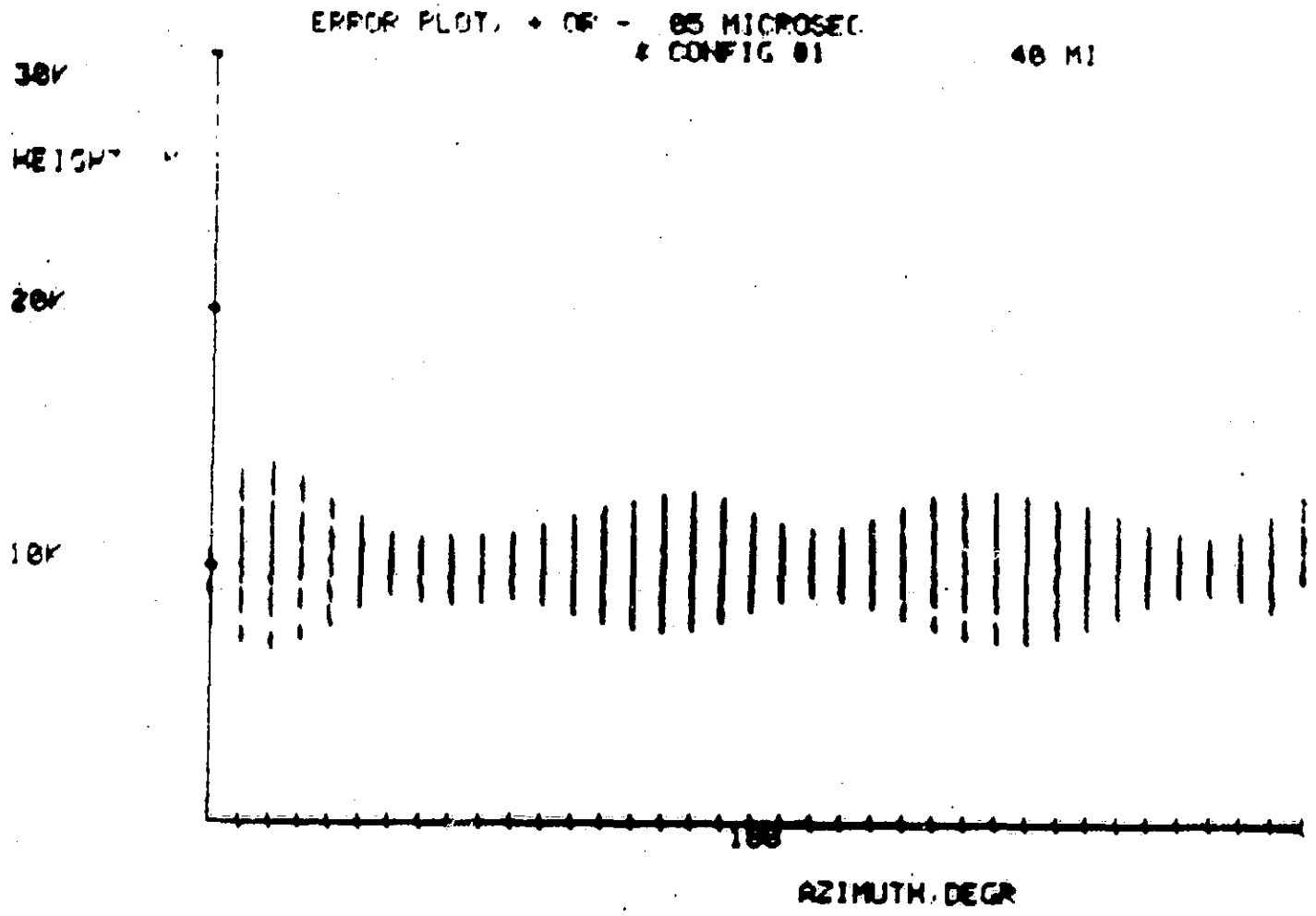

FIG. 22 ELEVATION-AZIMUTH ERROR PLOT, CONFIGURATION NO. 1, 160 MILES

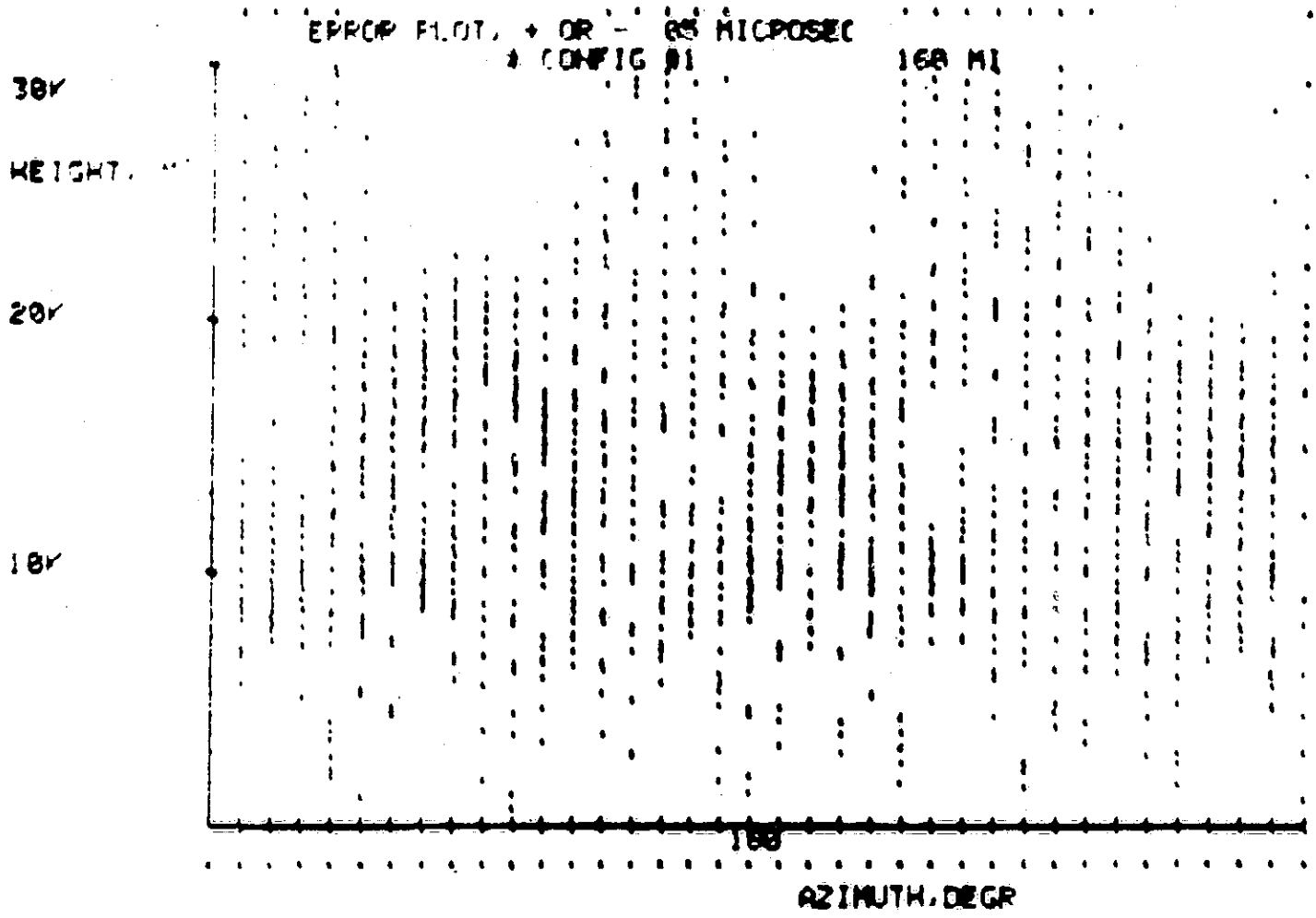

FIG. 23 RANGE-AZIMUTH ERROR PLOT, CONFIGURATION NO. 2, 5 MILES

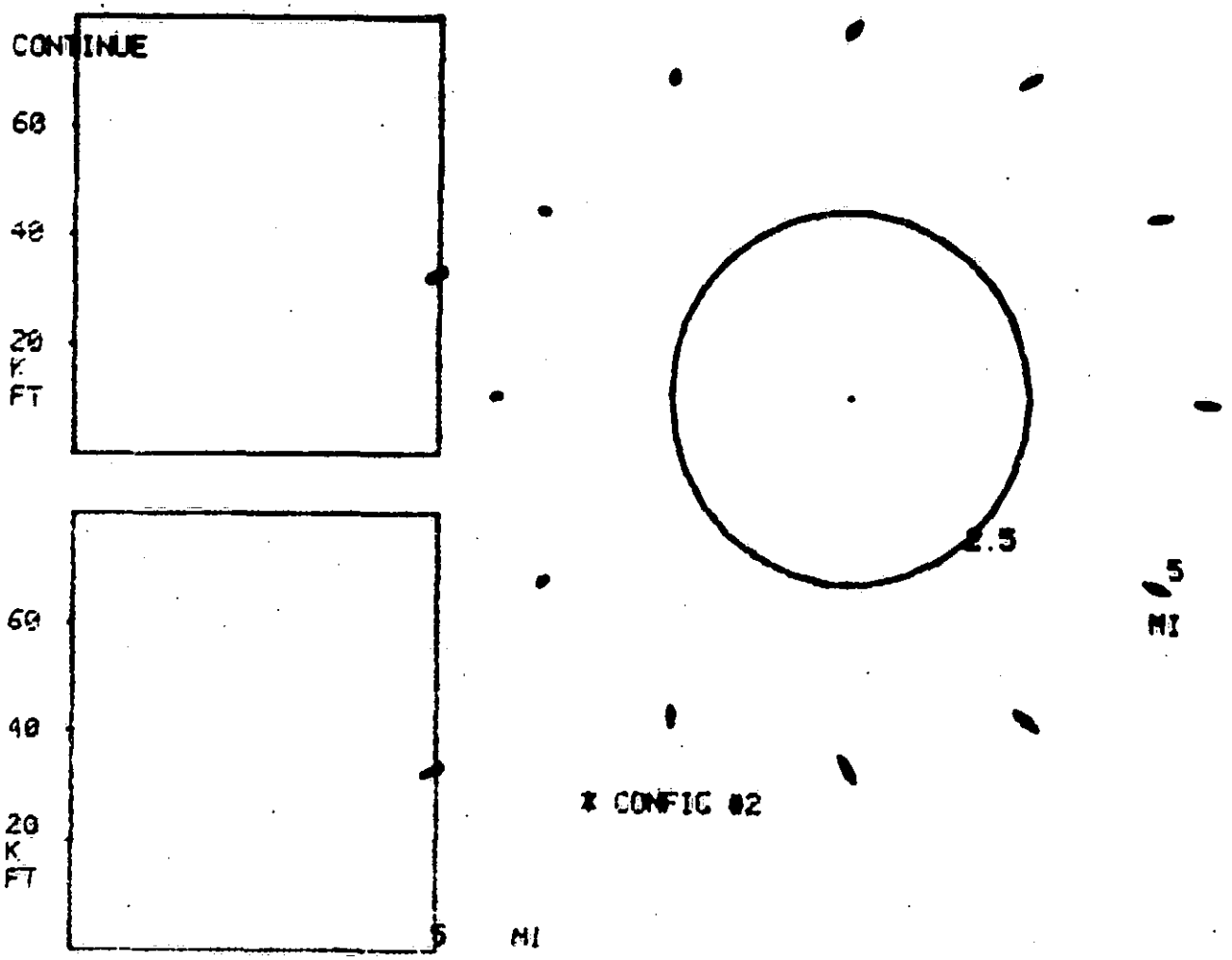

FIG. 24 RANGE-AZIMUTH ERROR PLOT, CONFIGURATION NO. 2, 10 MILES

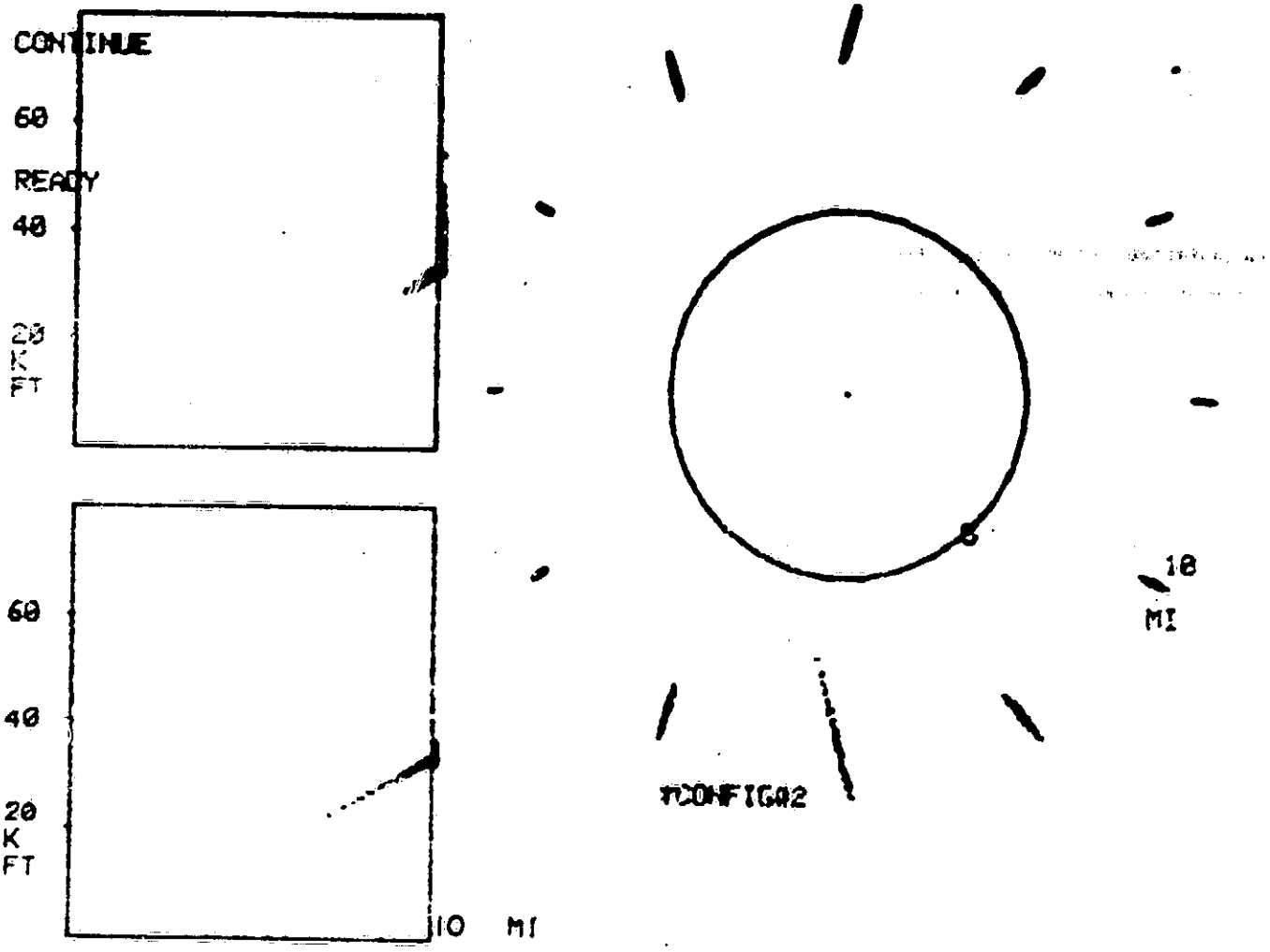

FIG. 25 RANGE-AZIMUTH ERROR PLOT, CONFIGURATION NO. 2, 20 MILES

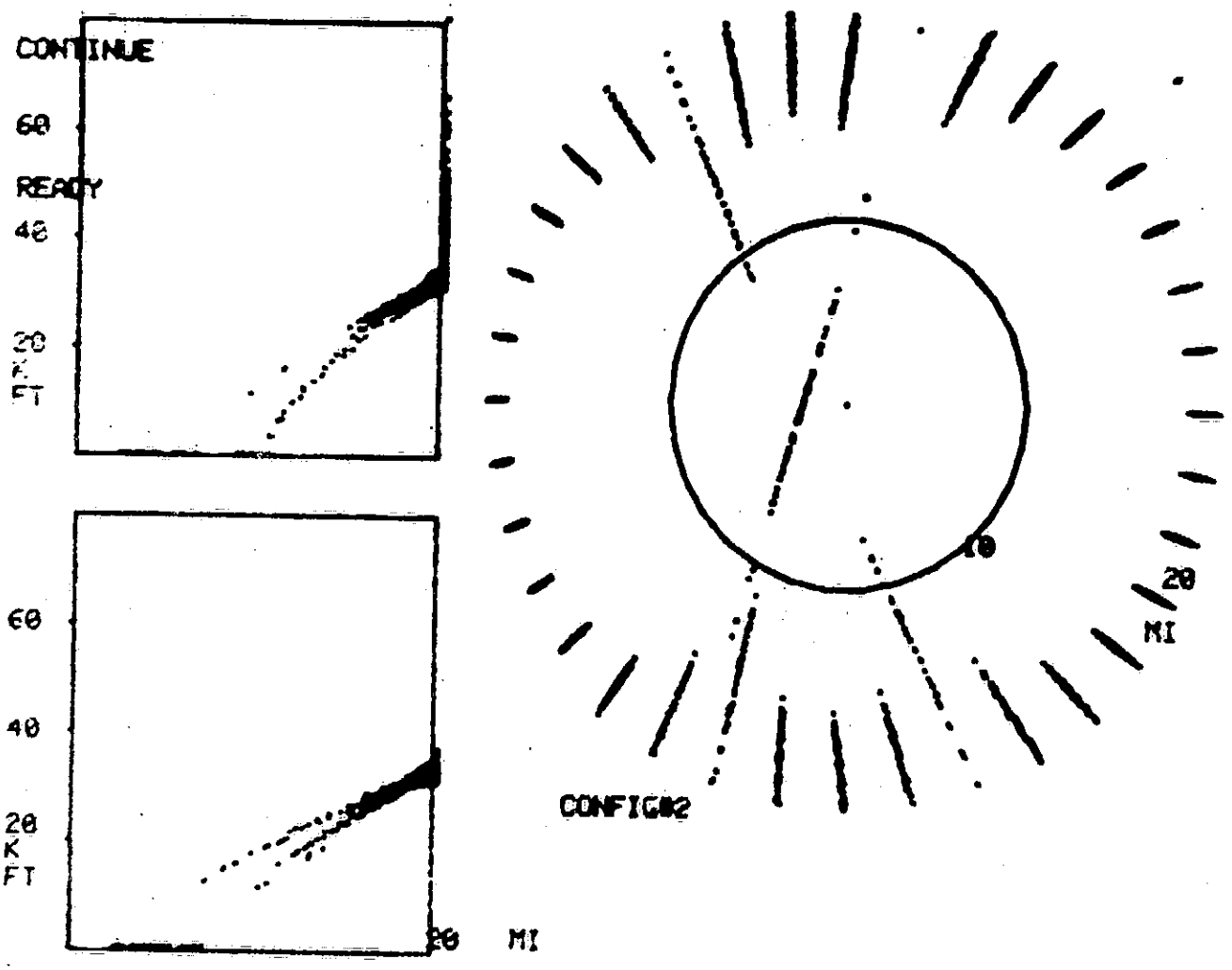

FIG. 26 RANGE-AZIMUTH ERROR PLOT, CONFIGURATION NO. 2, 40 MILES

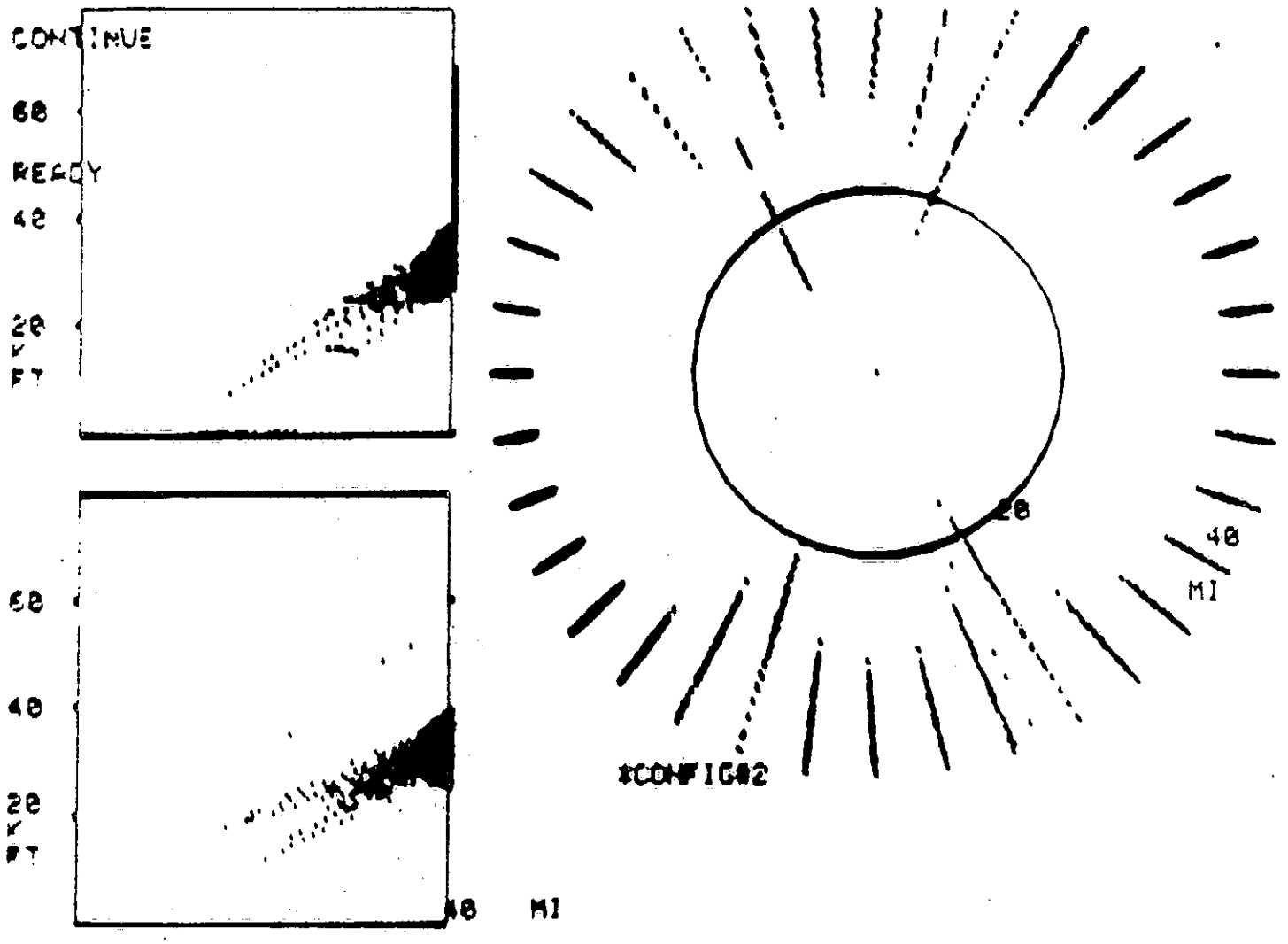

FIG. 27 RANGE-AZIMUTH ERROR PLOT, CONFIGURATION NO. 2, 160 MILES

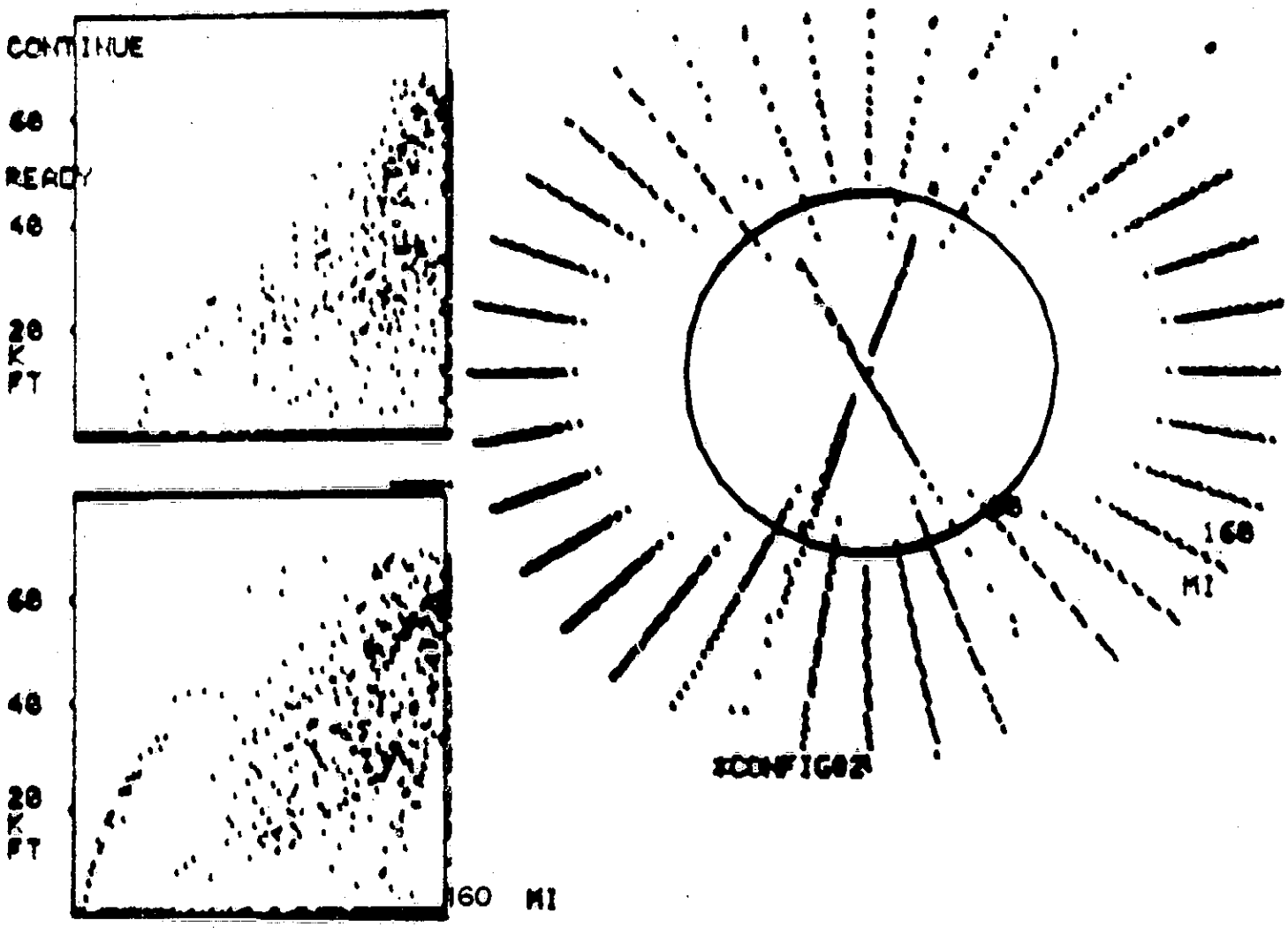

FIG. 28 ELEVATION-AZIMUTH ERROR PLOT, CONFIGURATION NO. 2, 5 MILES

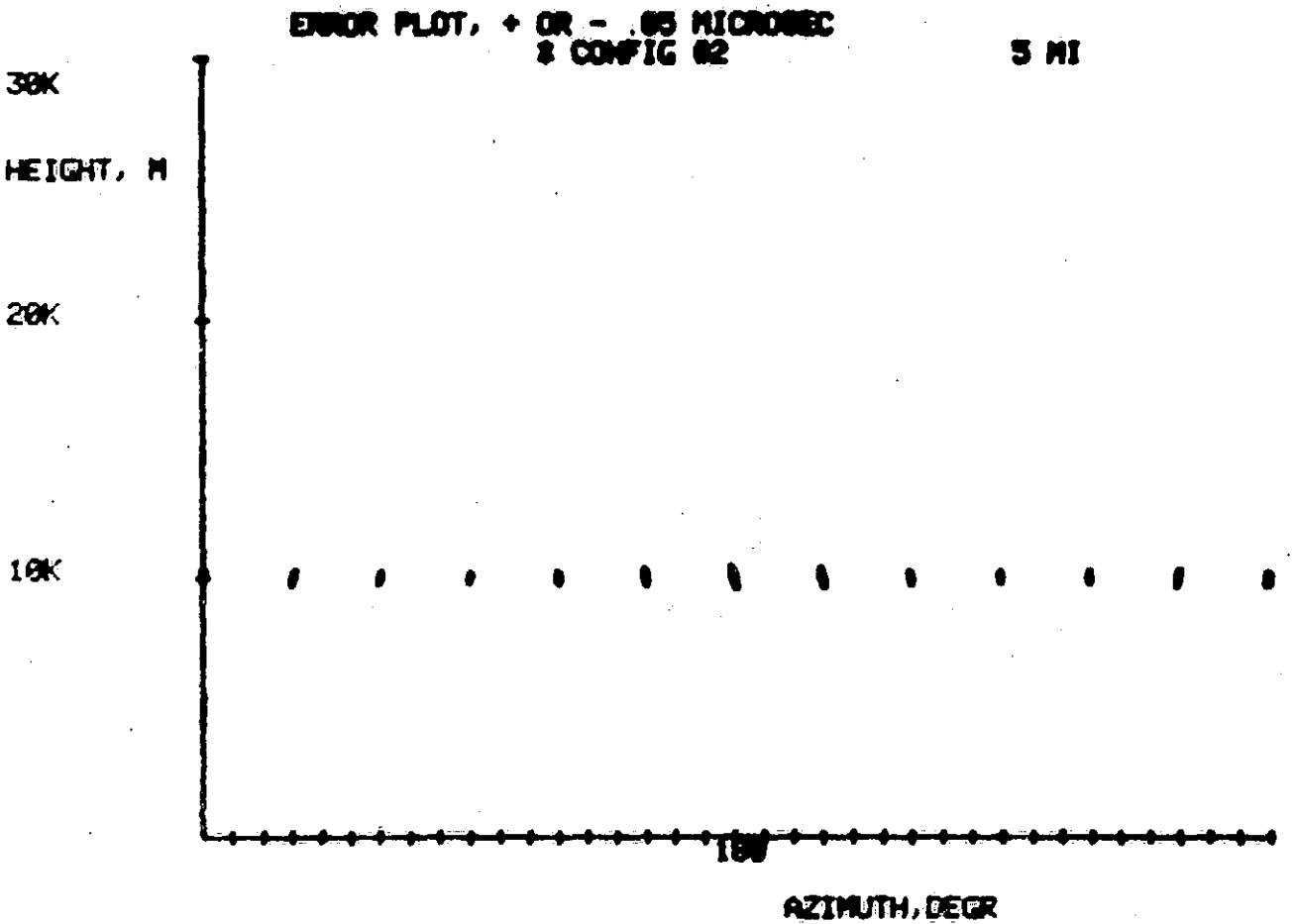

FIG. 29 ELEVATION-AZIMUTH ERROR PLOT, CONFIGURATION NO. 2, 10 MILES

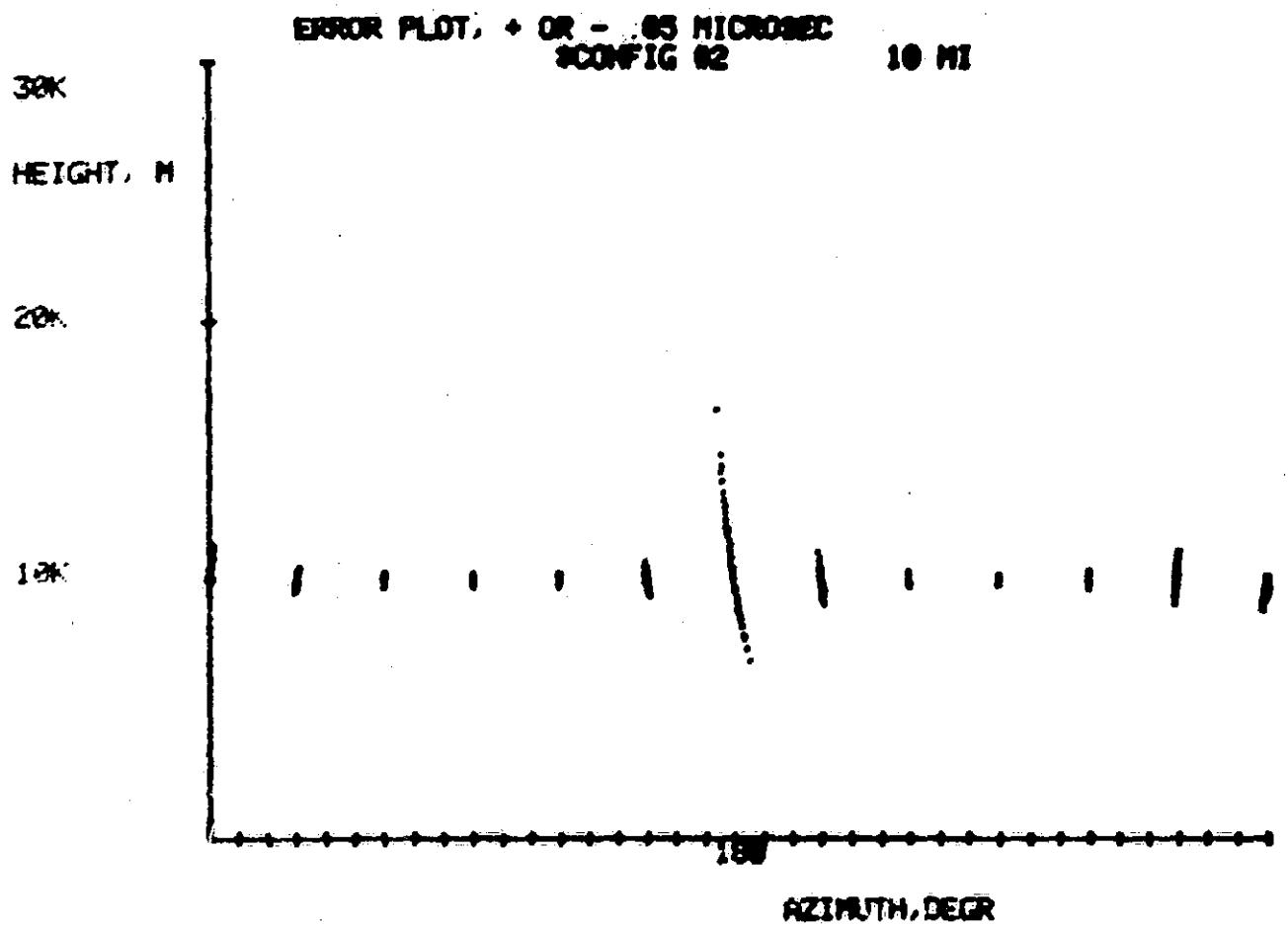

FIG. 30 ELEVATION-AZIMUTH ERROR PLOT, CONFIGURATION NO. 2, 20 MILES

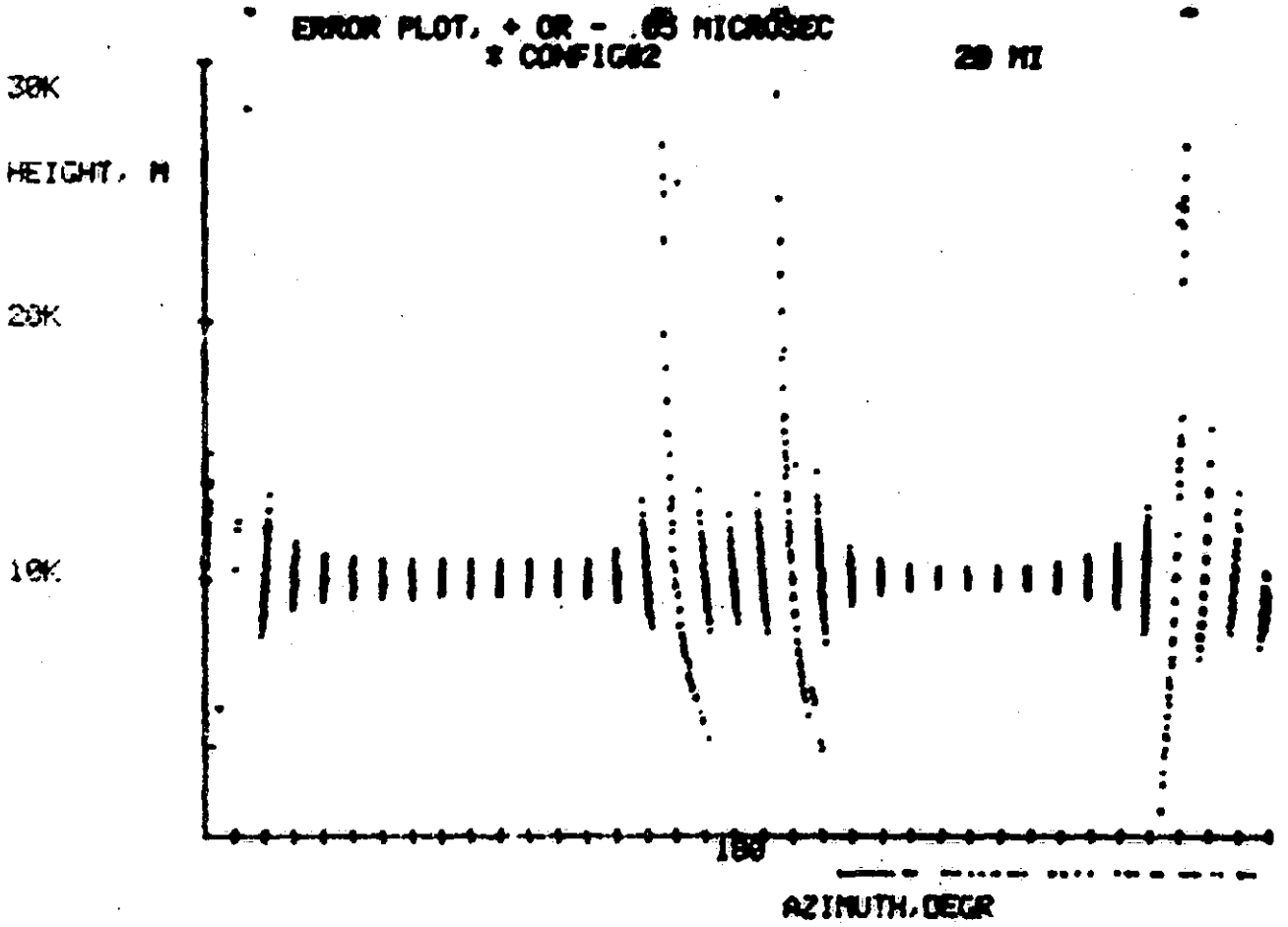

FIG. 31 ELEVATION-AZIMUTH ERROR PLOT, CONFIGURATION NO. 2, 40 MILES

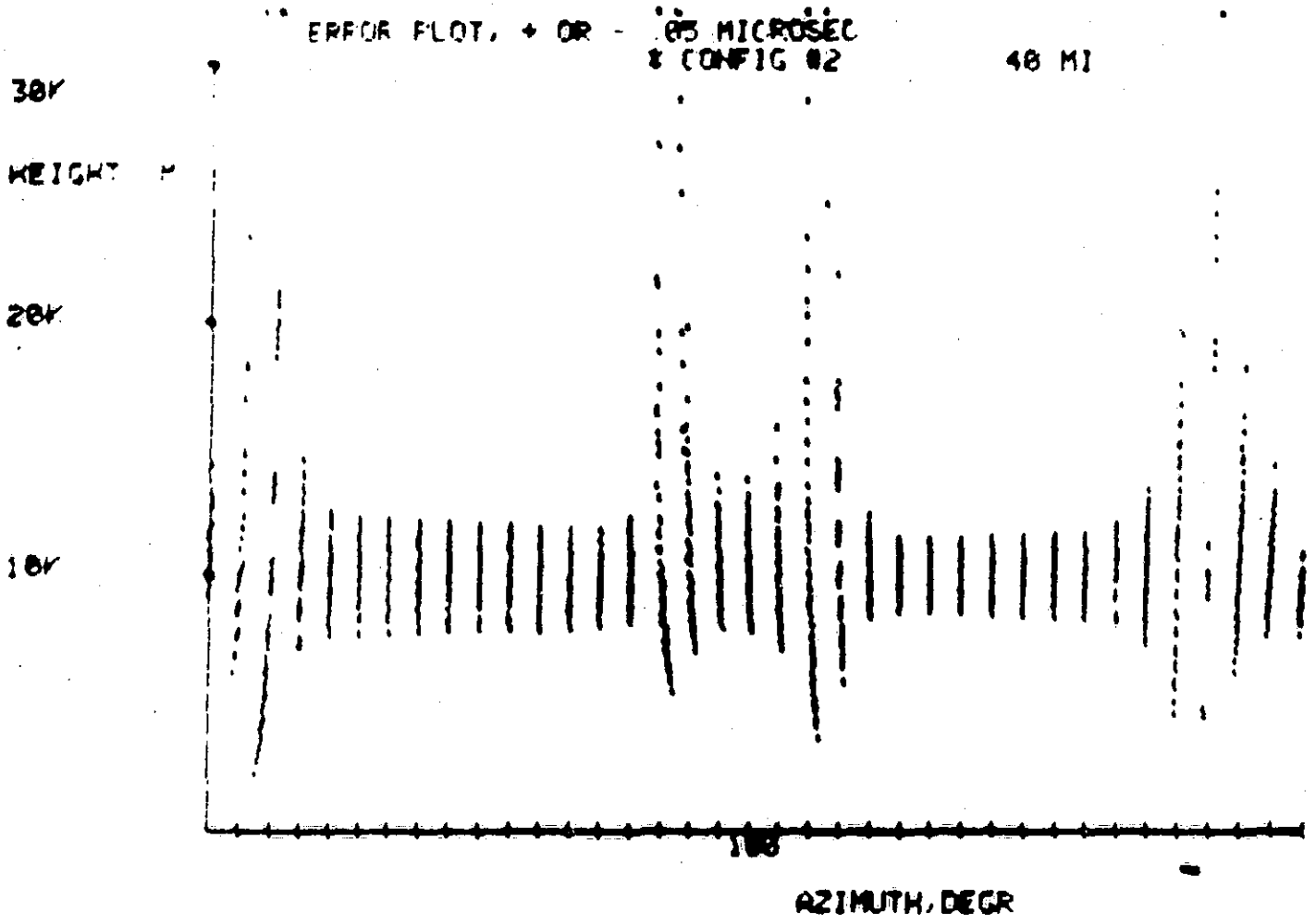

FIG. 32 ELEVATION-AZIMUTH ERROR PLOT, CONFIGURATION NO. 2, 160 MILES

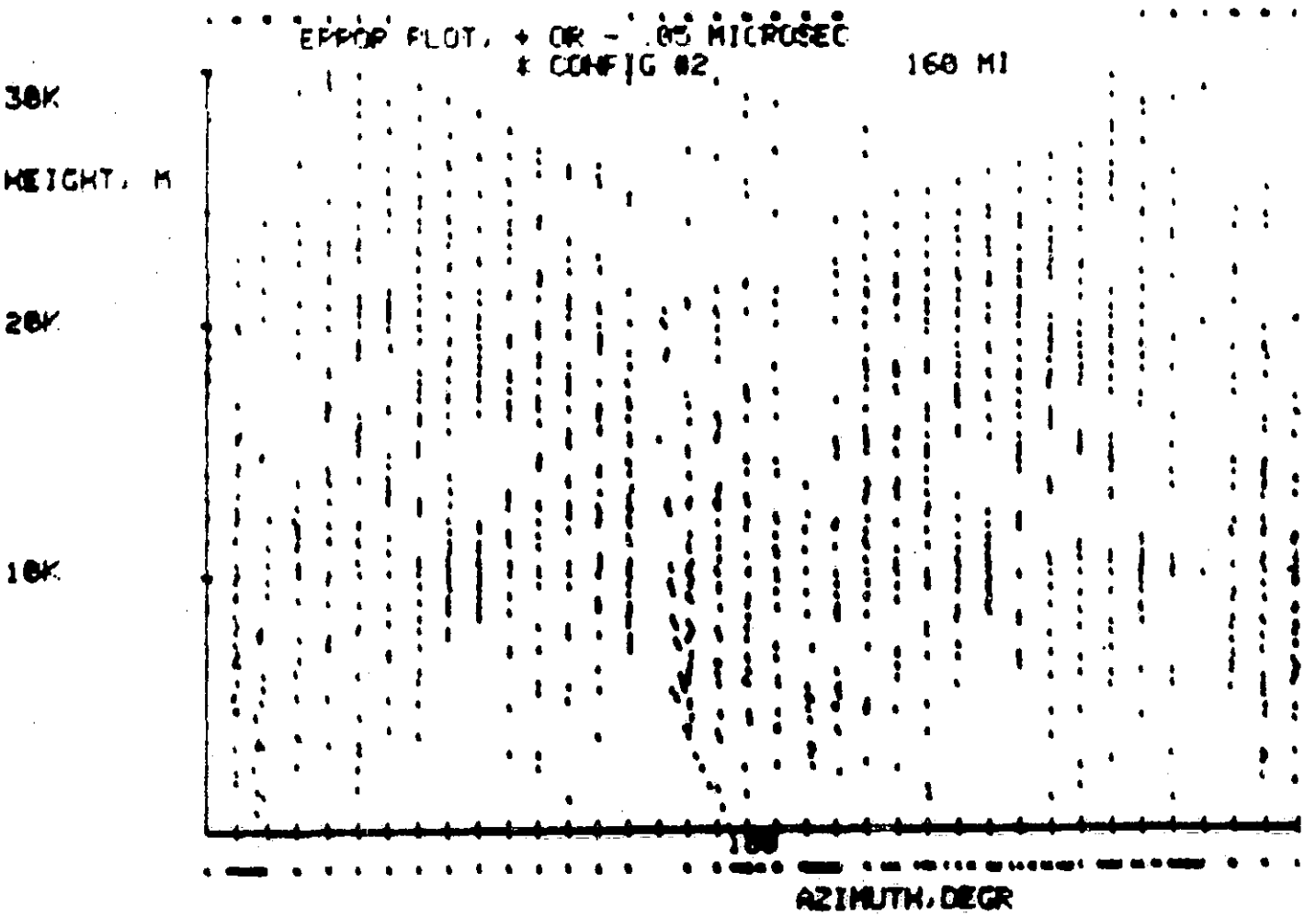

FIG. 33 RANGE-AZIMUTH ERROR PLOT, CONFIGURATION NO. 3, 5 MILES

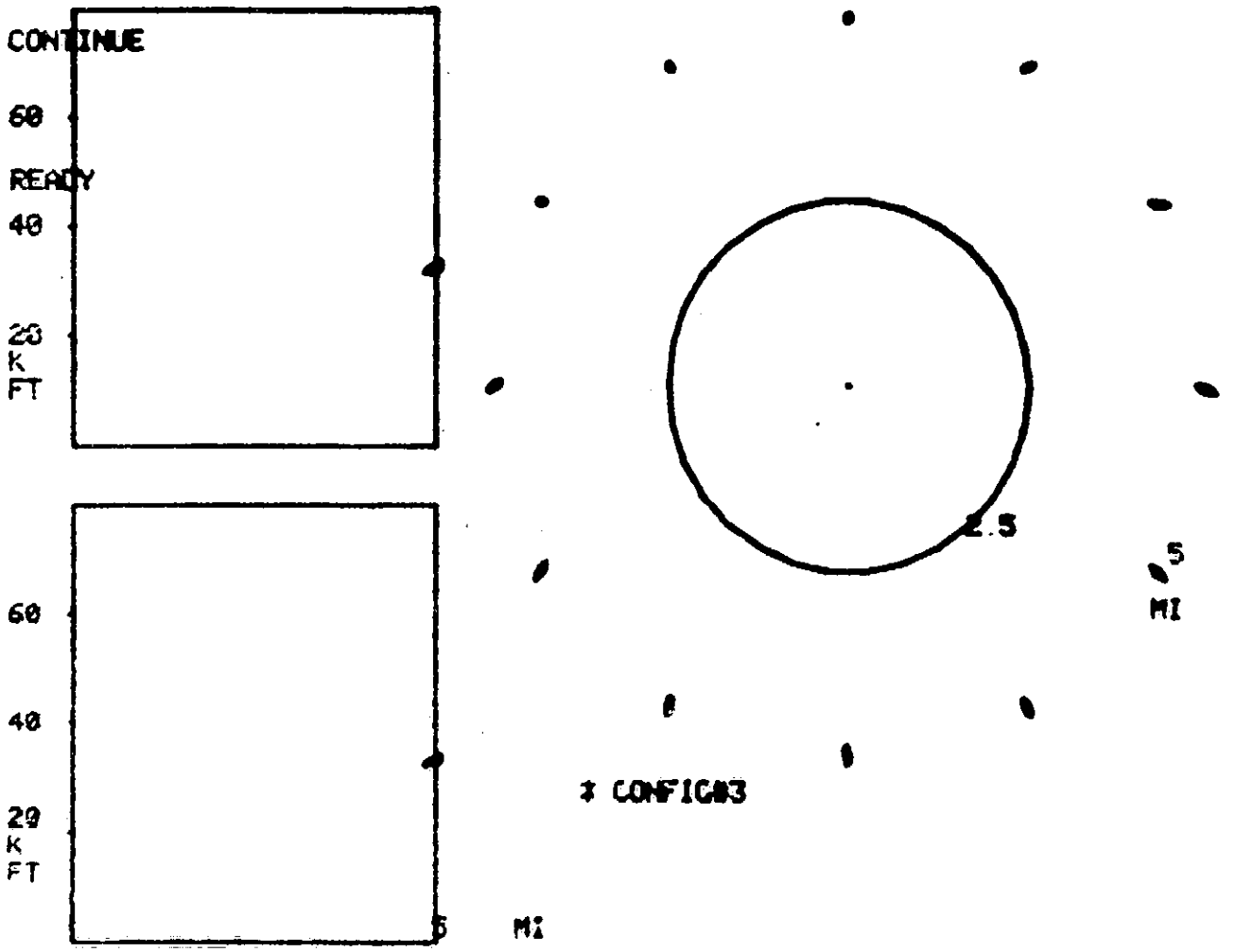

FIG. 34 RANGE-AZIMUTH ERROR PLOT, CONFIGURATION NO. 3, 10 MILES

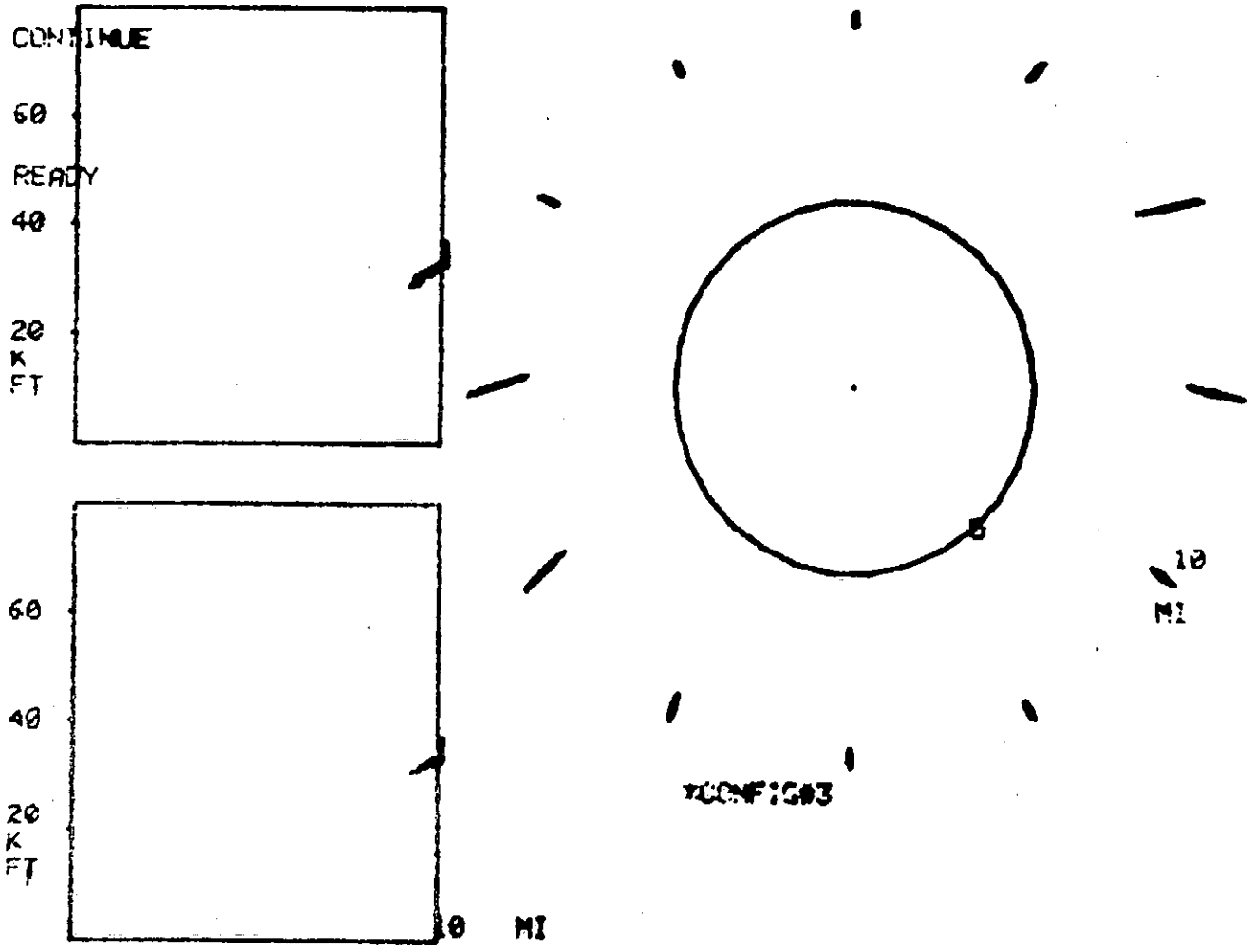

FIG. 35 RANGE-AZIMUTH ERROR PLOT, CONFIGURATION NO. 3, 20 MILES

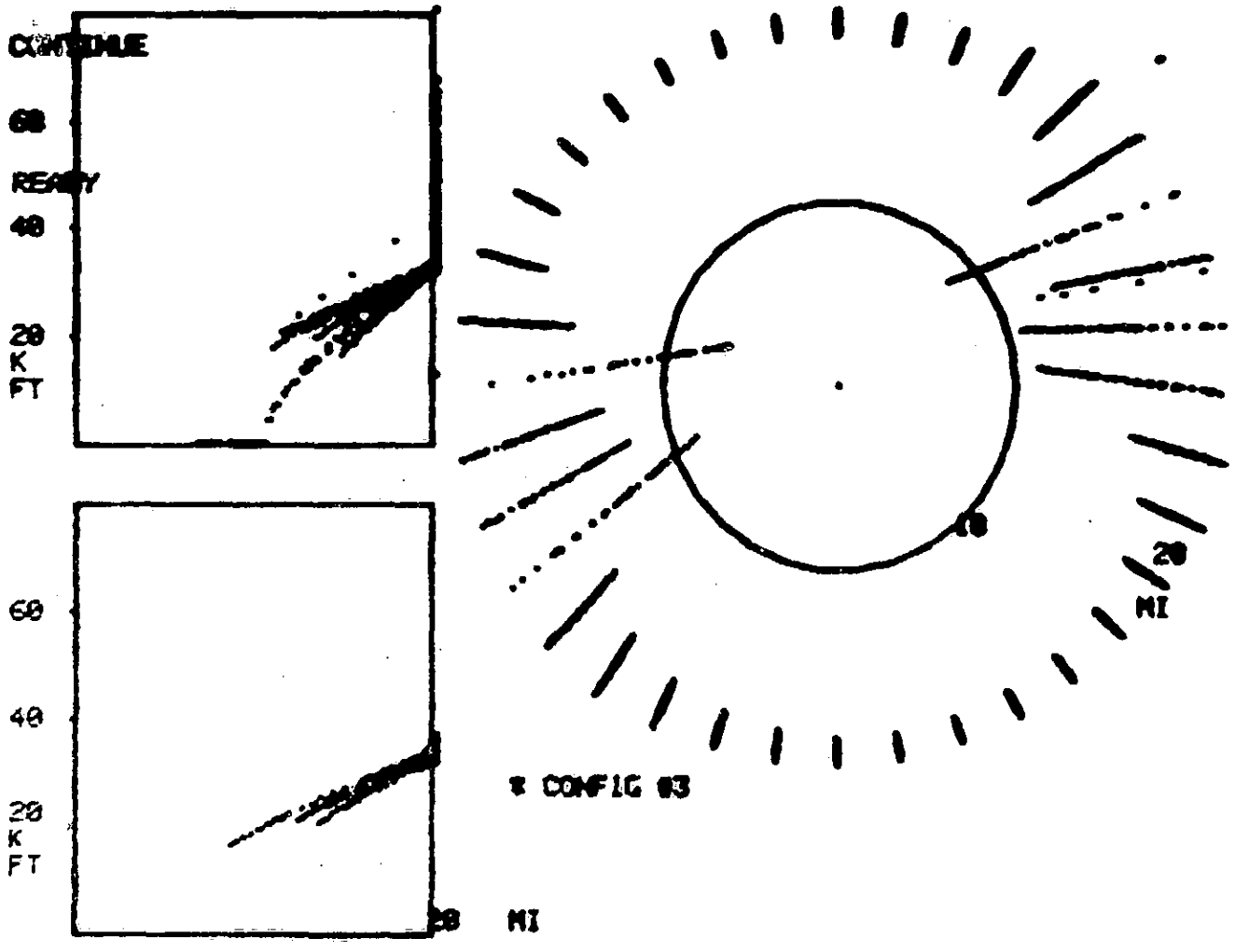

FIG. 36 RANGE-AZIMUTH ERROR PLOT, CONFIGURATION NO. 3, 40 MILES

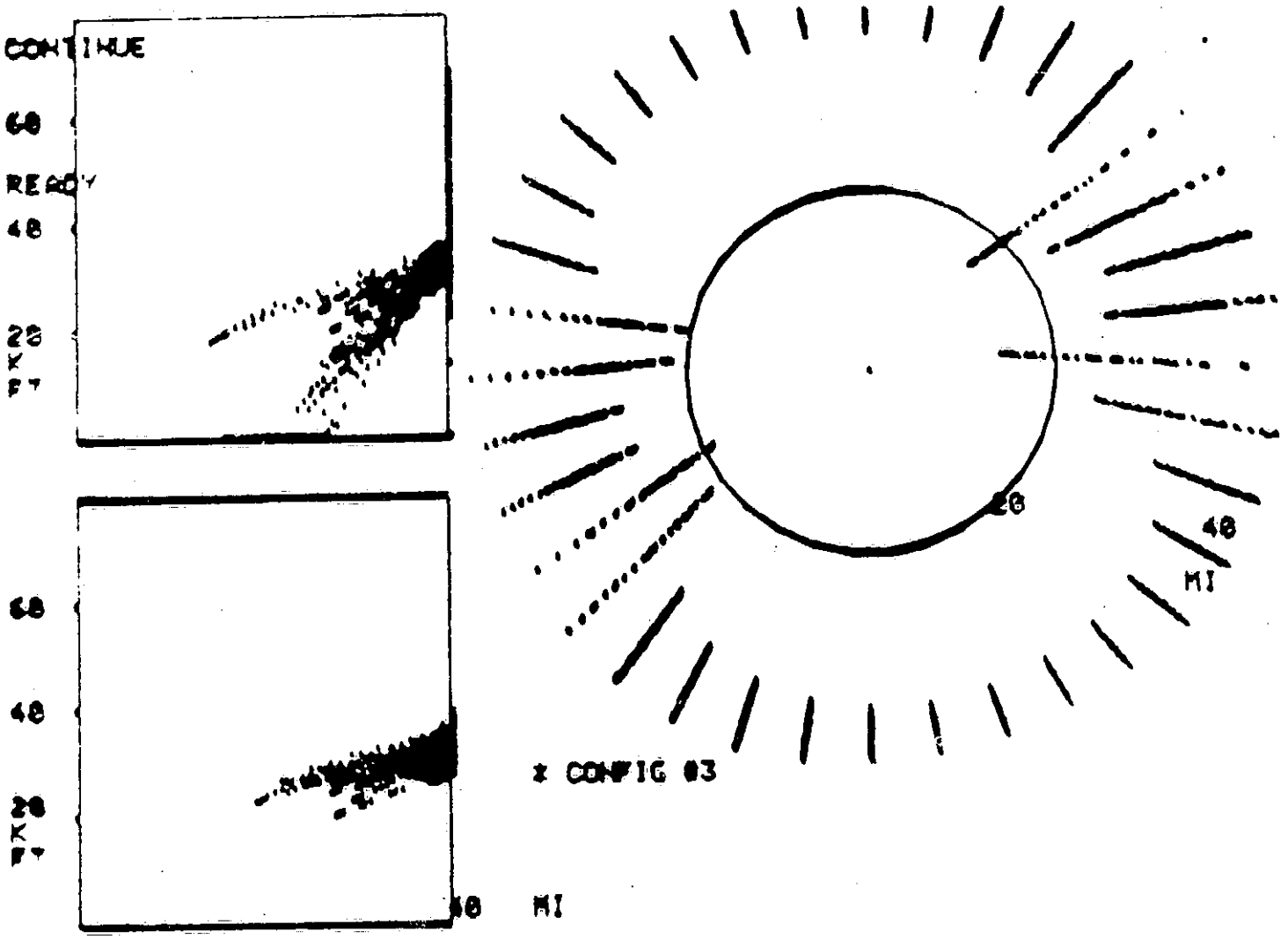

FIG. 37 RANGE-AZIMUTH ERROR PLOT, CONFIGURATION NO. 3, 160 MILES

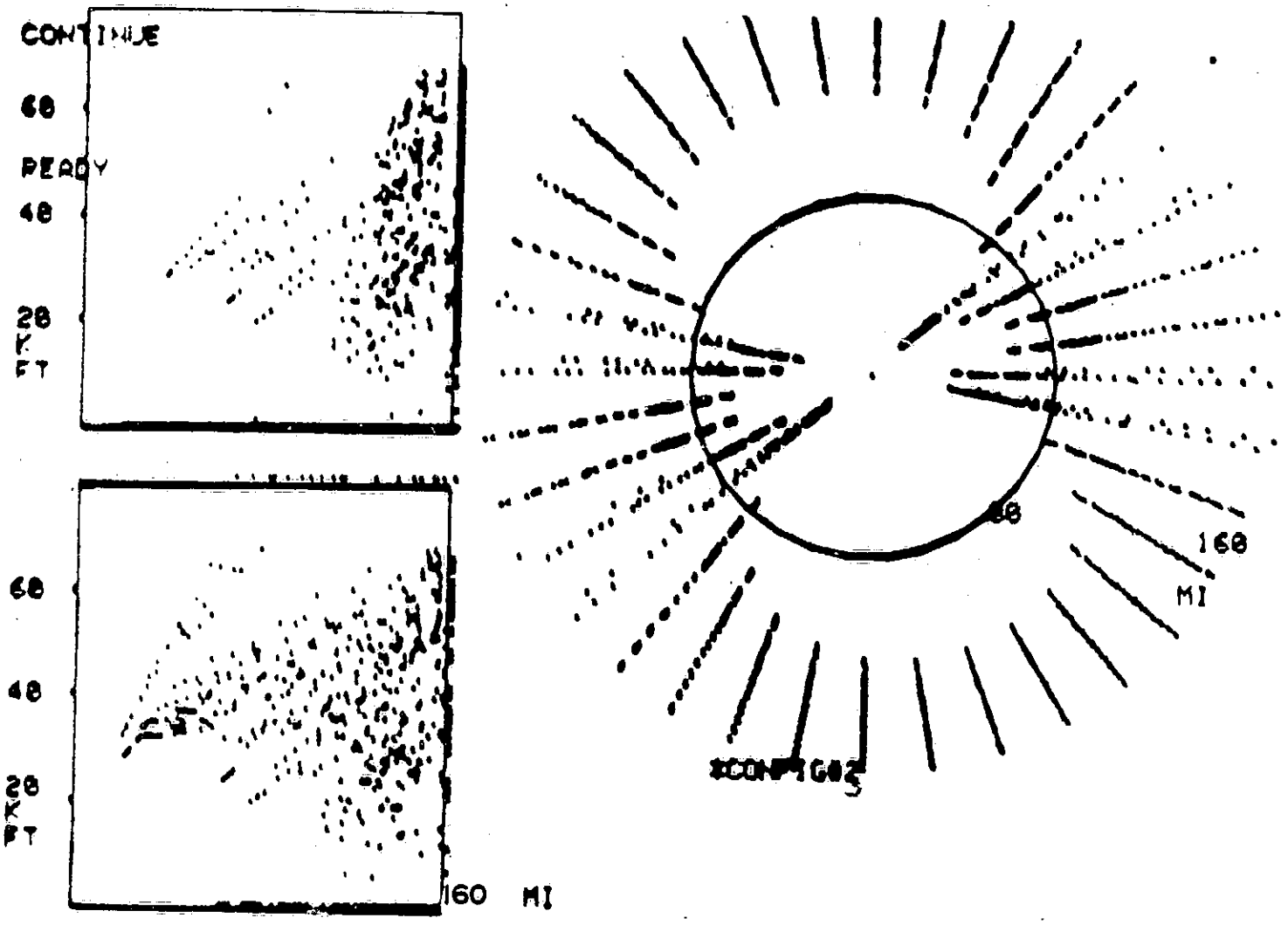

FIG. 38 ELEVATION-AZIMUTH ERROR PLOT, CONFIGURATION NO. 3, 5 MILES

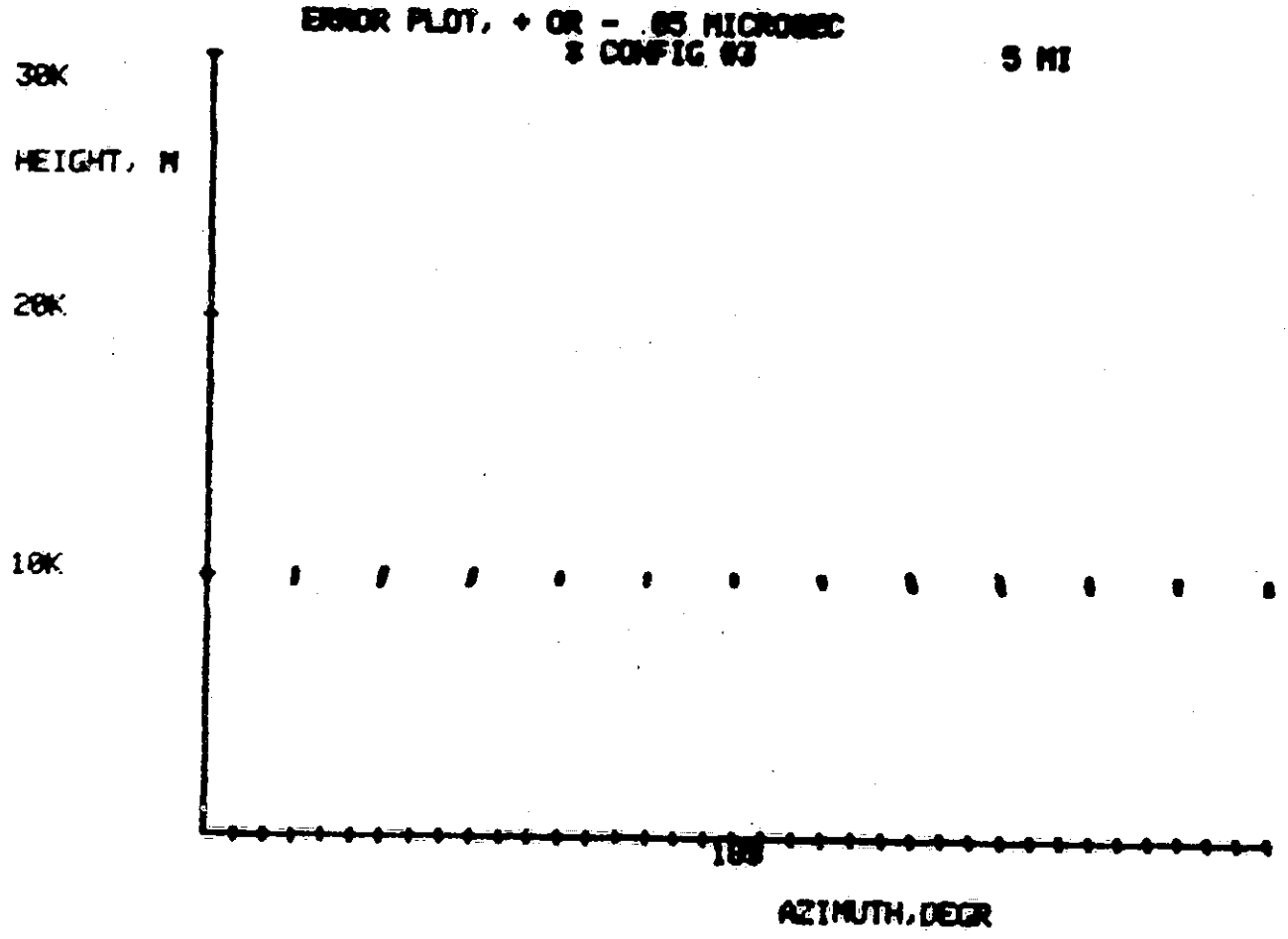

FIG. 39 ELEVATION-AZIMUTH ERROR PLOT, CONFIGURATION NO. 3, 10 MILES

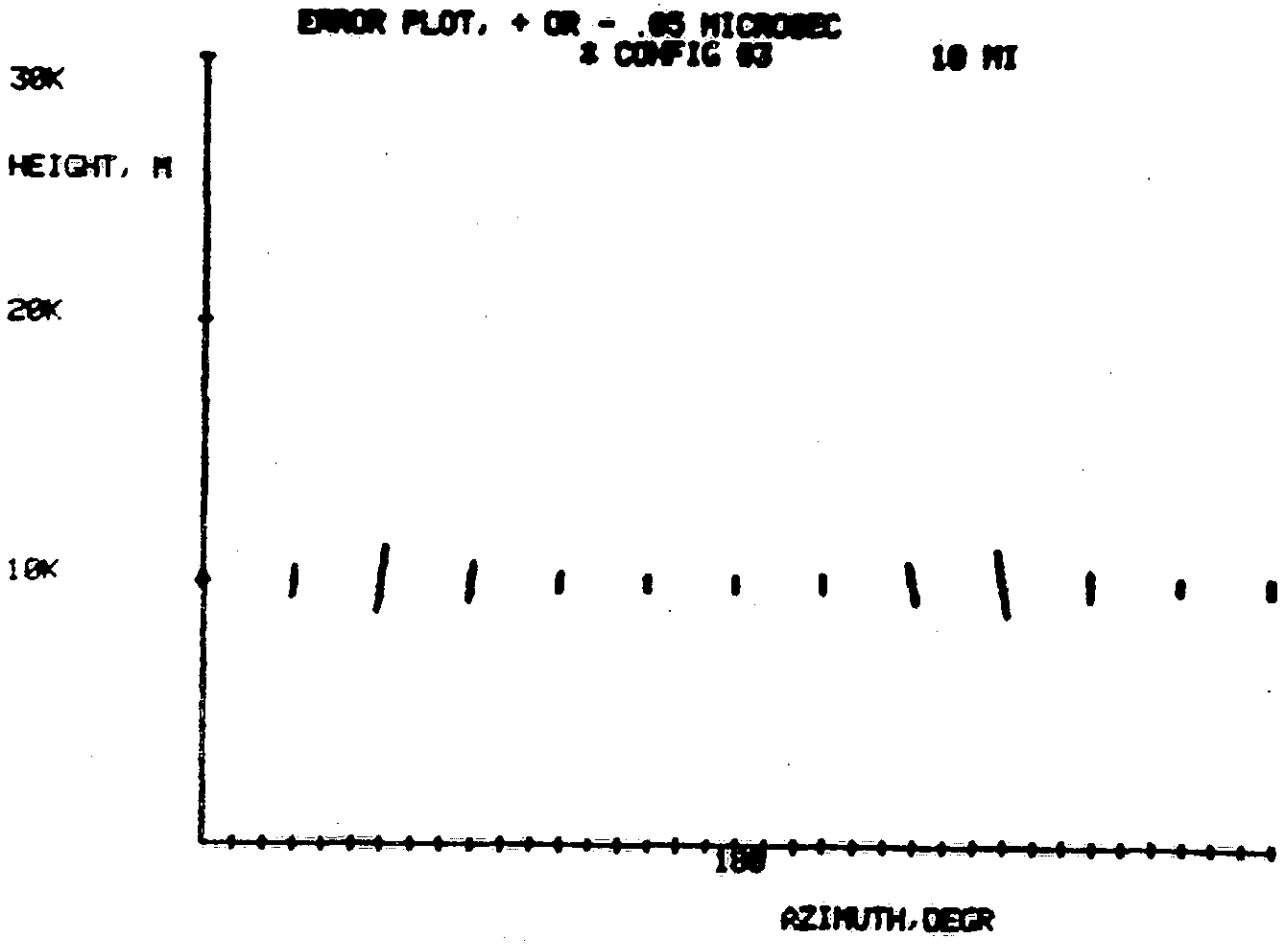

FIG. 40 ELEVATION-AZIMUTH ERROR PLOT, CONFIGURATION NO. 3, 20 MILES

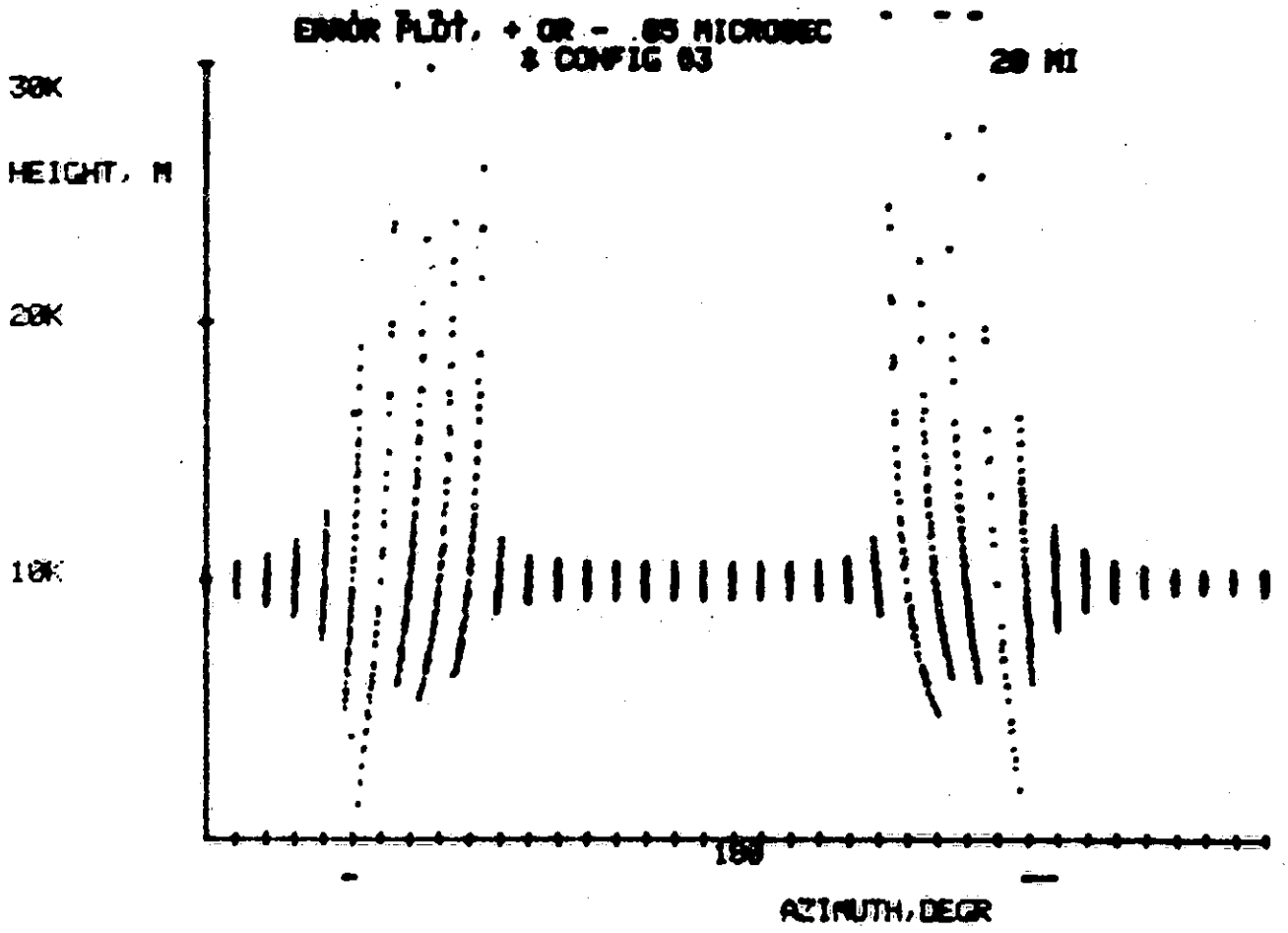

FIG. 41 ELEVATION-AZIMUTH ERROR PLOT, CONFIGURATION NO. 3, 40 MILES

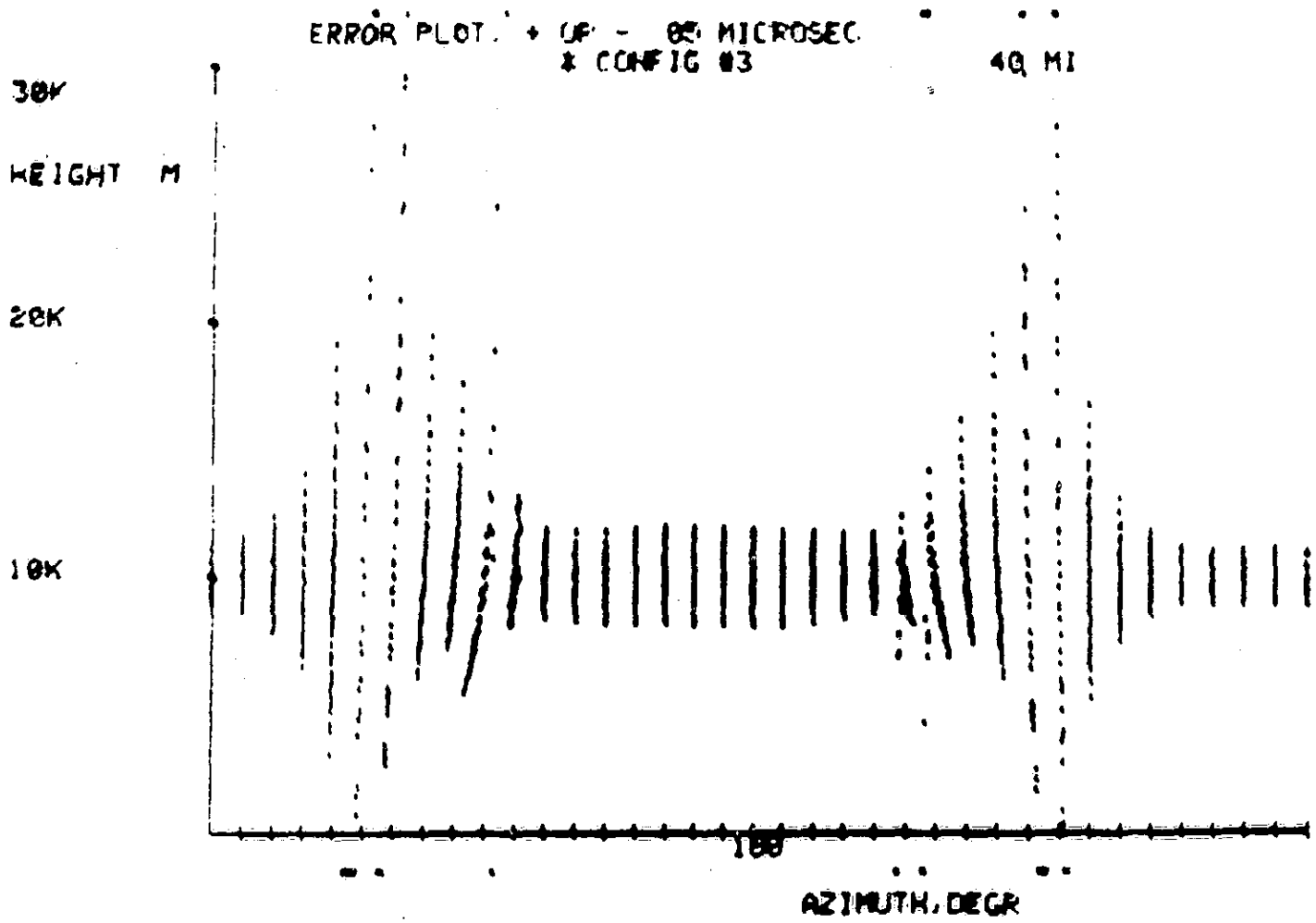

FIG. 42 ELEVATION-AZIMUTH ERROR PLOT, CONFIGURATION NO. 3, 160 MILES

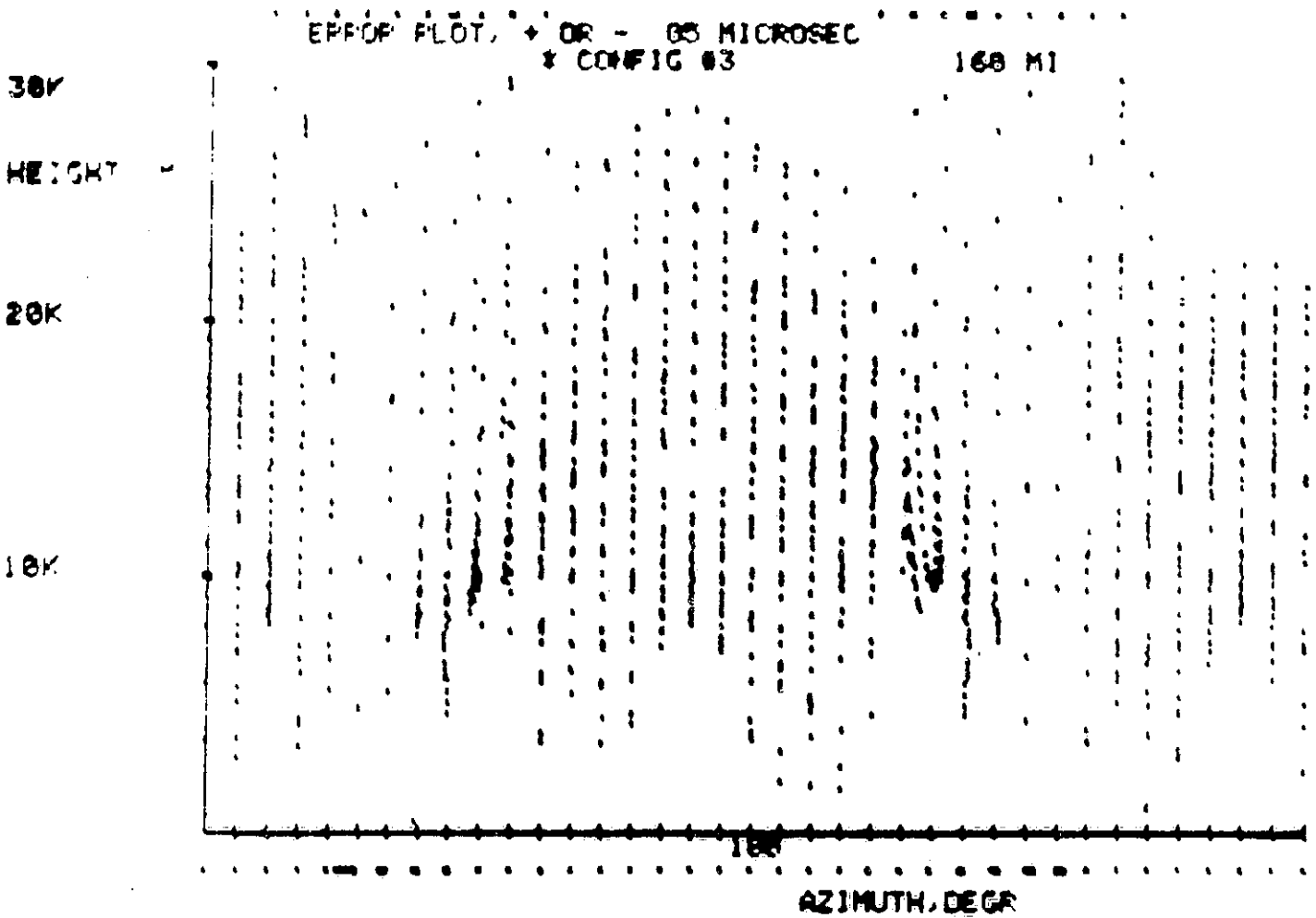

FIG. 43 RANGE-AZIMUTH ERROR PLOT, CONFIGURATION NO. 4, 5 MILES

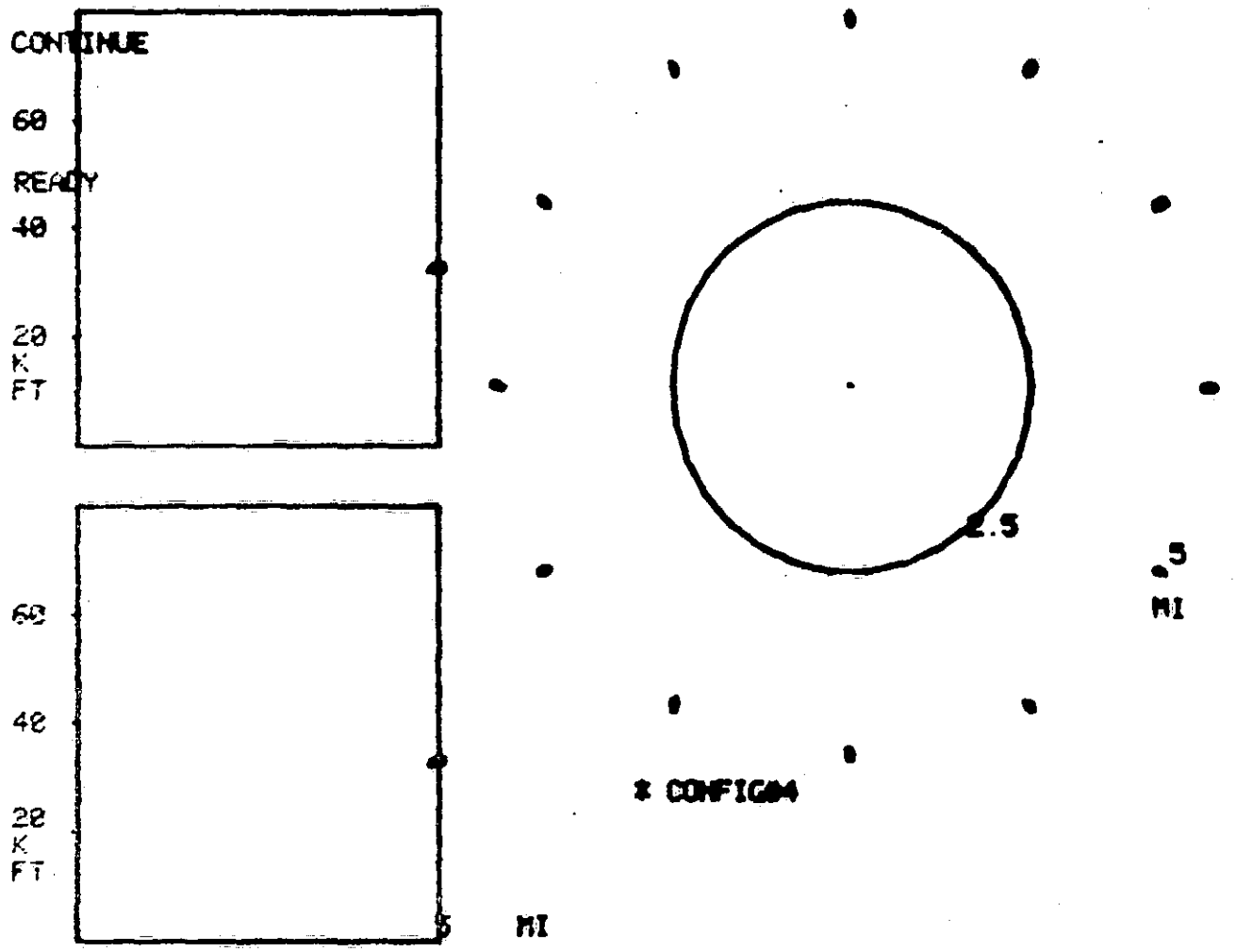

FIG. 44 RANGE-AZIMUTH ERROR PLOT, CONFIGURATION NO. 4, 10 MILES

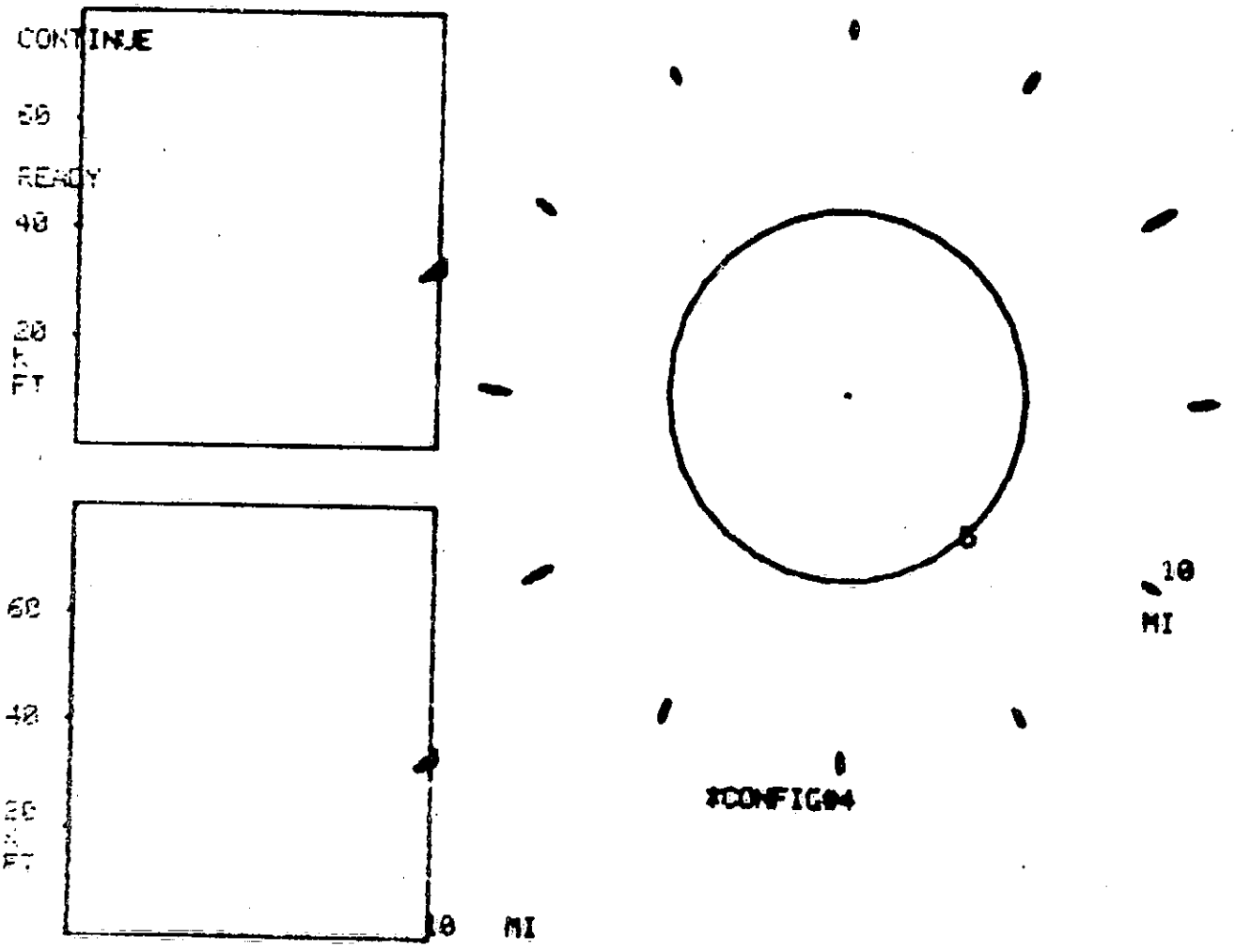

FIG. 45 RANGE-AZIMUTH ERROR PLOT, CONFIGURATION NO. 4, 20 MILES

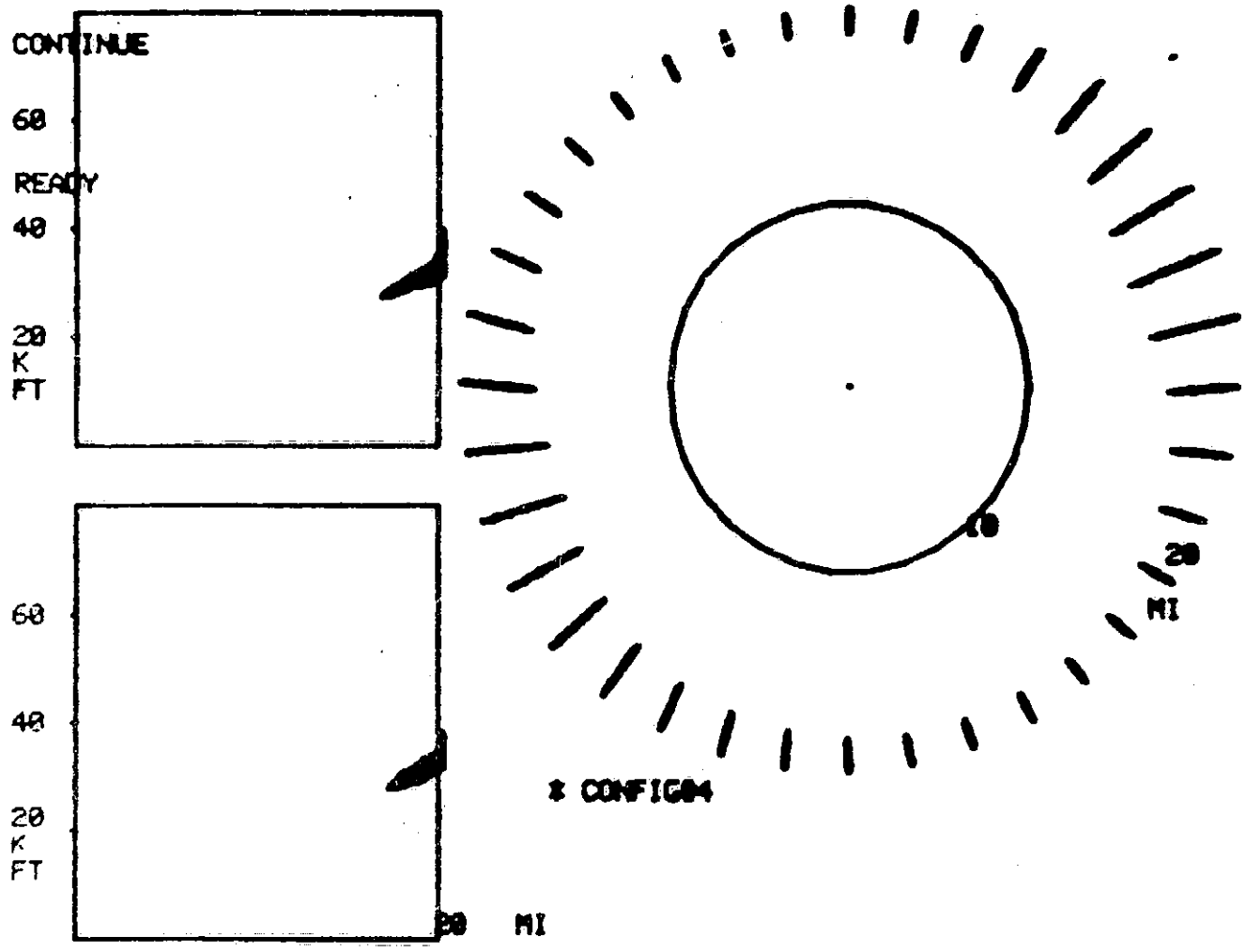

FIG. 46 RANGE-AZIMUTH ERROR PLOT, CONFIGURATION NO. 4, 40 MILES

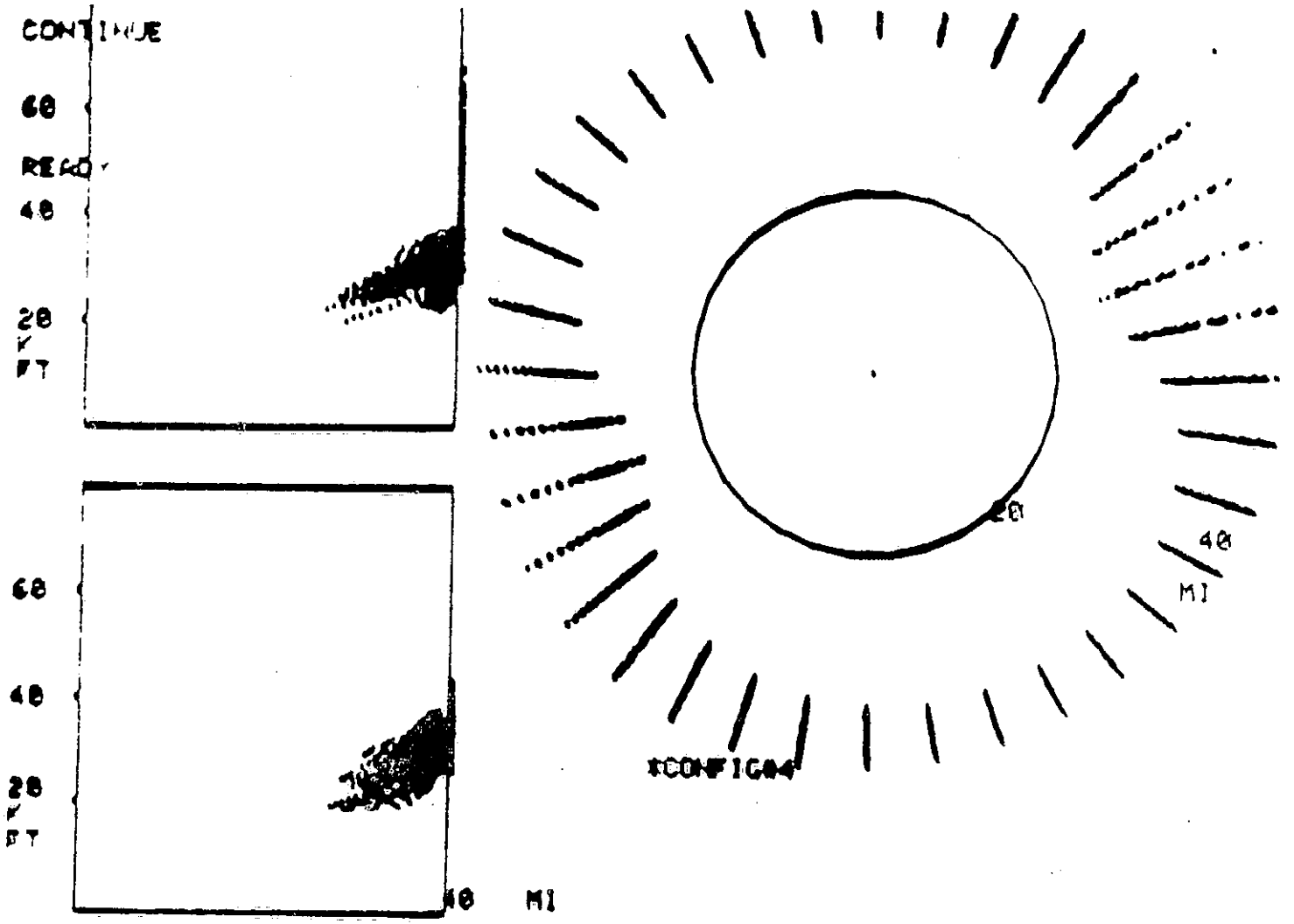

FIG. 47 RANGE-AZIMUTH ERROR PLOT, CONFIGURATION NO. 4, 160 MILES

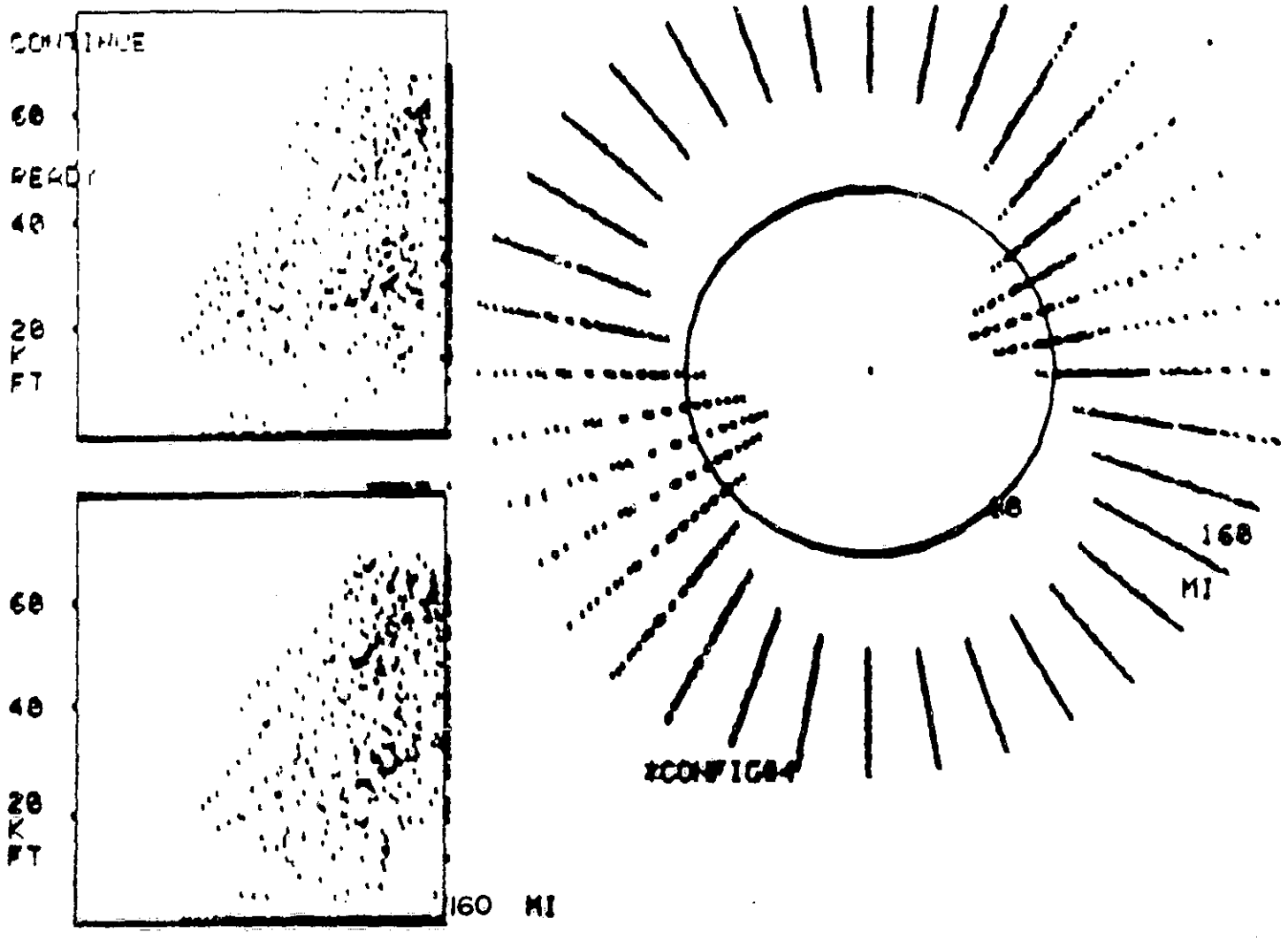

FIG. 48 ELEVATION-AZIMUTH ERROR PLOT, CONFIGURATION NO. 4, 5 MILES

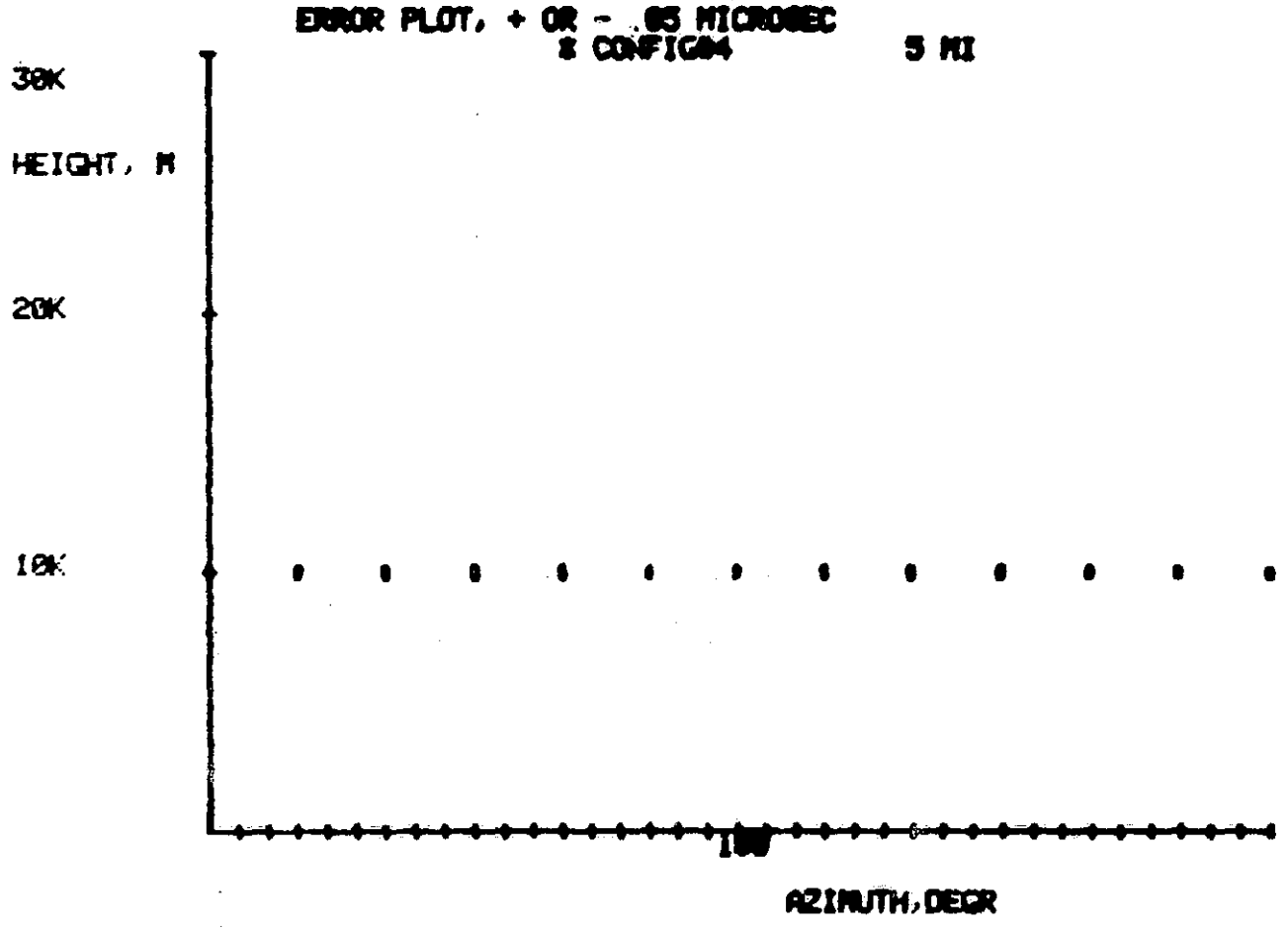

FIG. 49 ELEVATION-AZIMUTH ERROR PLOT, CONFIGURATION NO. 4, 10 MILES

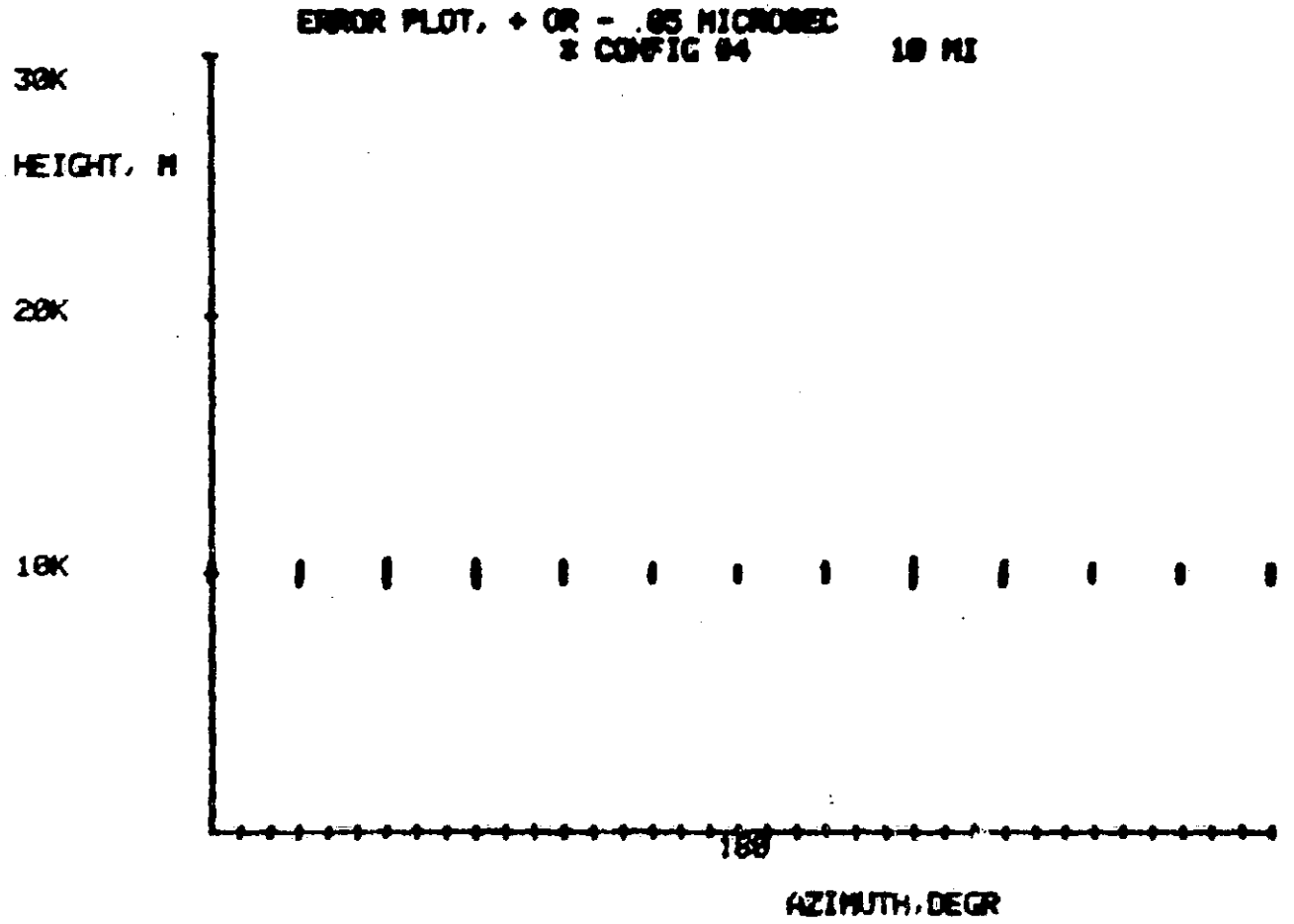

FIG. 50 ELEVATION-AZIMUTH ERROR PLOT, CONFIGURATION NO. 4, 20 MILES

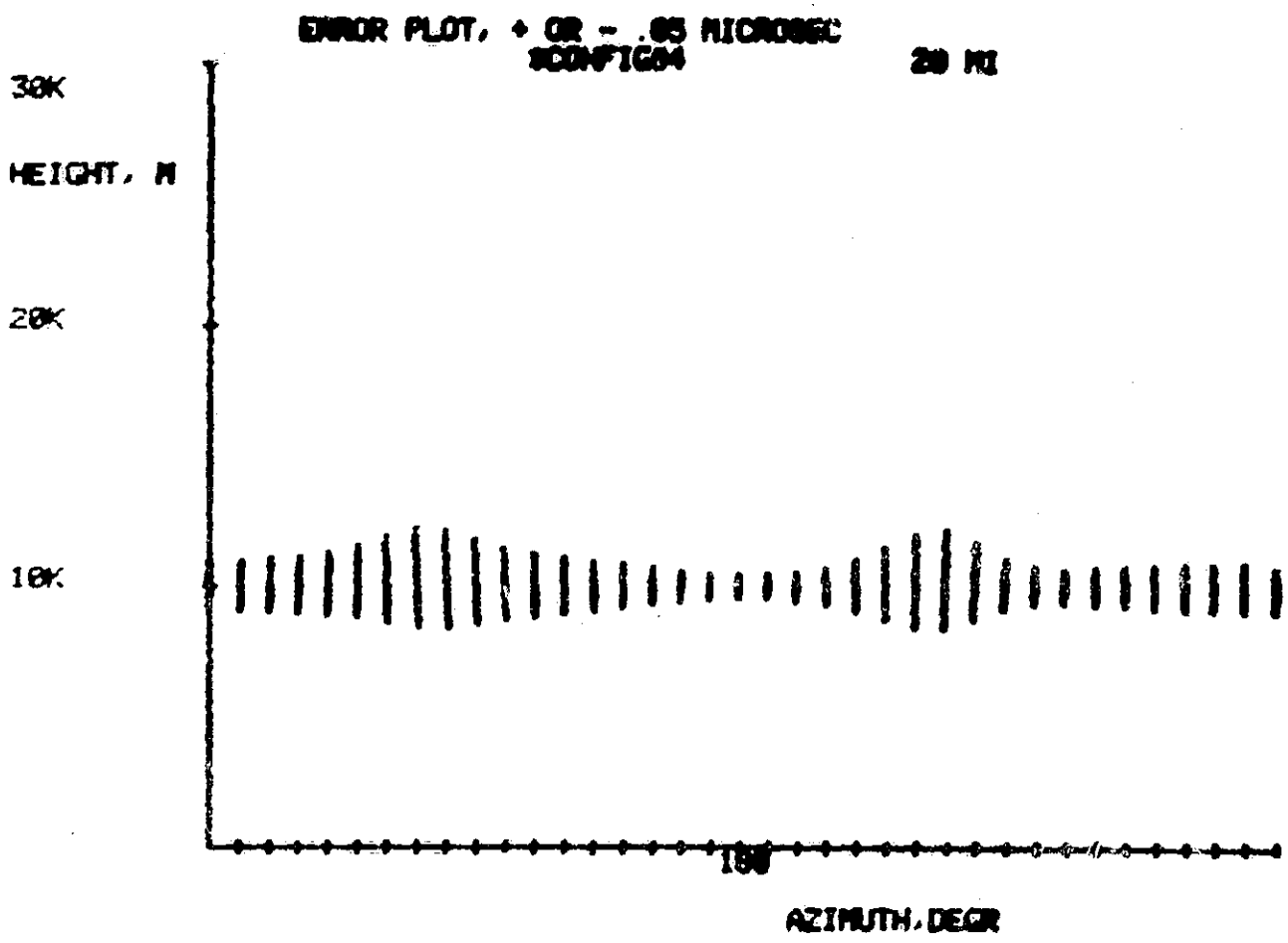

FIG. 51 ELEVATION-AZIMUTH ERROR PLOT, CONFIGURATION NO. 4, 40 MILES

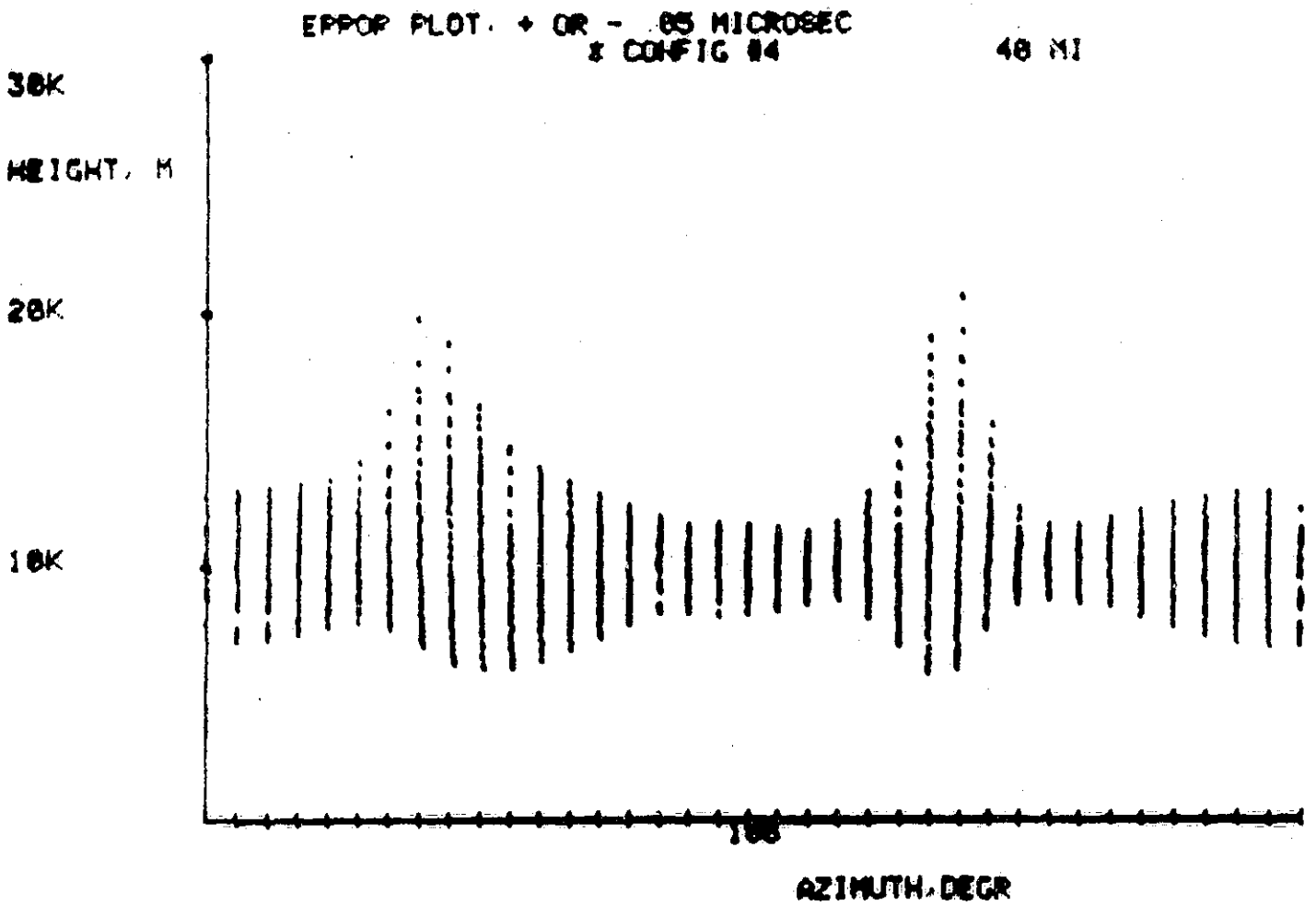

FIG. 52 ELEVATION-AZIMUTH ERROR PLOT, CONFIGURATION NO. 4, 160 MILES

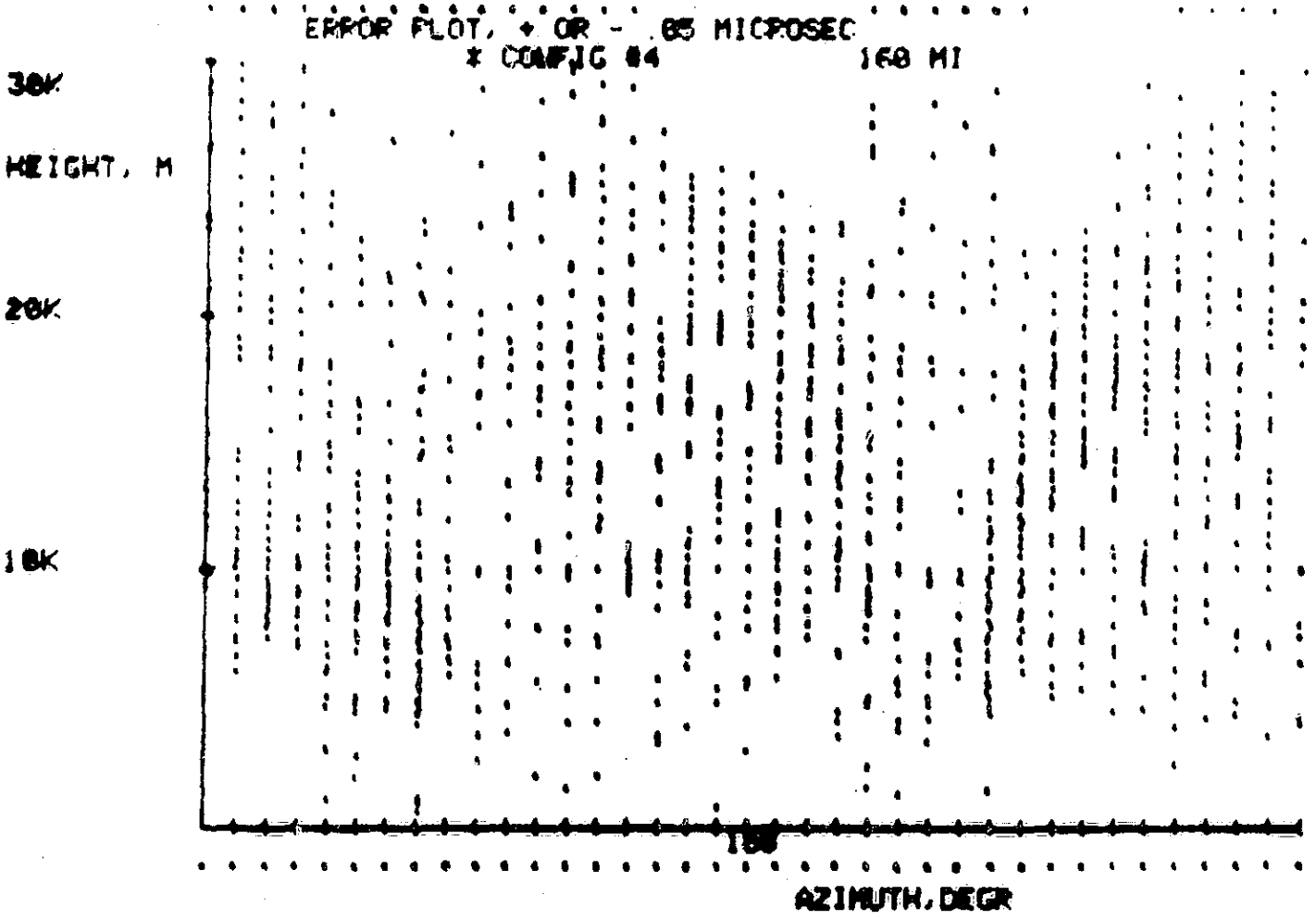

FIG. 53 RANGE-AZIMUTH ERROR PLOT, CONFIGURATIONS NO'S 2 AND 4 COMBINED, 20 MILE RANGE.

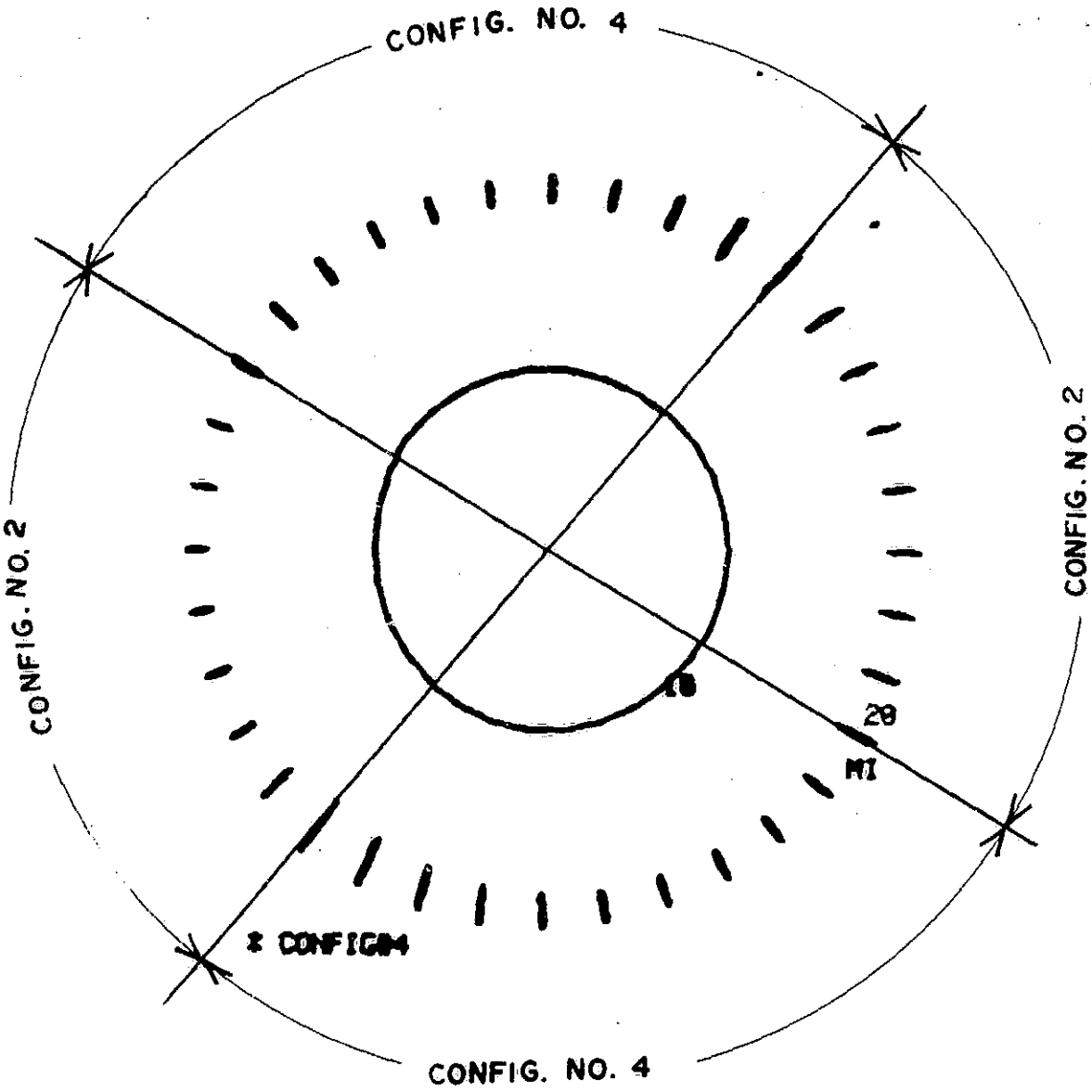

FIG. 54 ELEVATION - AZIMUTH ERROR PLOT, CONFIGURATIONS NO'S 2 AND 4 COMBINED, 20 MILE RANGE.

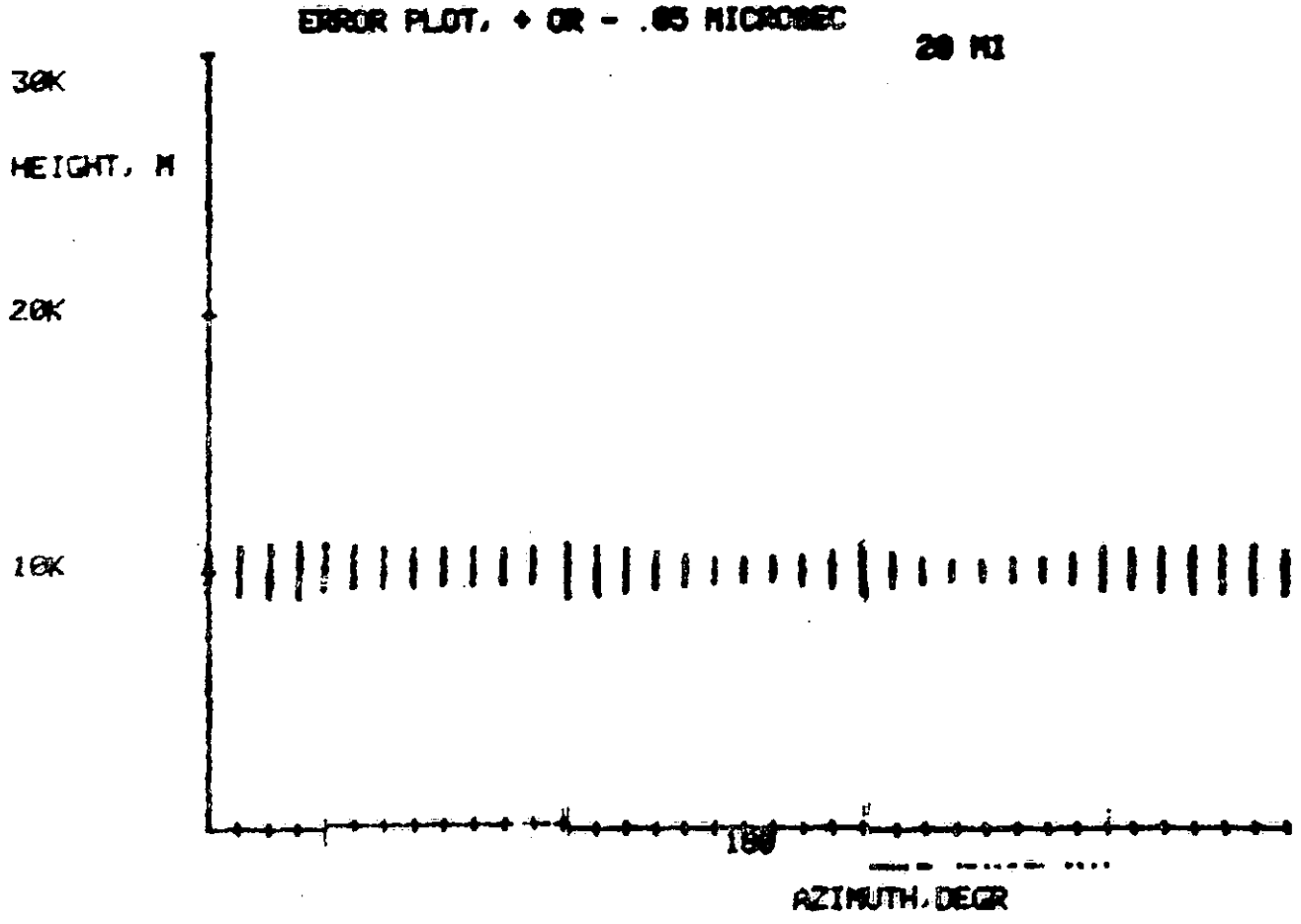

FIG. 55 MEASUREMENT UNCERTAINTY IN HEIGHT DUE TO ASSUMED QUANTIZING ERRORS OF 0.05 MICROSECONDS IN TØ, T1, T3, AND T4 PRIMARY CONFIGURATION

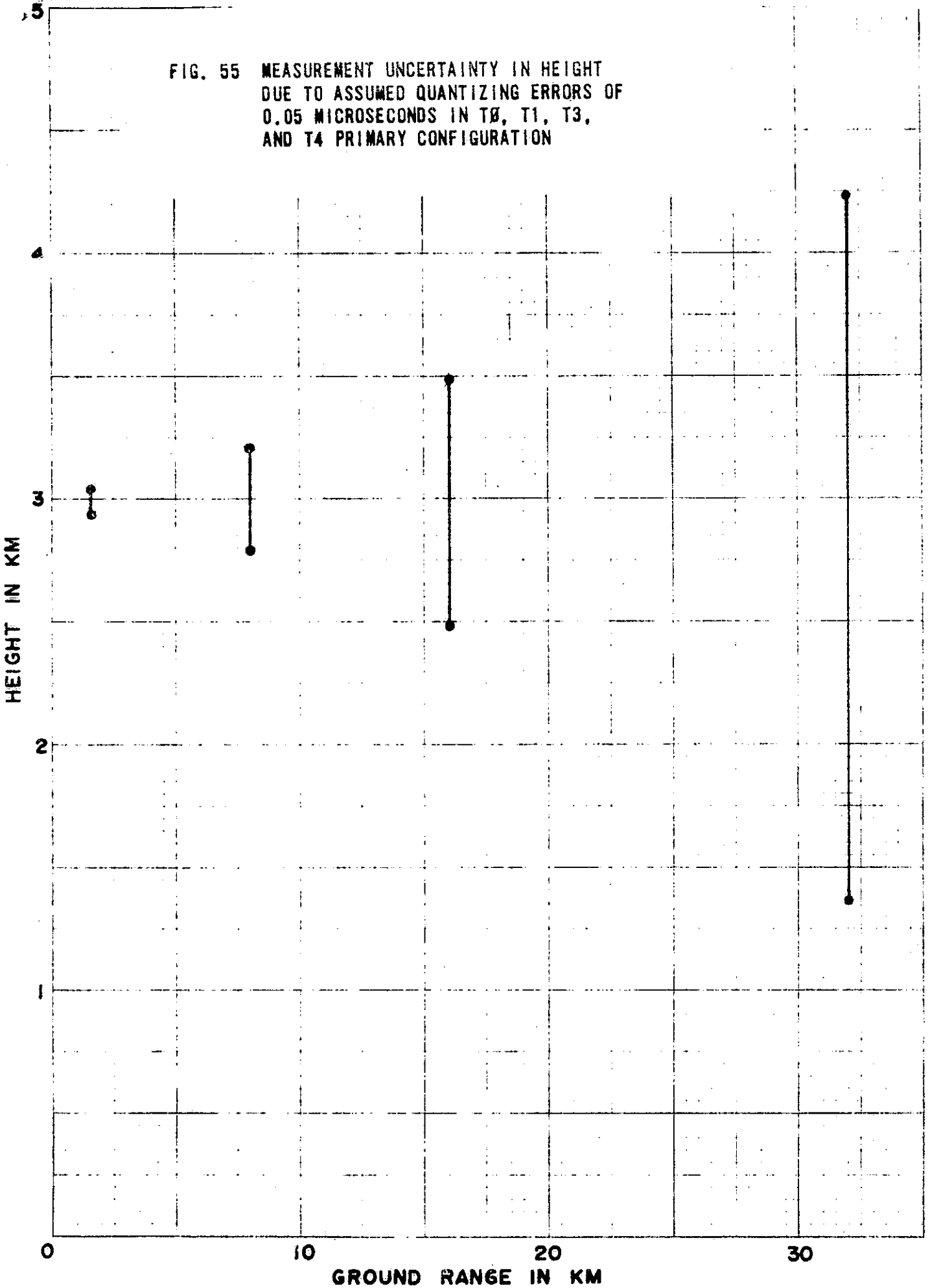

FIG. 58 MEASUREMENT UNCERTAINTY IN HEIGHT DUE TO ASSUMED QUANTIZING ERROR OF 0.05 MICROSECONDS IN TØ, T1, T3, AND T4 PRIMARY CONFIGURATION

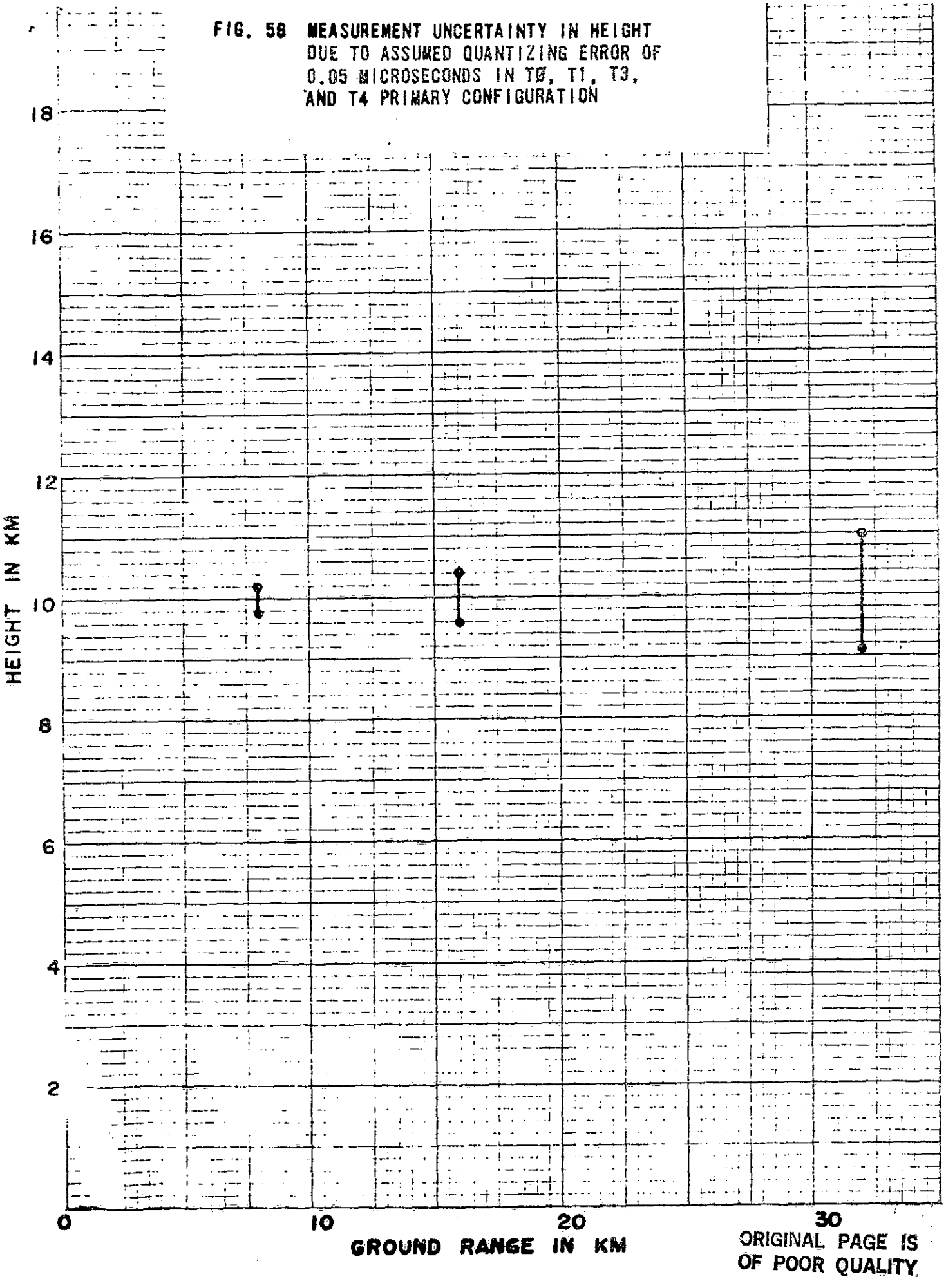

FIG. 57 LDAR TRACK OF C140 JET PLANE AT 30,000 FT. AT 450 KNOTS. AUGUST 18, 1976

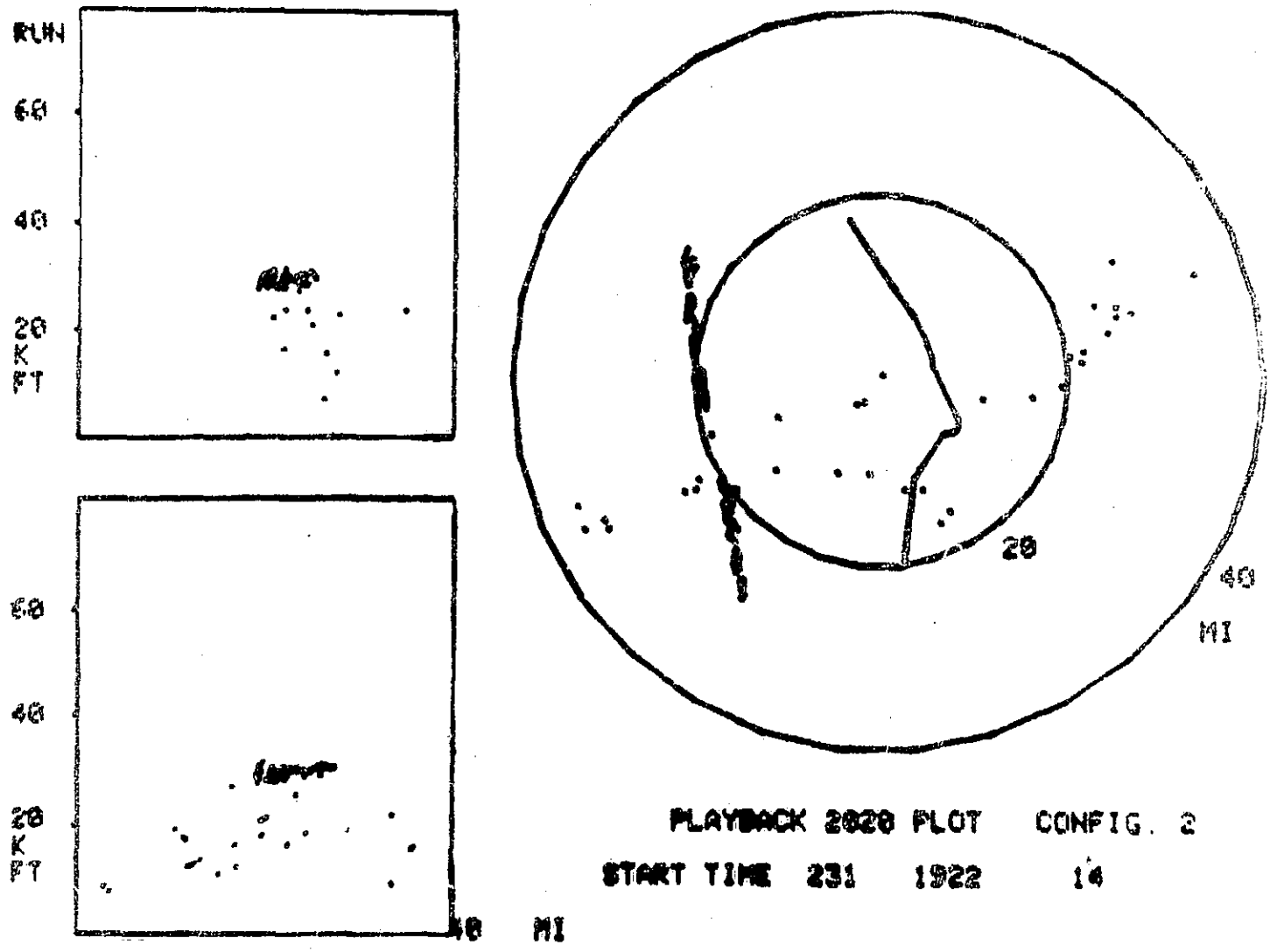

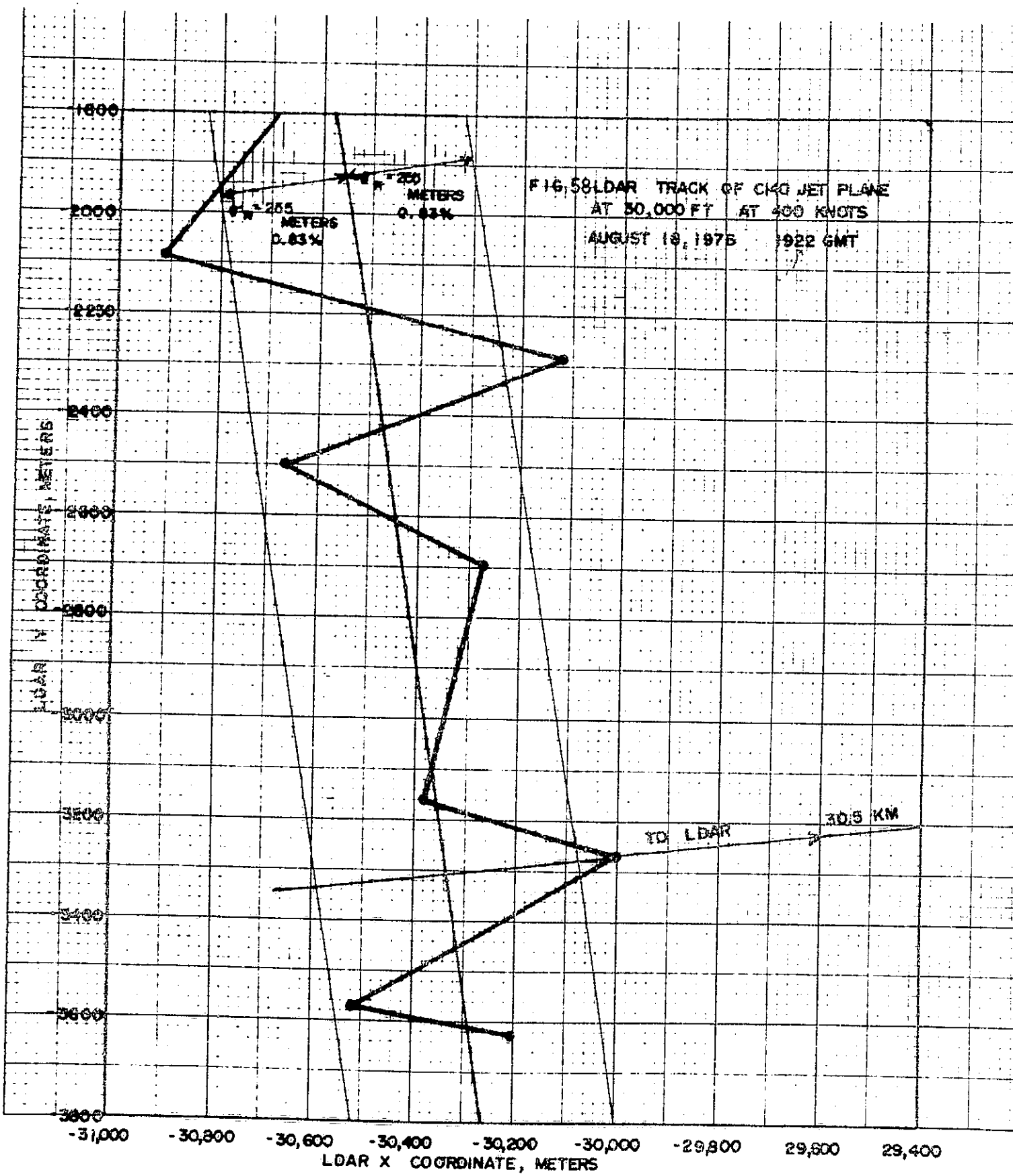

F16,58 LDAR TRACK OF C140 JET PLANE AT 30,000 FT AT 400 KNOTS AUGUST 18, 1975 1922 GMT

STANDARD TITLE PAGE

1. Report No.	2. Government Accession No.	3. Recipient's Catalog No.

4. Title and Subtitle	5. Report Date
AN ACCURACY ANALYSIS OF THE LDAR SYSTEM	March 8, 1977
	6. Performing Organization Code
7. Author(s)	8. Performing Organization Report No.
Dr. Horst A. Poehler	FEC-7146
9. Performing Organization Name and Address	10. Work Unit No.
Federal Electric Corporation FEC-720 Kennedy Space Center, Florida, 32899	11. Contract or Grant No. NAS 10-4967
	13. Type of Report and Period Covered
12. Sponsoring Agency Name and Address	Contractor Report
NATIONAL AERONAUTICS AND SPACE ADMINISTRATION KENNEDY SPACE CENTER, FLORIDA, 32899	14. Sponsoring Agency Code

15. Abstract An accuracy report of the LDAR System is presented. The effect of quantizing errors are modelled by use of a computer. The errors in the four configurations of the LDAR System are compared to the limiting errors in an ideal hyperbolic system. Performance data from the track of a jet plane and for the indicated position of a fixed lightning simulator are analyzed for dispersions in the data. Error models show the quality and the areas of highly accurate data, and show how the data deteriorates outside the primary measuring range.

16. Key Words

Lightning, Atmospheric Electricity, Thunderstorms, Measurements

17. Bibliographic Control	18. Distribution
May be announced in STAR	Publicly available

19. Security Classif.(of this report)	20. Security Classif.(of this page)	21. No. of Pages	22. Price
Unclassified	Unclassified	83	